

**NOVEL NANOPARTICLES TO STIMULATE THERAPEUTIC ANGIOGENESIS FOR
THE TREATMENT OF PERIPHERAL ARTERIAL DISEASES**

By
TAM PHUNG NGUYEN

DISSERTATION

Submitted in partial fulfillment of the requirements

for the degree of Doctor of Philosophy at

The University of Texas at Arlington

August 2022

Arlington, Texas

Dissertation Supervisor

Dr. Kytai T. Nguyen

Professor of Bioengineering

Supervising Committee

Dr. Ralph Mason, Professor of Radiology at UT Southwestern

Dr. Liping Tang, Professor of Bioengineering

Dr. Jian Yang, Professor of Biomedical Engineering at Pennsylvania State University

Dr. Hao Xu, Assistant Professor of Bioengineering

Abstract

Peripheral arterial disease (PAD) is a severe impairment of arterial vessels resulting in obstruction of normal blood flow in the legs, leading to acute or chronic lower limb ischemia, and subsequently, high morbidity and mortality rates. Common treatments for PAD, such as medications and surgical revascularization, have several limitations. For instance, medications used to lower cholesterol, reduce high blood pressure, control blood sugar, prevent blood clots, and relieve symptoms like leg pains may delay onset. Still, they cannot treat the established disease directly and often cause side-effects including bleeding, headache, and diarrhea. Meanwhile, many elderly PAD patients cannot undergo surgical options. Therefore, it is vital to develop an alternative therapy to treat PAD. The long-term goal for this thesis research is to develop novel biodegradable dual-modal imaging nanoparticles (DINPs) to precisely deliver therapeutic reagents that provide cell protection and facilitate the formation of blood vessels *de novo* at ischemic sites while allowing detection of the NP location and monitoring of their therapeutic effectiveness for PAD treatment. My results demonstrated DINPs were fabricated successfully with a homogenous size range around 150-200 nm. These DINPs retained their intrinsic imaging properties including fluorescent intensities in DAPI, FITC, and Cy5 channels as well as facilitating photoacoustic (PA) images at the deep tissue level of 11 mm in *ex vivo*. These DINPs were tracked on the EC uptake study via their intrinsic fluorescent properties. I also visualized DINPs in gastrocnemius muscle via the MSOT imaging system. EpoR plasmids released from EpoR DINPs demonstrated their properties in protecting cells damaged from stress conditions and facilitating tube formation in *in vitro* studies. In addition, EpoR DINPs enhanced angiogenesis to prevent ischemic legs from requiring amputation and improved physical capability on PAD

mice. In conclusion, our novel biodegradable DINPs are photostable, biodegradable, and able to encapsulate therapeutic EpoR plasmids in addition to showing intrinsic imaging properties including fluorescence and photoacoustic images to allow *in vivo* NP tracking/detection, thereby conferring distinct advantages over current imaging approaches. The EpoR DINPs could not only enhance the growth of blood vessels, but could also detect in deep muscle tissues during the treatment for adjusting the effective doses. This thesis research impact is significant in the bioengineering and health science fields as it is a paradigm shift to facilitate nanotechnology for the treatment of PAD.

Copyright © Tam Phung Nguyen

2022

All Rights Reserved

Acknowledgements

To complete my PhD program, I have received much motivation and support from my family in pursuit of my Ph.D. journey. As a big part of my success, I would like to say the deepest appreciation to my mentor, Dr. Kytai T. Nguyen, for her supervision and persistent support during my PhD program. She not only guided me step by step to complete my PhD thesis on the correct timeline, but also encouraged me to overcome personal problems in order to continue the program. Honestly, I consider Dr. Nguyen as my second mother in my life. She gave me invaluable suggestions and support to solve personal problems, so that I could return to do research quickly. She always motivated me to have positive thinking in order to strive through difficulties and challenges. Especially during the COVID-19 pandemic when most labs were shut down because of safety issues, she gave her PhD students great support to overcome COVID-19 associated issues in doing experiments.

On this occasion, I am also thankful to Dr. Liping Tang for his academic support and great suggestions to address issues and solve problems. I have learned various concepts and critical thinking for designing experiments and collecting data from him. He provided me with a great foundation to become an independent researcher as well as a mature scientist in the future.

Sincerely, I would like to thank my other committee members: to Dr. Xu for the training of animal peripheral arterial disease (PAD) model to evaluate my strategies for PAD imaging and treatment, and to Dr. Mason and Dr. Yang for their valuable time to review my work and give their best advice to improve my research. Especially, I would like to acknowledge Dr. Yang for providing his novel biodegradable imaging polymers to fabricate my novel therapeutic dual-imaging nanoparticles, and Dr. Mason for using his equipment (iThera MSOT 256TF, the cutting-edge technology and powerful optoacoustic imaging system) to measure the oxygen saturation in

the ischemic tissues for confirming model and monitor therapeutic outcomes and visualizing nanoparticle quantitation for managing PAD treatment.

I would like to thank the Bioengineering department for its support and assistance from the staff to process during my Ph.D. program.

I also would like this opportunity to thank Vy Tran, Priyanka Iyer, and Na Nguyen for contributing a great part in my thesis as well as working with me in other projects during my Ph.D. program, and all other members of the nanomedicine and drug delivery laboratory including Luis Soto, Harish Ramachandramoorthy and Uday Chintapula, for their wonderful friendship and encouragement. I would especially like to thank the previous Ph.D. student in Dr. Nguyen's lab, Dr. Aneetta Kuriakose, for training numerous experiments related to the project.

Lastly, I would like to acknowledge all funding sources including NIHR01 HL158204-01A1, STEM GRA, and a dissertation fellowship to support this research becoming feasible.

July 25th, 2022

Table of Contents

Abstract	i
Acknowledgements	iv
Table of contents	vi
List of figures	ix
List of tables	xi
Chapter 1 – Literature review	1
1.1 Peripheral arterial diseases (PADs)	1
1.2 Current treatment of PADs and their limitations	4
1.3 Surgical strategy on PAD treatment	6
1.4 Non-surgical strategy for PAD treatment	8
1.5 Gene therapy as a potential method for PADs	9
1.6 EpoR plasmids on PAD treatment	10
1.7 Nanoparticles on PAD treatment	11
1.8 Novel BPLPATs as imaging materials to formulate EpoR DINPs	12
1.8.1 Overview of dissertation research	14
1.8.2 Specific aims	16
1.8.3 Innovative aspects	17
Chapter 2 – Materials and Methods	18
2.1 Plasmid purification and characterization	18
2.1.1 Construction of plasmids	18
2.1.2 Plasmid purification	19
2.1.3 Plasmid Characterization	19

2.1.4 Plasmid-PEI complex preparation	20
2.2 The formulation and characterization of DINPs	20
2.2.1 DNP fabrication	20
2.2.2 Physical properties of DINPs	22
2.2.3 Plasmid loading of DINPs	22
2.2.4 Plasmid release profiles of DINPs	22
2.2.5 DINPs stability	23
2.2.6 Evaluation of intrinsic fluorescent properties of fabricated DINPs	24
2.3 The determination of <i>in vitro</i> effectiveness of EpoR DINPs	24
2.3.1 Cell culture	24
2.3.2 GFP plasmid expression	24
2.3.3 Evaluation of DNP imaging properties <i>in vitro</i> study	25
2.3.4 <i>In vitro</i> therapeutic effects of EpoR DINPs on HMMECs	25
2.3.5 Cytocompatibility of DINPs	26
2.4 The evaluation of <i>in vivo</i> therapeutic and imaging effects of EpoR DINPs	27
2.4.1 Creation of PAD mice	27
2.4.2 Imaging assessment of PAD mice	28
2.4.3 Biodistribution study of ICG DINPs	29
2.4.4 Investigation of the <i>in vivo</i> effectiveness of DINPs on PAD mice	29
2.4.5 Evaluation of histological staining	30
2.4.6 Toxicity assessment of DINPs	31
Chapter 3 – Results	32
3.1 DNP fabrication and characterization	32
3.1.1 Plasmid purification and characterization	32
3.1.2 DINPs fabrication and characterization	33

3.1.3 DINPs imaging properties	34
3.1.4 Drug release profiles	35
3.1.5 DNP stability	35
3.2 <i>In vitro</i> studies of EpoR DINPs	36
3.2.1 GFP expression	36
3.2.2 EpoR expression on EPCs	37
3.2.3 EpoR DINPs transfection study on EPCs	38
3.2.4 DINPs uptake study	40
3.2.5 <i>In vitro</i> therapeutic effects of EpoR DINPs on HMMECs	41
3.3 <i>In vivo</i> studies of EpoR DINPs	43
3.3.1 PAD models	43
3.3.2 Bio-distribution of ICG DINPs on PAD mice	46
3.3.3 Therapeutic effect of EpoR DINPs in LSCI and treadmill	48
3.3.4 Histology staining	50
Chapter 4 – Discussion/Conclusion	53
Chapter 5- Limitations and future work	58
References	61
Biographical Information	73

List of Figures

Chapter 1 – Literature Review	1
Figure 1. Atherosclerosis in the leg artery caused PAD	1
Figure 2. Prevalence of PADs (%) by aging men and women	2
Figure 3. Pathology of PAD	4
Figure 4. Three mechanisms improve blood perfusion in the body	5
Figure 5. Advantages and disadvantages of PAD treatment	6
Figure 6. The schematic diagram of EpoR DINPs on PAD imaging and treatment	15
Chapter 2 – Materials and Methods	18
Figure 7. EpoR plasmid map	18
Figure 8. The flow chart of DIMP fabrication	21
Figure 9. The left mouse PAD models	27
Chapter 3 - Results	32
3.1 DIMP fabrication and characterization	32
Figure 10. Gel electrophoresis of undigested and digested plasmids	32
Figure 11. The power forms of fabricated DINPs	33
Figure 12. TEM images of DINPs	34
Figure 13. The intrinsic fluorescent properties of DINPs	34
Figure 14. The release profile of EpoR DINPs	35
Figure 15. DIMP stability	36
3.2 <i>In vitro</i> studies of EpoR DINPs	36
Figure 16. Transfection study of free plasmids on LentiX cells	37
Figure 17. Transfection study of PEI: plasmids complexes on EPCs	38
Figure 18. The dose dependent study of EpoR DINPs on EPCs	39
Figure 19. The uptake study of DINPs on EPCs	40

Figure 20. The quantitative analysis of DINPs uptake on EPCs	40
Figure 21. The Cytoviva images of DINPs absorbed HMMECs	41
Figure 22. <i>In vitro</i> therapeutic effects of EpoR DINPs on HMMECs	42
Figure 23. <i>In vitro</i> tube formation of EpoR DINPs	43
3.3 <i>In vivo</i> studies of EpoR DINPs	43
Figure 24. Blood perfusion on PAD mice via LSCI	44
Figure 25. The established PAD mice reduction of blood perfusion on LSCI	45
Figure 26. MSOT images of blank DINPs on a PAD mouse	45
Figure 27. The biodistribution study of ICG PLGA NPs through IV and IM injections	46
Figure 28. The representative <i>in vivo</i> images of ICG DINPs	47
Figure 29. The <i>ex vivo</i> biodistribution study of ICG DINPs on PAD mice	48
Figure 30. <i>In vivo</i> therapeutic effects of EpoR DINPs on PAD mice	49
Figure 31. H&E staining of gastrocnemius muscle on treated PAD mice	51
Figure 32. Immunohistochemistry staining of CD31, CD34, and EpoR biomarkers	52

List of Tables

Table 1 . Plasmid characterization.....	32
Table 2 . Characterization of DINPs.....	33

Chapter 1

Literature Review

1.1. Peripheral arterial diseases (PADs)

PAD is a peripheral arterial progressive disorder characterized by stenosis and/or occlusion of large and medium-sized arteries because of atherosclerosis. According to the National Heart, Lung, and Blood Institute (NHLBI), atherosclerosis is the main reason for reducing or fully blocking the oxygen-rich blood flow throughout the body (**Figure 1**). The disease affects both men

and women, and its prevalence increases dramatically with age³. From the Centers for Disease Control and Prevention (CDC), PAD manifests in the elderly, approximately 20% of individuals over 80 years-old^{4,5} (**Figure 2**) and affected at least 8.5 million

individuals in the United States in 2015 and over 200 million people worldwide,⁶ with high rates of morbidity and mortality. It is the most common arterial disease of the lower body, in which non-coronary arteries become narrowed, leading to critical

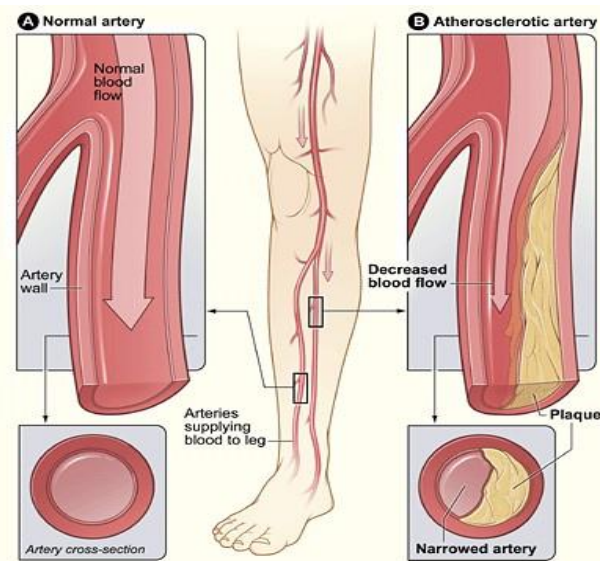


Figure 1. Atherosclerosis in the leg artery caused PADs. Figure A (left side) represents a normal artery supplying high blood perfusion to the leg, whereas its diameter shows full on the cross-section at the bottom-left side. On the other hand, Figure B (right side) represents a narrowed atherosclerotic artery restricting the blood flow through the plaque site. The atherosclerosis plaque blocked partial blood perfusion to the leg, which is PADs, whereas its diameter was occupied by more than 50% by the plaque lesion (yellow) on the cross-section at the bottom-right side. NHLBI Sources on July 17, 2022. <https://www.nhlbi.nih.gov/health/peripheral-artery-disease/causes>

limb ischemia (CLI). Gradually, CLI patients fall to conditions of immobility, uncontrollable pain,

ulceration, and toe and foot necrosis to limit their quality of life⁷. Eventually, the CLI conditions get worse with a poor prognosis including high rates of amputations (30% in one year) and mortality (20-25% in one year and 40-50% in five years)⁸ because of the poor quality of current therapies^{9,10}. Therefore, due to our aging population with high

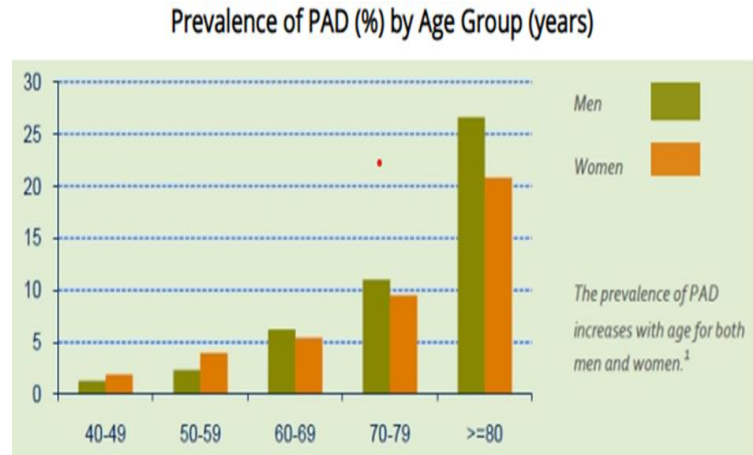


Figure 2. The prevalence of PAD in the US. PADs tend to increase in elderly people. PADs in men were a little bit higher than PADs in women after 60-years-old. There was approximately 20% or more of individuals over 80-years-old both men and women. CDC Sources on July 17, 2022. <https://www.cdc.gov/heartdisease/PAD>.

prevalence and mortalities, it is essential to explore new strategies to improve life quality and expectancy of PAD treatment and management.

Atherosclerosis (AS) is chronic progressive inflamed vascular disease characterized by patchy intimal plaques that cause narrow or blocked arteries. Its complications, one of the leading causes of high mortalities, resulted in 18.6 million deaths worldwide (30% of all deaths) according to the World Health Organization in 2021 and 868,662 deaths in the US (1 in 3 all deaths) including coronary heart disease (42.1%), followed by stroke (17.0%) according to Heart Disease and Stroke Statistics 2021¹¹. This paper reported its mortality rate as the highest among all death forms of cancer and lung diseases combined. Atherosclerosis is also the main reason causing PADs, occupied by 90% of PAD patients. Percutaneous transluminal angioplasty (PTA) is considered a minimally-invasive technique including balloon angioplasty with/without stent implantation, and has been extensively indicated for revascularization narrowed/occluded arteries to immediately supply blood flow to ischemic legs. It improves the short-term mortality rate of treated patients;

however, the inflation step during the balloon angioplasty or pre-dilation step in stent implantation may injure the arterial walls further, subsequently activating platelet aggregation post-procedure and re-narrowing the arteries in the long-run, leading to serious complications such as late thrombosis and restenosis,^{12,13} one of the biggest hurdles of PTA. Moreover, stent implantation in the legs can be fractured or in malposition due to their large motion¹⁴⁻¹⁶. These limitations encourage scientists to explore a non-surgical PAD treatment that enhances therapeutic effects without causing serious complications.

It has recently been proven that angiogenesis is a potential strategy to promote vessel formation in ischemic tissues.¹⁷ Instability limits growth factor delivery, enhancing therapeutic efficiency and showing potential side effects,¹⁸ while gene therapy modifies defective cells by delivering nucleic acid molecules, often through viral vectors, which have drawbacks such as immunogenicity and/or mutagenesis. To overcome these limitations, polymeric NPs have been developed as alternative gene carriers.¹⁹⁻²¹ Poly(lactic-co-glycolic acid) PLGA is the Food and Drug Administration (FDA) approved biodegradable polymer with good encapsulation properties that provide controlled, sustained release of its payload²² while Polyethylenimine (PEI) is the cation polymer that transports plasmids to nuclei resulting in higher transfection efficiency²³; however, its limitations include cell membrane destabilization, protein binding and immune responses affecting clinically translational application.^{24,25} NPs promoted significant angiogenesis with dense capillaries, improved collateral circulation, and enhanced gene expression compared to that of naked plasmids.²⁶⁻²⁸ To date, delivery of growth factors has not yielded satisfactory angiogenesis in PAD,²⁹⁻³² potentially because the cells at the ischemic site could not survive the ischemic environment. Historically, the location and amounts of administered NPs *in vivo* could not be quantitatively or accurately assessed. Few reliable, noninvasive imaging modalities are

available to monitor PAD development or therapy³³ even though monitoring the progress of therapeutic intervention is critical. These observations highlight the importance of developing novel nanoparticles as an image-guided approach for PAD management.

1.2. Current treatment of PADs and their limitations

The restriction of narrowed/blocked arteries leads to an increase of shear stress in pre-existing arterioles and hypoxic ischemia, inducing inflammation, monocyte recruitment, upregulation of various factors including VEGF, PDGF, NOS and HIF that promote arterial remodeling. This will trigger arteriogenesis, which is the process of arteriolar connection and dilation and angiogenesis, which is the formation of new capillaries (**Figure 3**). There are 3 mechanisms to enhance blood

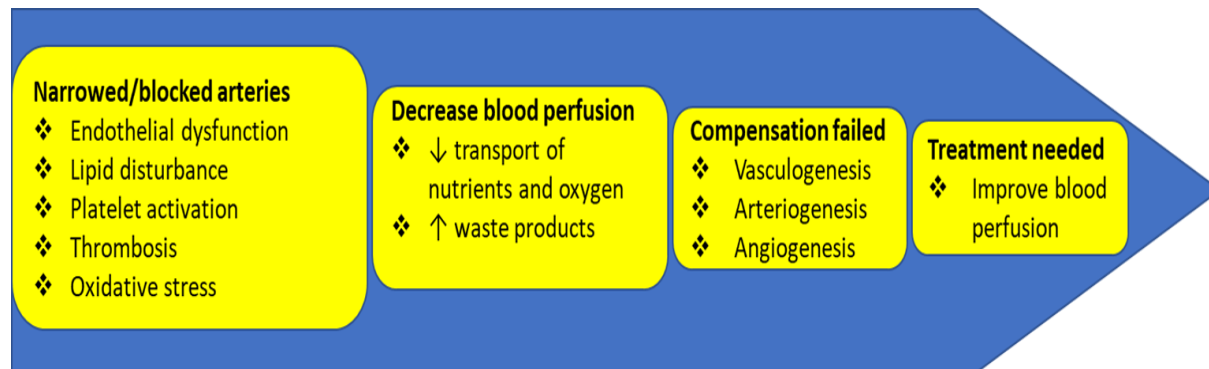


Figure 3. Pathology of PAD. The pathology of PAD mostly relates to atherosclerosis where lipids gradually build up on the lumen of the damaged artery, called plaque. The plaque results in narrowed/blocked arteries decreasing blood perfusion, which reduced the transport of nutrients and oxygen. The disease is getting worse when lipid disturbance causes inflammation leading to platelet activation, thrombosis, and oxidative stress. Hemodynamic consequences of PADs depend on the degree of narrowed arteries and the dilation of the collateral network of small arteries (arteriogenesis). Enhancing blood perfusion by vasculogenesis is only triggered in embryo while angiogenesis is limited by scarcity of growth factors. The hallmark of PAD is marked when the compensation mechanisms fail. Initially, PADs show symptoms during walking when the collateral arterial dilation maximizes but cannot supply enough blood perfusion. Gradually, the disease progresses more severely when the demands of the blood supply is not enough for the resting metabolism. Therefore, treatment is needed to reduce the symptoms, enhance patient life quality, and prevent amputation consequences.

perfusion to hypoxic ischemic tissues including vasculogenesis, arteriogenesis, and angiogenesis; however, vasculogenesis only occurs in embryo while arteriogenesis is limited due to the small

numbers of pre-existing arterioles (**Figure 4**). Therefore, inducing angiogenesis by using growth factors has been considered as a potential strategy for PAD treatment. The current standard therapy

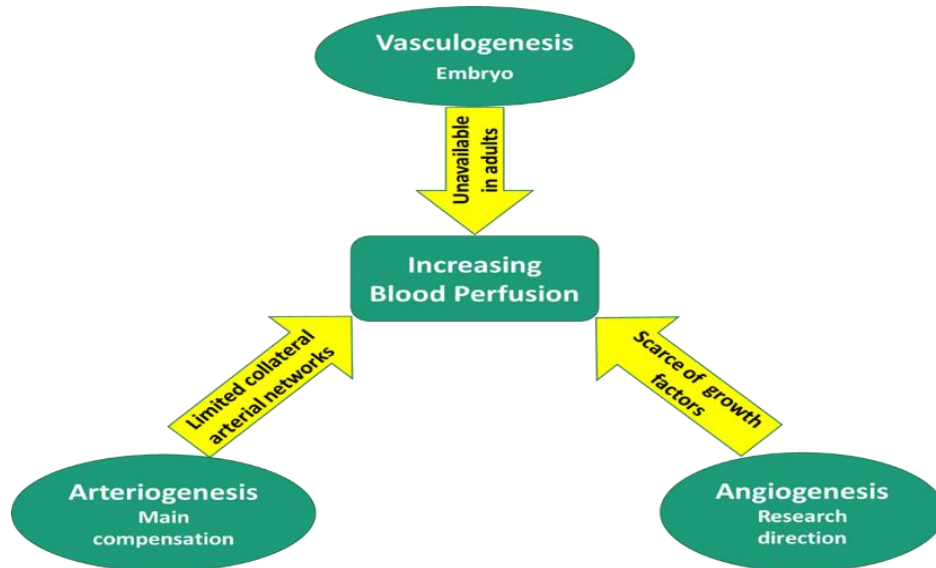


Figure 4. Three mechanisms improve blood perfusion in the body. Vasculogenesis is the process of blood vessel formation during embryogenesis via the differentiation of endothelial precursor cell, so it is unavailable for adults. Arteriogenesis is the process of enlarging pre-existing collateral small arteries to replace occluded arteries, but these arteries never supply blood demand as much as the main arteries do. Angiogenesis is the process of sprouting new capillaries regulated by chemical signals in the body. This mechanism is believed to enhance enough blood demand in PAD patients, so research direction has been focused on enhancing angiogenesis by delivering various growth factors to the ischemic tissues. The yellow arrows indicate limitation of each mechanism in the body.

for PADs has been investigated on improving the blood perfusion via endovascular surgery (including balloon angioplasty, stenting, and bypass procedure) and non-surgery (angiogenic induction). The advantages and disadvantages of all methods on PAD treatment were summarized in **Figure 5**, indicating imbalances of benefits and drawbacks on two main strategies: surgery and non-surgery. Surgery provides a great benefit on short-term effects to immediately restore blood flow on narrowed/blocked arteries to save patients' legs and lives; however, long-term effects are still hurdles because of serious complications such as late-thrombosis and restenosis. On the other hand, non-surgery takes advantage of gradually enhancing angiogenesis without serious complications, but its therapeutic outcomes are still limited and need to be improved.

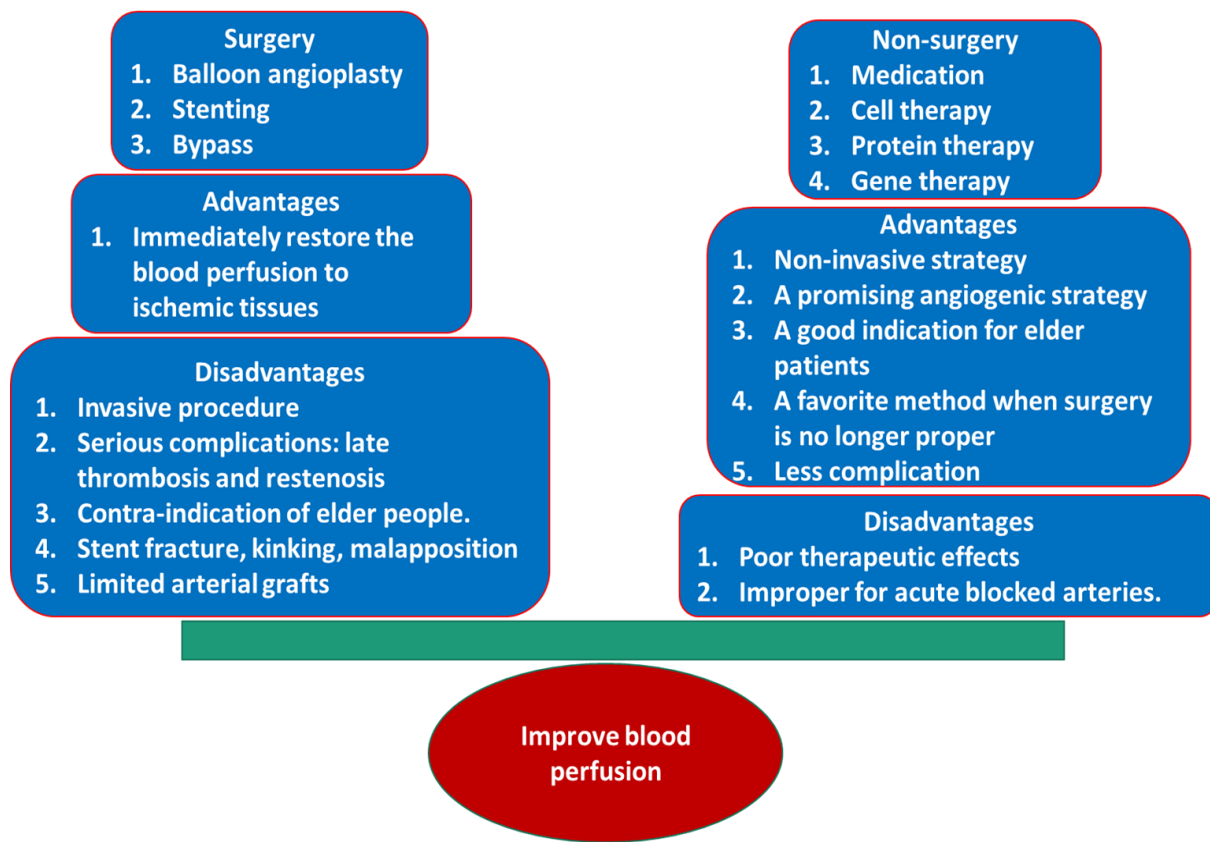


Figure 5. Advantages and disadvantages of current PAD treatments. Surgery significantly and immediately enhances blood perfusion via endovascular intervention, while non-surgery provides blood perfusion gradually via medication. Surgery has benefits on short-term outcomes but shows serious complications such as late thrombosis and restenosis. Moreover, this strategy mostly is a contraindication in elderly patients where they contract background diseases. On the other hand, a non-surgical method can improve blood perfusion in both short and long terms. Although this method cannot restore blood flow as quickly as surgery, it can avoid disadvantages from that invasive method.

1.3. Surgical strategy on PAD treatment

While late-thrombosis can cause patient death immediately, restenosis will limit their life quality and expectancy. Percutaneous transluminal angioplasty (PTA) is a minimally invasive procedure with/without stent implantation, extensively indicated for revascularization femoral narrowed/occluded arteries to immediately restore blood perfusion to the lower leg without invasive vascular surgeries. This procedure significantly improves blood flow throughout the blocked segments to reduce the short-term morbidity and mortality rate of patients; however, over-

inflating the balloon during the angioplasty procedure or pre-dilation step in stent implantation can peel off or damage ECs on the surface of the femoral arterial walls. Subsequently, denuding ECs activates platelet aggregation post-procedure, causing late thrombosis complications, injuring ECs, triggering inflammatory mechanisms, combining to lipid deposition on the arterial walls, and causing re-narrowed arteries long-term known as restenosis,^{12,13} one of the biggest hurdles of PTA. To overcome late thrombosis, antiplatelet drugs such as warfarin, aspirin, and clopidogrel will be required to prevent platelet aggregation^{34,35}, but these medications increase the risk of bleeding and a prolonged hospital stay.^{36,37} Similarly, the second PCI will be performed on restenosis or in-stent restenosis to enhance blood perfusion, but poor prognosis on these patients can be predicted. Although stents and drug eluting stents (DES) have positive outcomes in the treatment of coronary arteries, they have several significant issues when applied to the legs including stent fracture, kinking, malapposition, impaired vascular healing, and high rates of thrombosis and restenosis, probably because of extensive motion of the lower extremity.¹⁴⁻¹⁶ This might be due to the greater motion of the lower extremity, leading to higher torsion, compression, flexion, and extension at the implanted stent. Drug eluting balloons (DEB) would overcome the drawbacks of stent technology as they could actively transfer drugs/compounds locally to increase treatment efficacy and reduce stent usage in the lower extremity. Various clinical trials have consistently shown the effectiveness of DEBs compared to that of uncoated balloons in reducing neointimal formation in PAD patients after angioplasty^{14,15,38,39}. Yet late restenosis is still a major limitation of this vascular intervention. This might be due to the limited amount of drug transfer to the arterial wall and the delayed vascular healing after angioplasty. When endovascular intervention is unavailable, bypass surgery is the indication to revascularize the blood flow over the blocked/narrowed sites of the artery by suturing donor arteries bridging from an upstream artery to a downstream artery. The

donor arterial sources can be autograft, allograft, xenograft, or prosthesis. The bypass surgery is classified as a major invasive procedure, so it is usually a surgical contraindication for elderly patients with medical background diseases. While the less invasive interventions including balloon angioplasty and stents showed serious complications, the invasive treatment for PADs includes bypass surgery and is related to another major challenge, which is that approximately 50% of patients do not have adequate autogenous veins for the bypass procedure⁴⁰⁻⁴⁵. When forced to use prosthetic grafts, the 5-year patency of these grafts is about 40-50% for the artery above and 15-30% below the knee⁴⁶. Performing endovascular and vascular therapies to revascularize the blood flow of narrowed arteries only shows the short-term therapeutic effects, while it causes serious complications such as late thrombosis and restenosis. Moreover, the contraindication of vascular surgery on elderly PAD patients increases difficulties for physicians to choose the best therapeutic options as well as limits chances for patients to get the best expected outcomes. Thus, it is essential to investigate the strategy that enhances the blood perfusion without using invasive procedures and avoids severe complications on post-treatment.

1.4. Non-surgical strategy for PAD treatment

For patients who cannot undergo endovascular intervention, angiogenic therapies such as cell-based therapy⁴⁷⁻⁴⁹, pharmacological treatment^{50,51}, protein therapy, and gene therapy⁵² are used. The therapeutic angiogenesis has proven to be a potential strategy to mitigate patients' symptoms as it promotes blood vessel formation to supply oxygen-rich blood and nutrients to deficit tissues.¹⁷ Although these therapies demonstrated promising results in preclinical studies and Phase I trials, there are no significantly different outcomes of mortalities, amputations, or amputation-free survivals observed in clinical trials followed up to two years^{47,52}.

Current pro-angiogenic protein therapy has recently been proven as a potential strategy to promote capillary formation in ischemic tissues.¹⁷ It requires the administration of exogenous pro-angiogenic factors to protect ECs under hypoxic environments, recruit EPCs to remodel the extracellular matrix for tubule formation and finally sprout new blood vessels for enhancing blood perfusion.²⁹ However, this strategy is limited by protein instability, leading to the therapeutic failure and potential side effects.¹⁸ Pharmacological therapy has not reduced ischemic symptoms in damaged legs or the disease's progression,^{53,54} while stem cell therapy has very poor cell retention at ischemic areas⁵⁵ where they are easily attacked and cleared out by the immune system. Infusions of bone marrow mononuclear cells for rejuvenating endothelial progenitor cells failed to show improvements of major amputation rates, rest pain, quality of life, and ankle-brachial index in JUVENTAS trial (NCT00371371).⁵⁶ Moreover, some cancers have been reported from either undifferentiated or over-activated self-renewal stem cells.⁵⁷

1.5. Gene therapy as a potential method for PADs

Gene therapy is the most common approach to optimize therapeutic angiogenesis.³² Among pro-angiogenic genes applied for PAD treatments, vascular endothelial growth factor (VEGF), fibroblast growth factor (FGF), hepatocyte growth factor (HGF), stromal derived growth factor (SDF), and platelet derived growth factor (PDGF) have been most extensively studied in preclinical and clinical trials.^{58,59} However, they have failed to demonstrate benefits on primary outcomes in phase 2 or 3 clinical trials. Gene therapy has some limitations including low therapeutic effects, limited genes, protein availability over time mostly due to short half-life and enzymatic degradation,⁶⁰ or uses of single growth factor plasmids.⁶¹ Since gene therapy modifies defective cells by delivering nucleic acid molecules often through viral vectors, it also relates to

drawbacks such as immunogenicity and/or mutagenesis. To overcome unmet needs, trending research has been explored for new growth factor expressed plasmids to facilitate angiogenesis for improving therapeutic effects of PAD treatments.

1.6. EpoR plasmids on PAD treatment

Administration of the mentioned angiogenic factor expressed plasmids still shows inadequacy in producing functional and mature vessels in randomized phase 2 clinical trials for PAD patients.⁶²⁻⁶⁴ EpoR, a 66-78 kDa transmembrane receptor of erythropoietin (Epo) upregulated in hypoxic environment,^{65,66} played important roles in cellular survival pathways, promotion of EC proliferation, enhancement of EPC recruitment, stimulation of angiogenesis, and maintenance of vascular integrity under stress conditions.⁶⁷⁻⁷⁴ Recently, EpoR has been explored as a pro-angiogenic agent for upregulating the expression of VEGF and VEGFR.^{69,75-78} EpoR expression triggers the Epo/EpoR signaling pathway and serves as vasodilators/vasoconstrictors, modulators of vascular tone synthesis, and elicitors of pro-angiogenic programs in stem cells and angiogenic signaling pathway initiators.^{67,79,80} EpoR plasmids were also reported to recruit EPCs in hypoxia-induced pulmonary hypertension.⁸¹ Particularly, EpoR plays major roles in enhancing angiogenesis in peripheral ischemia⁶⁹ and preventing cell apoptosis and inflammation⁷¹. Together with its anti-sense (RopE), EpoR transcripts have demonstrated synergistic upregulation of EpoR expression *in vitro* and in a canine lung.⁸² Although EpoR expression plays important roles in therapeutic angiogenesis, limited research has been investigated on its use in PAD treatments. Polyethylenimine (PEI), the polymer that can form complexes (called proton sponge) with plasmids via electrostatic forces and transport them to nuclei, provides higher transfection efficiency;²³ however, it causes cytotoxicity when used high doses.^{83,84} The proton sponge can

escape the lysosomal degradation in transfected cells to enhance transfection efficiency.²⁴ Therefore, delivering complexes of EpoR plasmids and PEI would be a potential selection to enhance angiogenesis as well as the blood perfusion on PADs.

1.7. Nanoparticles on PAD treatment

Although gene therapy is the most commonly used approach to stimulate therapeutic angiogenesis that can eradicate PAD, safety and effective delivery are one hurdle for gene therapy.⁸⁵ Delivering therapeutic DNA molecules or plasmids can be performed via direct injection or viral vectors.^{86,87} Yet these techniques are limited by ineffective therapeutic efficiency and extensive side effects¹⁸ because of their inability to penetrate through the cell membrane, enzymatic degradation, immunogenicity concerns, and their low performance in reducing amputation rates in CLI patients.^{88,89} To overcome these limitations, there is a need to develop novel therapeutic non-viral nanocarriers encapsulated therapeutic plasmids to eliminate the side-effects of using viral vector carriers while enhancing the bioavailability of plasmids at ischemic tissues. Polymeric NPs have been developed as alternative gene carriers.¹⁹⁻²¹ Polymeric NPs including natural polymers (alginate, chitosan, gelatin, and so on) and synthetic polymers have been investigated for controlled drug delivery and different biomedical applications due to their great biocompatibility, physiochemical/mechanical, and most importantly, biodegradability properties.⁹⁰⁻¹⁰⁴ Polymeric NPs demonstrated many advantages such as ease of fabrication, protection of therapeutic reagents against the harsh environment experienced in systemic circulation, and an ability to provide sustained drug delivery to relevant cells/tissues.^{105,106} In the last decade, PLGA has been applied for biomedical applications because of FDA approval, tailored biodegradable rate, and easy fabrication, modification, and storage.¹⁰⁷ PLGA NPs, non-viral

nanocarriers, provide good encapsulation properties and biphasic release profile including burst and sustained release of its payload.²² Delivery of EpoR PLGA NPs studied by our group has been shown to upregulate pulmonary EpoR expression and its downstream signals to attenuate stress-induced damage in rat lung tissues⁹⁰. In addition, other investigators have tailored PLGA nanostructures that possess superior encapsulating properties for probucol delivery to tissues and retention in rabbit femoral arteries and the hindlimb muscle.¹⁰⁸ Delivery of PLGA NPs encapsulating human VEGF plasmids to rabbit ischemic peripheral sites also showed significant angiogenesis with dense capillaries, improved collateral circulation, and enhanced gene expression compared to that of naked plasmids.¹⁰⁹ Furthermore, intramuscular administration of sphingosine-1-phosphate (S1P) loaded PLGA NPs to mice hindlimbs demonstrated their effectiveness as suitable carriers of pro-angiogenic factors by enhancing blood perfusion and capillary densities as well as minimizing limb necrosis and dysfunction in ischemic muscles.^{110,111} Our lab has fabricated various NPs that provided a controlled and sustained release of different payloads such as drugs, dyes, plasmids, and proteins.^{90,94,98} Especially, VEGF loaded NPs showed the sustained release of these therapeutic agents at the intended sites and enhanced endothelial proliferation and vascular remodeling.^{90,112-115} Although various growth factor encoded plasmid loaded NPs have been investigated in pre-clinical and clinical studies of PAD treatment, there is no previous study to evaluate the induced expression of EpoR via NP delivery to treat PADs.

1.8. Novel BPLPATs as imaging materials to formulate EpoR DINPs

Although PLGA NPs demonstrated outstanding benefits to deliver therapeutic agents compared to free drugs, they have not yielded satisfactory effects in PAD management.²⁹⁻³² Historically, location and amounts of administered NPs *in vivo* could not be quantitatively or

accurately assessed during the treatment. On cancer management, various NPs have been developed and have emerged as a novel imaging and therapeutic approach by facilitating diagnosis and treatment in a single setting^{116,117}. However, few nanoparticles have been developed for imaging applications in ischemic conditions to provide therapeutic agents for relevant cells such as vascular cells and to enable tracking and monitoring NP distributions in different tissues¹¹⁸⁻¹²². Few reliable, noninvasive imaging modalities are available to monitor PAD progress or therapeutic effects³³ even though monitoring the progress of therapeutic intervention is critical. These observations highlight the importance of developing novel nanoparticles as an image-guided approach for PAD management.

Dr. Yang's lab at Penn State University (PSU) has developed biodegradable multifunctional citric acid-derived elastomers for drug delivery and bio-imaging in tissue engineering.¹²³⁻¹³² Citrate based biomaterials have been explored as imaging polymers via intrinsic properties of photoluminescence.^{129,130} For instance, biodegradable photoluminescent polymers (BPLPs) demonstrated intrinsic fluorescent properties compared to photobleaching organic dyes and/or cytotoxic quantum dots.¹³⁰ Tunable fluorescent properties of BPLPs including high intensity, quantum yield, and photostability have been observed on the noninvasive biodegradable materials in the murine studies via fluorescence imaging.¹²⁹ However, the big challenge of the optical imaging is detectability in deep tissues, which are significantly inconvenient in *in vivo* imaging. To improve the limitation, aniline tetramer (AT) was inserted into BPLPs platforms to form new BPLPAT materials for providing dual imaging modality including fluorescent and photoacoustic (PA) imaging properties, which are helpful for *in vitro* and *in vivo* studies. Increasing AT ratios enhances PA signals while reducing fluorescent intensity of BPLPATs. *Ex vivo* PA images of BPLPAT scaffolds were successfully acquired at 11 mm tissue depth of chicken breast.¹³³ *In vivo*

PA imaging of BPLPAT disks was clearly observed next to a rat sciatic nerve (deep tissue implantation).

The dual-modal imaging of BPLPATs makes them potential materials to approach imaging and treatment of PADs. Therefore, I have optimized the formulation of dual imaging nanoparticles (DINPs) by using BPLPAT polymers to maximize the much-desired fluorescence and photoacoustic imaging for PAD treatment. To promote therapeutic angiogenesis and to overcome the limitations of current technologies for PAD therapies, I developed novel biodegradable DINPs for controlled release of EpoR plasmids to facilitate therapeutic angiogenesis long-term while allowing the detection of these DINPs at ischemic regions with a high sensitivity and penetration depth.

1.8.1. Overview of dissertation research

Chronic ischemia caused by partial or complete impairment of peripheral arteries affects over eight million individuals in the United States, resulting in high rates of morbidity and mortality. Current treatment options focus on drug therapy for symptomatic relief^{43,134} or improving blood flow via endovascular interventions, which are not suitable for over 50% of elderly PAD patients⁴³. Delivery of growth factor loaded NPs to ischemic tissues has promoted angiogenesis and improved collateral circulation¹³⁵. However, issues related to these therapeutic carriers include poor cell protection and blood vessel formation under hypoxia, difficulty in determining their *in vivo* bio-distribution, and low therapeutic efficacy *in vivo*¹³⁶⁻¹³⁸.

To overcome these limitations, the ultimate goal of this thesis research is to develop novel biocompatible and degradable **dual-modal imaging nanoparticles** (DINPs) that provide cell protection and facilitate therapeutic angiogenesis under stress conditions such as ischemia for peripheral arterial disease (PAD) treatment. These intramuscularly injected DINPs can be retained

at the ischemic regions, recruit stem cells such as endothelial progenitor cells (EPCs), and deliver therapeutic EpoR plasmids to promote angiogenesis, thereby forming blood vessels *de novo*, while providing detection tools to directly trace their bio-distribution, degradation, and therapeutic efficacy *in vivo* (Figure 6).

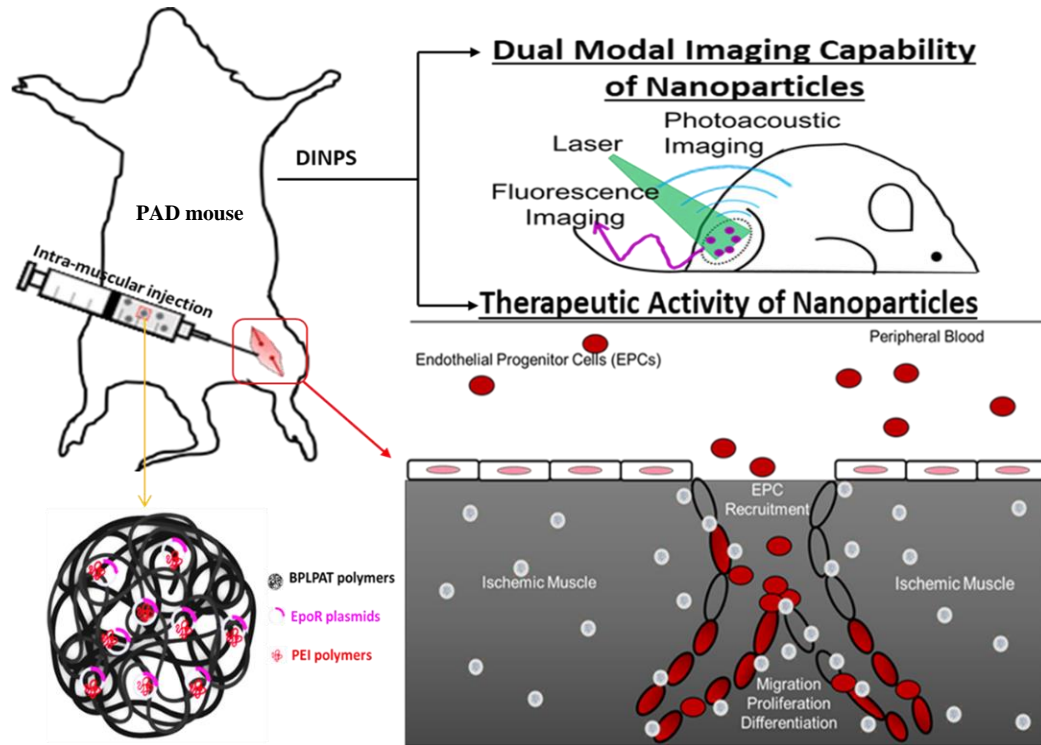


Figure 6. The schematic diagram of EpoR DINPs on PAD imaging and treatment. PAD mice will be intramuscularly injected with EpoR DINPs to the gastrocnemius muscle. EpoR released from DINPs will protect cells in ischemic tissues and enhance endothelial progenitor cell recruitment to the lesion for increasing angiogenesis. Multispectral optoacoustic tomography (MSOT) will be applied to verify the model, track DINP locations and doses, and assess therapeutic outcomes. Laser speckle contrast imaging (LSCI) and treadmill will be used to evaluate blood perfusion and physical restoration, respectively.

1.8.2. Specific aims

Aim 1: Formulation and characterization of DINPs made of optimized biodegradable photoluminescent polymers-aniline tetramers (BPLPATs) and loaded with erythropoietin receptor (EpoR) plasmids. Various DINPs were fabricated by using BPLPATs loaded with different

therapeutic agents for different purposes. Synthesized DINPs were characterized for physical and intrinsic fluorescent properties. Drug loading and release profiles were also determined to learn the biphasic release curve of EpoR DINPs. DNP stability was performed to assess its safety in animal studies. Lastly, intrinsic fluorescent properties of DINPs were visualized under microscopes at high magnification.

Aim 2: Determination of the in vitro effectiveness of EpoR DINPs on endothelial cells (ECs) and their intrinsic fluorescent properties to track EC uptake. Therapeutic EpoR plasmids were performed on ECs via protection and tube formation studies. The therapeutic agent should both enhance angiogenesis and prevent the hypoxia-induced apoptosis resulting from ischemia; I chose erythropoietin receptor (EpoR) as our therapeutic agent based on its known major roles in facilitating stem cell mobilization^{67-69,139}, preventing cell apoptosis and inflammation⁷⁰⁻⁷², and enhancing angiogenesis.^{69,73} Imaging properties of DINPs were also observed in the uptake study.

Aim 3: Evaluation of the in vivo therapeutic and imaging effects of EpoR DINPs on PAD mice. ICG DINPs were intramuscularly injected to the gastrocnemius muscle to assess the bio-distribution of DINPs in the body. The detection and therapeutic effectiveness of DINPs in PAD treatment were investigated *in vivo* using an animal model of hind limb ischemia by femoral artery ligation.¹⁴⁰ Blood perfusion and an endurance test were performed to evaluate the therapeutic effects of EpoR DINPs. Deep tissue imaging benefits of DINPs were determined via PA images. MSOT was used for DINPs tracking and hemoglobin saturation. Histology staining was analyzed for EpoR expression, capillary density, and EPCs recruitment.

1.8.3. Innovative aspects

The innovation of this thesis research includes **1)** the use of dual imaging materials (fluorescent/photoacoustic imaging) BPLPATs to formulate DINPs for tracking NPs *in vitro* and post-treatment tracking and detecting the DINPs bio-distribution and therapeutic effects *in vivo*; **2)** the application of gene therapy using EpoR plasmids to facilitate stem cell mobilization and cell survival under hypoxic conditions to form new blood vessels effectively.

Chapter 2

MATERIALS AND METHODS

2.1. Plasmid purification and characterization

2.1.1. Construction of plasmids

pEpoR-M61 vectors were used to investigate the *in vitro* and *in vivo* therapeutic effects of EpoR expression on angiogenesis. **Figure 7** shows the general construction of EpoR plasmids designed from GeneCopoeia, Inc. EpoR genes were inserted on the upstream of the enhanced green

fluorescent protein (eGFP) or mCherry fluorescent protein expressed genes followed by the internal ribosome entry site 2 (IRES2) element on the M61 backbone. Three different plasmids including human EpoR (h.EpoR genes inserted to M61), mouse EpoR (m.EpoR genes inserted to M61) and empty vector (M61 without EpoR genes) were obtained for this thesis research. h.EpoR plasmids encoding human EpoR transmembrane protein were

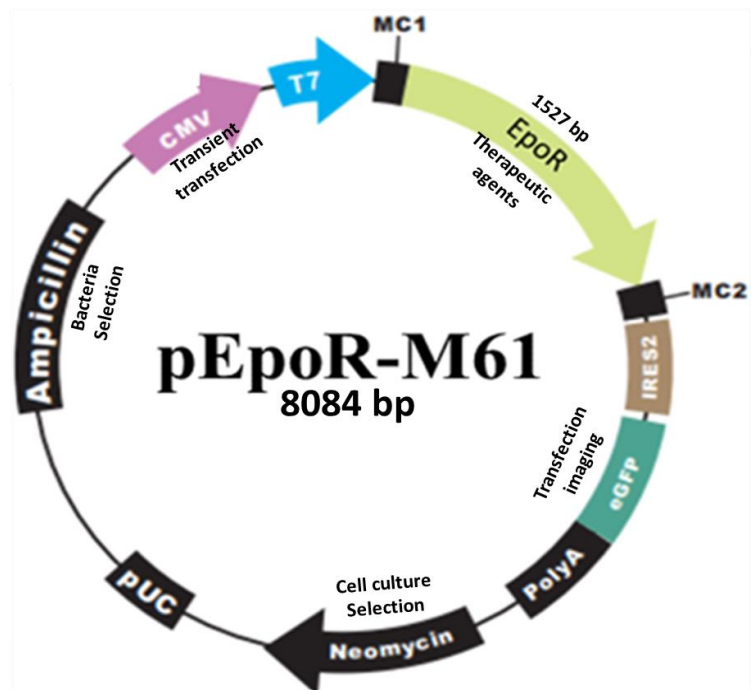


Figure 7. EpoR plasmid map. The EpoR plasmid will express two proteins including GFP or mCherry (not shown) for tracking of transfection and EpoR transmembrane protein to enhance angiogenesis. The IRES2 element is between EpoR and GFP for encoding separately EpoR and GFP protein. The plasmid backbone also contains the other two genes, which help for bacterial culture selection (Ampicillin) and cell culture selection (Neomycin).

used for *in vitro* studies, whereas m.EpoR plasmids that encode mouse EpoR transmembrane protein were applied in mouse PAD models. Empty vectors as well as h.EpoR and m.EpoR express

GFP for tracing transfection in cells/tissues. Especially for nanoparticle transfection studies on EPCs, I used plasmids carrying mCherry fluorescent protein to enhance the fluorescent signals instead of using the GFP plasmids.

2.1.2. Plasmid purification

Escherichia coli (*E. coli*) bacteria transformed with h.EpoR, m.EpoR, or empty vectors/plasmids were purchased from GeneCopoeia. *E. coli* bacteria were grown in the standard Luria Bertani (LB) medium with ampicillin antibiotic (100 mg/l) shaken 175 RPM at 37⁰C for 12-16 hours. Bacteria pellets were harvested by centrifuging at 6000 g for 15 minutes at 4⁰C; then plasmids were purified by using EndoFree Plasmid Giga (Qiagen) following the manufacturer's instructions. The purified plasmids were redissolved in Tris-EDTA (TE) buffer and aliquoted to 200 μ l in 0.2 ml PCR tubes for future usages. The entire plasmid purification process was described in Qiagen EndoFree plasmid purification kit protocols.

2.1.3. Plasmid characterization

Plasmid concentration and purification were measured via Thermo Scientific 2000 1-position Spectrophotometers by using 3 different wavelengths including 280 nm, 260 nm, and 230 nm. Briefly, one drop (1 μ l) of samples was used for measuring absorbance. The blank Tris-EDTA (TE) buffers were used to measure the background before reading plasmid samples for accurate measurement. The software built in the device analyzed the absorbed data to provide the plasmid concentration and ratios of 260 nm/280 nm for assessing purity of plasmids from protein and phenol contamination and 260 nm/230 nm for assessing purity of plasmids from high salt contamination. Plasmid structural integrity was determined by running Agarose Gel

Electrophoresis. The digested and undigested plasmids were mixed with 6x DNA loading buffer to electrophorese at 110 V for 30 minutes and imaged using the BIO-RAD ChemiDoc Touch Imaging System. The digested samples were cut at two sites using BamHI and NotI enzymes to separate the EpoR genes from the M61 backbone.

2.1.4. Plasmid-PEI complex preparation

600 µg of glucose was added to 200 µl plasmid solution (3 µg plasmids/µl TE buffer). The solution of plasmid and glucose was mixed with 1 mg/ml branched Polyethylenimine (bPEI) 10kDa MW (Polysciences) at the plasmid:bPEI ratio 1:3 (w/w) for 1 hour at room temperature under the rotation¹⁴¹. This solution (W1) was used to fabricate DINPs, as described in the next section.

2.2. The formulation and characterization of DINPs

2.2.1. DINP fabrication

The novel biodegradable photoluminescent polymers-aniline tetramers (BPLPATs) synthesized in Dr. Yang's lab at PSU were used to formulate the biodegradable dual-modal imaging nanoparticles (DINPs). DINPs were synthesized using a modified double emulsion technique as previously described.¹⁴²⁻¹⁴⁵ Briefly, the solution W1 of glucose:plasmids:bPEI (1:1:3 w/w ratio) was added drop-wise to 5 ml of the organic phase solution (O) of BPLPAT in acetone (20 mg/ml). The solution was emulsified by sonicating at 10W for 15s. By adding glucose to the aqueous phase (W1), it served as a cryoprotectant and enhanced the aqueous phase (W1) immiscible in the organic phase (O) to form a primary emulsion¹⁴⁴. Then the primary emulsion was added dropwise to 20 ml aqueous phase (W2) of 5% w/v polyvinyl alcohol (PVA) 31kDa and

emulsified using ultra-sonication at 25W for 1 minute. The suspension was evaporated overnight to remove acetone and centrifuged at 15,000 RPM for 15 minutes to collect DINPs (pellets). The supernatant was used to measure the plasmid loading efficiency via an indirect method, while the pellets were washed 1x with deionized (DI) water and resuspended in 2 ml of DI water. The final suspension was aliquoted to 200 μ l in 2 ml eppendorf tubes and kept in a -80°C freezer for 2 days

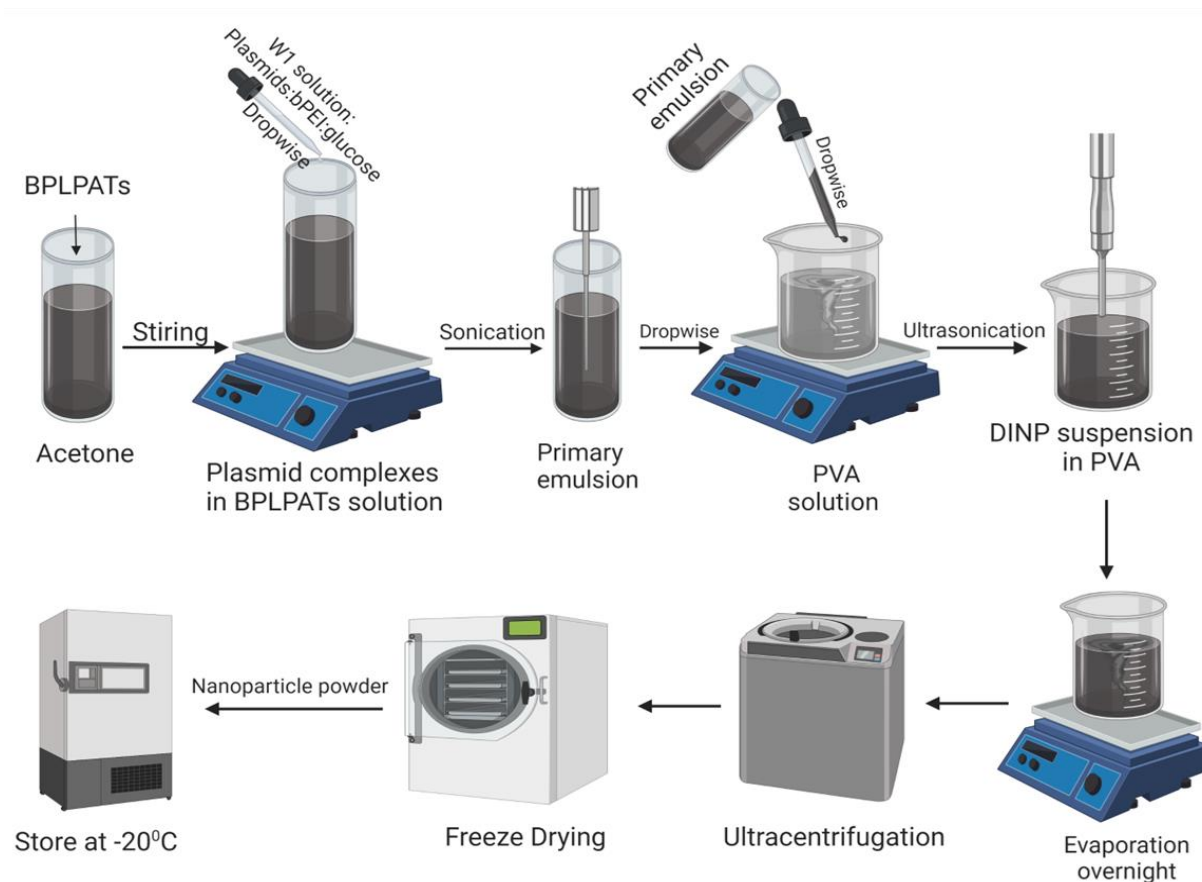


Figure 8. The flow chart of DINP fabrication. DINP fabrication is followed by the modified double emulsion technique. The W1 phase is the plasmid complexes mixed with glucose in TE buffer, which is plasmids:bPEI:glucose solution. The organic (O) phase is a biodegradable photoluminescent polymer-aniline tetramers (BPLPATs) in acetone. The W2 phase is 5% (w/v) polyvinyl alcohol (PVA) 31kDa in water. Briefly, the W1 solution is added in dropwise to the O phase under stirring and sonicated at 10W for 15 seconds to create the primary emulsion. Then this primary emulsion is added to the W2 phase under stirring and ultrasonicated at 25W for 60 seconds (10 seconds off between 30 seconds on). The final emulsion is stirred overnight to evaporate acetone and ultracentrifuge to collect DINPs in pellets. The pellets are washed with DI water and ultracentrifuged a second time to collect the final pellets. The powder form of DINPs is created by resuspending the final pellets in 2 ml of DI water and keeping it in -80°C for 2 days before freeze-drying for 1 day. The powder form of DINPs is stored at -20°C for short-term usage or -80°C for long-term storage. DINPs loaded various agents are formulated when different W1 solutions are used.

before freeze-drying to collect the powder form of DINPs (**Figure 8**). By preparing different W1 solutions, four different DINPs including h.EpoR DINPs, m.EpoR DINPs, empty vector DINPs, and blank DINPs were fabricated for different purposes.

2.2.2. Physical properties of DINPs

Sizes, size distributions, and zeta-potentials of DINPs were measured using NanoBrook 90Plus PALS analyzer (Brookhaven Instruments, Holtsville, NY). Briefly, 20 μ l of DIMP suspension (1 mg DINPs/ml KNO₃ 10mM) was added to 3 ml KNO₃ 10mM in the BI-SCP cuvette to measure the sizes of DINPs. The size distributions of DINPs were calculated by using the population standard deviation formula (Equation 1). The zeta potential was evaluated by using the surface zeta potential (SZP) electrode. The probe was dipped in the BI-SCP cuvette containing 10 μ l DINPs samples in 1.5 ml KCl 1mM to read the zeta potential of DINPs. The DIMP morphology was observed under the transmission electron microscope (TEM) (Hitachi, H-9500 HRTEM).

$$SD = \sqrt{\frac{\sum |x - \bar{x}|^2}{n}} \quad (1)$$

2.2.3. Plasmid loading of DINPs

To study the loading efficiency, the amount of plasmids in the supernatant during DINPs fabrication (not loaded in DINPs) was measured by using PicoGreen DNA assays (Thermofisher, Waltham, MA) as described in the literature¹⁴⁶. The efficiency was determined as the loaded amount against the total amount used for the DIMP fabrication (Equation 2).

$$Plasmid\ loading\ efficiency\ ((\%)) = \frac{Loaded\ plasmids\ (mg)}{Initial\ plasmids\ (mg)} \times 100\% \quad (2)$$

2.2.4. Plasmid release profiles of DINPs

The technique was used to plot the release profile of plasmids from DINPs as described previously¹⁴⁷. Briefly, 20 mg plasmid loaded DINPs were resuspended in 20 ml 1x DNase and RNase-free phosphate buffered saline (PBS) pH 7.40 and aliquoted 5 ml to 15 ml conical centrifuge tubes. These tubes were continuously shaken at 37°C. At designated times (0 hours, 2 hours, 6 hours, 18 hours, 1 day, 2 days, 3 days, 7 days, 14 days, 21 days, and 1 month), 1 ml of each sample was collected and centrifuged at 16,000G for 20 minutes to collect the supernatant for processing plasmid precipitation, while the pellets were resuspended in fresh PBS and put back in the tubes. Plasmids in the supernatant were precipitated in ethanol with 10% (v/v) of 3M sodium acetate pH 5.2 mixed at the supernatant: ethanol (1:2) ratio. The solution was kept in -80°C overnight to enhance plasmid precipitation. The precipitated solution is centrifuged at 16,000G for 15 minutes at 4°C and washed 2x with 70% cold ethanol. The plasmid pellet was air-dried and resuspended in TE buffer and quantified by PicoGreen assays to quantify the amount of released plasmids for each sample (time point). The accumulated released plasmids were calculated and plotted over an incubated time range.

2.2.5. DINPs stability

DINP stability was determined in reference to size changes in various fluids including PBS, media containing serum, and human simulated body fluid (SBF) over 72 hours to reveal any particle aggregation as previously described⁹⁴. In brief, DINPs were incubated in different fluids, and changes in their average diameters were measured over the time range. At each designated time-point, sizes of DINPs were measured using NanoBrook 90Plus PALS analyzer (Brookhaven Instruments, Holtsville, NY).

2.2.6. Evaluation of intrinsic fluorescent properties of fabricated DINPs

Fabricated blank DINPs were resuspended in DI water at a concentration of 1 mg/ml; then the stock DINPs suspension was diluted 10 µg/ml for imaging purposes. 100 µl of DNP suspension was pipetted on the coverslip and evaporated for 1 hour. The dried DINPs were added with one drop of aqueous mounting media before taking their images in various fluorescent channels including DAPI (ex385/em450), FITC (ex470/em525), and CY5 (ex640/em690) channels.

2.3. Determination of the *in vitro* effectiveness of EpoR DINPs

2.3.1. Cell culture

Human primary skeletal muscle microvascular endothelial cells (HMMECs) were obtained from Applied Biological Materials (ABM Inc.) and cultured in completed M199 media containing 20% fetal bovine serum (FBS) (Gelifescience) and 1% Penstrep (Life technologies) at 37⁰C and 5% CO₂. HMMEC culture media were renewed every two days. Umbilical cord-derived endothelial outgrowth cells (EOCs) were purchased from AngioBiocore (Indianapolis, IN). EOCs are a population of endothelial progenitor cells (EPCs), so they were considered as EPCs through the project. EPCs were cultured in endothelial cell growth medium 2 completed with supplement mix C-39216 (Promocell, Germany) and replenished with 10% FBS and 1% Mycozap (Lonza, Houston, TX). In this project, HMMECs were mainly used to test the *in vitro* therapeutic effects of nanoparticles including protection studies and tube formation studies. Since HMMECs took time to grow and were sensitive, EPCs were selected for all the other studies of this project.

2.3.2. GFP plasmid expression

Purified plasmids including empty vector, h.EpoR, and m.EpoR were used to transfect

LentiX cells to verify the quality of collected plasmids for DINPs fabrication. The cell transfection studies were performed by using lipofectamine 3000 kits (ThermoFisher, Waltham, MA) as described in the transfection protocol from the company. Transfected cells were tracked under the fluorescent microscope (ECHO revolve microscope, RVL2-K model, San Diego, CA) in FITC channels for various time-points.

2.3.3. Evaluation of Dinp imaging properties *in vitro* study

EPCs were seeded on the coverslip at the confluent density overnight before being incubated with blank Dinp suspensions at various concentrations (0, 250, 500, and 1000 $\mu\text{g/ml}$) for 2 hours. The treated EPCs were washed 3 times with PBS 1x to remove excess DINPs. Cells were fixed with 4% formaldehyde solution for 5 minutes. Nuclei were stained with one drop of nucBlue for counter staining for fluorescent microscope imaging. The samples were observed using our Cytoviva microscope and ECHO microscope to track the cellular uptake of DINPs by EPCs.

2.3.4. *In vitro* therapeutic effects of EpoR DINPs on HMMECs

Pre-transfected HMMECs were used for the *in vitro* protection and tube formation study as described previously¹⁴⁸. Briefly, HMMECs were pre-transfected with various DINPs one day before experiments. In the HMMEC protection study from ROS species, pre-transfected HMMECs were seeded in 96-well plates overnight at the confluent density. The cells were then washed with PBS 1x pH 7.40 and replenished with 200 μM H_2O_2 in low serum M199 media (1% FBS) for the 1-day study. Cells treated with VEGF (5 ng/ml) served as the positive control while non-transfected HMMECs exposed to H_2O_2 served as the negative control. At 24 hours, the cell culture

supernatant was removed and washed once with PBS 1x before cell viability was assessed by using MTS assays following the manufacturer's instruction (CellTiter 96 AQueous One Solution Cell Proliferation Assay, Promega, and Madison, WI). In the tube formation study, pre-transfected HMMECs were seeded on reduced growth factor Matrigel® matrix basement membrane (Corning, Glendale, AR) in 48 well plates with low serum M199. Treated cells were kept in the hypoxic chamber (<1% oxygen and 5% carbon dioxide in nitrogen) at 37⁰C for 12 hours. HMMECs treated with VEGF (5 ng/ml) and non-transfected cells were used for the positive and negative controls, respectively. Phase contrast images were taken at 12 hours to analyze the tube formation efficiency by using NIH ImageJ software.

2.3.5. Cytocompatibility of DINPs

Cell toxicity and hemocompatibility of DINPs were investigated by incubating vascular smooth muscle cells (SMCs) and heparin-anticoagulated human blood with DINPs at various concentrations (0, 50, 100, 200, 500, and 1000 µg/ml), respectively. On cell toxicity, the cell viability over a time range (24 and 48 hours) was studied via MTS assays following the manufacturer's instructions. Hemocompatibility of DINPs was evaluated by detecting the number of adherent platelets via lactate dehydrogenase (LDH) assays (Takara Bio INC.), assessing platelet activation by flow cytometry as described previously^{123,124,128,149}, and determining whole blood clotting kinetics^{123,150}. Poly(octamethylene citrate) (POC) was used as a control since it has been demonstrated to be well-suited for vascular graft coating applications partly because of its excellent hemocompatibility^{131,150,151}.

2.4. The evaluation of *in vivo* therapeutic and imaging effects of EpoR DINPs

2.4.1. Creation of PAD mice

A mouse model of unilateral hindlimb ischemia as previously described¹⁵² was used in this thesis research. Aging is an important factor responsible for impaired angiogenesis in PADs, and blood perfusion of ischemic hindlimbs in old mice was significantly decreased compared to young mice after surgery¹⁵³. Briefly, 6–8 month-old retired Balb/c mice (age relevant to the old age of humans)¹⁵³⁻¹⁵⁶ of both sexes were purchased from Charles River Laboratory and housed at the UTA animal facility center at least one week before experiments. The left femoral artery and its branches were used for the ligation to generate hindlimb ischemia models based on the procedures described by Padgett *et al*¹⁵⁷. The intact right hindlimb was used for a control non-ischemic limb.

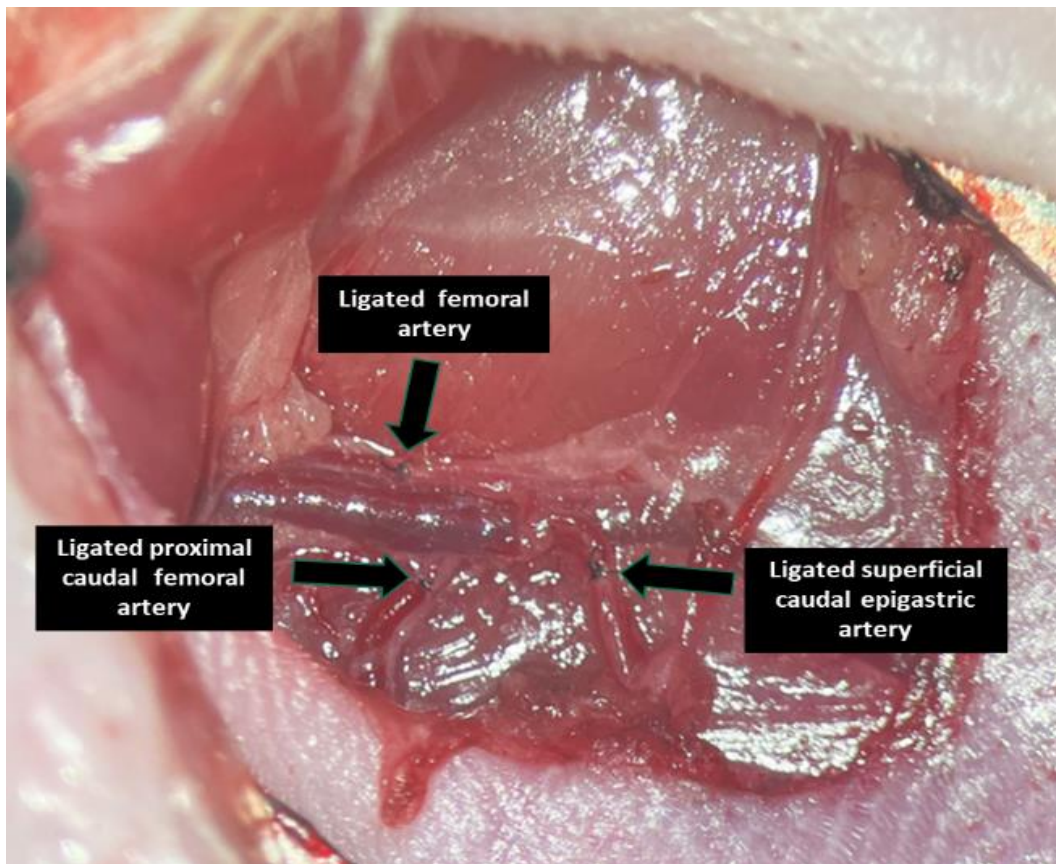


Figure 9. The left mouse PAD models. Balb/c mice at 6–8 months old were used to create the model. The left femoral artery and its branches including the proximal caudal femoral and superficial caudal epigastric arteries were exposed and isolated from the nerve before ligating with non-absorbable sutures 10-0. Three black arrows represent the ligation knots of arteries listed above. The right femoral artery was kept intact and served as the control of the study.

Briefly, mice were prepared for the ligated surgery followed IACUC standard operative procedures (SOPs) by subcutaneously injecting Buprenorphine SR 1.0 mg/kg and anesthetizing with isoflurane 2% in oxygen inhalation. A shaved incision of 1 cm was created on the front of the left thigh. The bundle of femoral and vessels were exposed. The femoral artery and its branches were carefully separated and ligated by using unabsorbable sutures 10-0 (**Figure 9**), and then the incisions were closed using absorbable sutures 7-0. Ligated mice were measured using blood perfusion to verify the ischemic tissues before returning to recovery cages. These mice were randomly selected from different treatment and control groups in any animal study. All *in vivo* experiments followed the animal protocol approved by the institutional animal care and use committee (IACUC) at the University of Texas at Arlington.

2.4.2. Imaging assessment of PAD mice

Initially, PAD mice were examined to verify the model and compare imaging modalities. In each case, the legs were shaved and thoroughly depilated to ensure optimal acoustic and optical contact. Mice were anesthetized and maintained with isoflurane (~2%) in air or oxygen with a nose cone (snorkel). Blood perfusions were measured by using laser speckle contrast imaging (LSCI) (PeriCam, PSI NR system, Perimed, Las Vegas, NV). The evaluation of oxy- and deoxy-hemoglobin in ischemic tissues was determined via multispectral optoacoustic tomography (MSOT) InVision 256-TF small animal imaging system (iThera). MSOT provides high-resolution images at depths up to several centimeters, revealing vascular oxygen saturation throughout the leg muscles of animals¹⁵⁸⁻¹⁷² as well as visualizing DINPs. More importantly, MSOT was used to verify that observations would match with the traditional technologies. Briefly, the animal holder was placed in the imaging chamber, and multiwavelengths (680, 730, 760, 798, 874, 930, 972 nm)

were chosen to exploit the spectral characteristics of oxy- and deoxy-hemoglobin to image ischemic and non-ischemic thighs. I evaluated differential perfusion between control and ischemic legs using LCSI and MSOT of the PAD models. 5 mg of blank DINPs was injected into the ischemic gastrocnemius muscle to verify the ability to assess their retention after administration.

2.4.3. Bio-distribution study of ICG DINPs

About 2 mg of ICG DINPs were resuspended in 50 μ l saline and intramuscularly injected along the ischemic gastrocnemius muscle on PAD mice for the bio-distribution study. Saline served as a control group. Bio-distribution of ICG DINPs was assessed by an *in vivo* fluorescent imaging system (Kodak *in vivo* Fx Pro system) via whole animal *in vivo* imaging and *ex vivo* organ imaging. *In vivo* optical imaging was used to observe the fluorescent intensity at 3 different timepoints (0, 4, and 24 hours). At 4 and 24 hour- timepoints, 4 mice/group were sacrificed to collect various organs including liver, kidneys, spleen, and gastrocnemius muscles (injured and healthy legs) for *ex vivo* imaging. The tissues were further homogenized by Precellys Evolution Homogenizers (Bertin Instruments), and fluorescent intensities of lysed samples were determined via a spectrophotometer (Tecan Infinite M200 Spectrophotometer). Quantification of DIMP distribution was determined as the amount of DINPs per gram of tissue.

2.4.4. Investigation of the *in vivo* effectiveness of DINPs on PAD mice

Three different doses of EpoR DINPs (1, 2, and 4 mg DINPs/mouse) were used to find the optimal dose of EpoR DINPs that induces maximum therapeutic effects while causing the least side-effects. Therapeutic effects were evaluated by blood perfusion and physical functionality. The optimized dose was used for further *in vivo* testing. Animals were divided into five groups: (1)

sham (saline as a negative control), (2) VEGF (positive control), (3) free EpoR plasmid (equivalent amount of EpoR plasmids in DINPs), (4) EpoR DINPs (the optimal dose found from the pilot study), and (5) empty vector DINPs (the same dose used for EpoR DINPs). The un-ligated (non-ischemic) legs of the same animal were used to calculate blood perfusion ratio (ischemic/non-ischemic leg ratio). PAD mice on the 2nd day were intramuscularly injected with 50 μ l volume of the corresponding solution as described above. Treated animals were weekly imaged using LCSII and evaluated by an endurance test to assess limb recovery as described¹⁷³. Briefly, the treadmill device (Panlab Touchscreen Treadmill, Harvard Apparatus, Holliston, MA) was started at a low speed (6 m/min), then the velocity was raised 2 m/min every 2 minutes for 12 minutes and kept constant at 18 m/min thereafter. Exhaustion was defined as the mouse spending more than 5 seconds on the shock grid without reengaging the treadmill. Animals were sacrificed at 7 and 21 days after treatment for histology analysis^{95,128,158}.

2.4.5. Evaluation of histological staining

Gastrocnemius muscles were collected, sectioned, stained, and analyzed by H&E and immunohistology staining. Cross-sections of muscle embedded in paraffin were cut in 5 μ m thickness and put on the glass slides (3-5 sections/slide). H&E staining was performed to analyze the muscular structure and tissue inflammation. All immunohistology staining was performed by fluorescent labeled secondary antibodies, as detailed in Abcam immunostaining protocols. Briefly, sample antigens were retrieved using different methods depending on specific markers including CD31, CD34, EpoR, Ki67, desmin, and smooth muscle cells (α -SMA). Then a diluted primary antibody was incubated at 4^oC overnight in moisture. The samples were washed with PBS 2x for 5 minutes before incubating diluted FITC labeled secondary antibody for 1 hour at room

temperature. The nuclei were counter-stained to DAPI before adding mounting media. The slides were covered with coverslips and sealed with nail polish. Fluorescent images were taken under a fluorescent ECHO Revolve microscope. To assess angiogenesis, primary anti-CD31+ antibodies were used to quantify ECs. The capillary density (capillaries/mm²) labeled with CD31 was determined as the number of capillaries per total area (square millimeter). To determine the potential of EpoR DINPs on EpoR expression and EPC recruitment, tissue sections were immunostained with primary anti-EpoR antibodies and anti-CD34 antibodies, respectively. Similarly, FITC labeled secondary antibody was incubated on the treated samples for one hour before taking fluorescent images. To evaluate neovascularization, tissue sections were co-stained for the presence of endothelial cells (CD31), smooth muscle cells (α -SMA), pericytes (desmin), and nuclei DAPI counterstain. Neovascularization was quantified by measuring the density of vessels per unit area and maturation of blood vessels containing positive stains of all ECs, SMCs, and pericytes.

2.4.6. Toxicity assessment of DINPs

Potential side effects were monitored from biweekly body weight for up to 4 weeks. To determine potential cardiotoxicity, I examined biomarkers such as troponins. Lung toxicity was detected by the tumor necrosis factor; kidney toxicity via serum creatinine, blood urea nitrogen, and kidney injury molecule-1, and liver toxicity using alanine aminotransferase and LDH.

Chapter 3

RESULTS

3.1. DINP fabrication and characterization

3.1.1. Plasmid purification and characterization

Three different plasmids were successfully purified by EndoFree Qiagen kits. I collected 8.8 mg mEpoR, 6.2 mg hEpoR, and 5.5 mg empty vector per kit. Their purifications were described as the purity of the collected plasmids in **Table 1**.

Table 1. Plasmid characterization

	Empty Vector	h.EpoR	m.EpoR
Yield	5.5 mg	6.2 mg	8.8 mg
260 nm/280 nm ratio	1.92	1.93	1.91
260 nm/230 nm ratio	2.27	2.26	2.26

Gel electrophoresis showed the wide bands of the supercoil (undigested) h.EpoR plasmids and

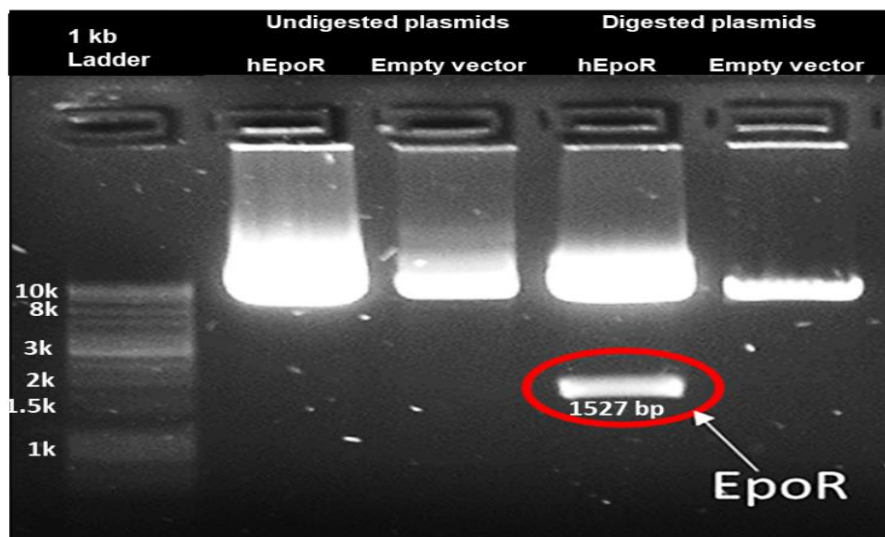


Figure 10. Gel electrophoresis of undigested and digested plasmids. The results showed the h.EpoR band was observed between 2 k and 1.5 k bands after digestion, which is proper for the size of h.EpoR genes (1527 base pairs). The backbone band was the same level as the empty vector.

empty vector. The digested h.EpoR plasmids separated two bands on the gel including the backbone (larger) band at the same level with the empty vector and the h.EpoR genes

(shorter) band sized close to 1.5k base pairs (**Figure 10**).

3.1.2. DINPs fabrication and characterization

I have successfully fabricated several types of DINPs loaded with different plasmids or dyes using modified standard double emulsification methods¹⁴²⁻¹⁴⁵ and used them for our *in vitro* and *in vivo* studies. As shown in **Figure 11**, I synthesized different types of DINPs: i) blank DINPs, ii)

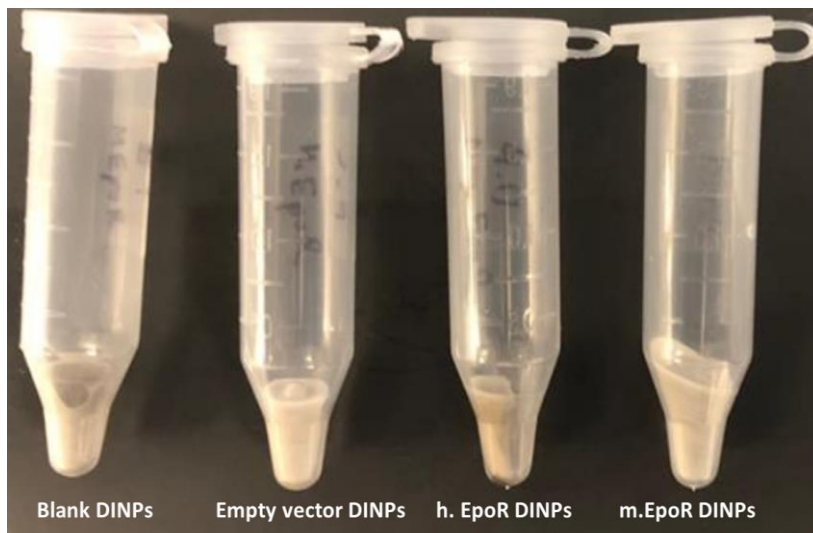


Figure 11. The powder forms of various fabricated DINPs. Various DINPs were fabricated including blank DINPs, empty vector DINPs, h.EpoR DINPs, and m.EpoR DINPs. DNP powder had light gray color in soft fluffy forms after freeze-drying. They were stored in a dry condition and covered by aluminum foil to protect from light.

empty vector DINPs, iii) h.EpoR DINPs (for *in vitro* studies using mammalian cells) and iv) m.EpoR DINPs and ICG DINPs (for therapeutic and biodistribution animal studies). DNP sizes, surface charges, and plasmid loading efficiencies were determined. The average sizes of DINPs ranged from 283 to 378 nm (**Table 2**). Our method effectively encapsulated various plasmids

Table 2. Characterization of DINPs

Types of DINPs	Sizes (nm)	Polydispersity (PDI)	Zeta Potential (mV)
Blank DINPs	378 ± 130	0.213	-35.98 ± 8.49
Empty vector DINPs	331 ± 126	0.184	-33.51 ± 2.08
h.EpoR DINPs	283 ± 143	0.138	-28.82 ± 4.09
m.EpoR DINPs	333 ± 144	0.146	-39.14 ± 1.82

inside DINPs (average 80% loading efficiency).

3.1.3. DINPs imaging properties

TEM images of EpoR DINPs showed spherical shapes around 200 nm diameters (**Figure 12**). The diameters were different due to different methods used to measure the diameters of NPs. The intrinsic fluorescent properties of blank DINPs were observed under microscopes by using different fluorescent channels including DAPI (excitation wavelength 385 nm/emission wavelength 450 nm), FITC (excitation wavelength 470

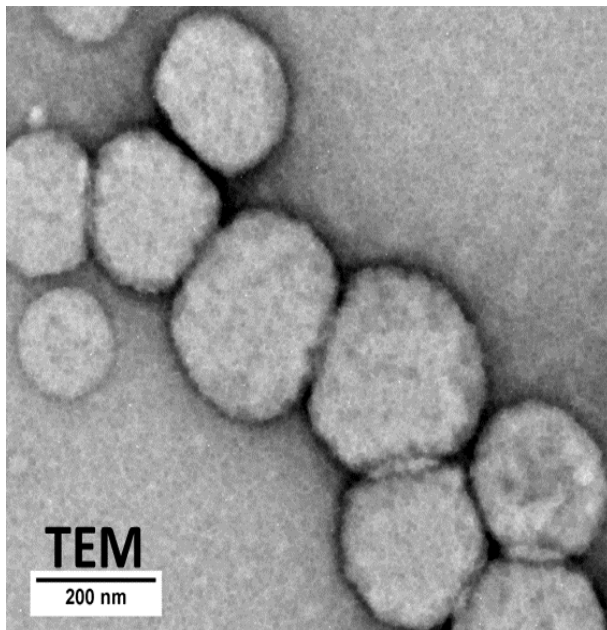


Figure 12. TEM images of EpoR DINPs. The EpoR DINPs suspension 1 mg/ml was prepared to add on the TEM grid for taking DNP images. DINPs were visualized in uniformly spherical shapes ranging from 150 nm-200 nm.

nm/emission wavelength 525 nm), and CY5 (excitation wavelength 640 nm/emission wavelength 690 nm) channels (**Figure 13**).

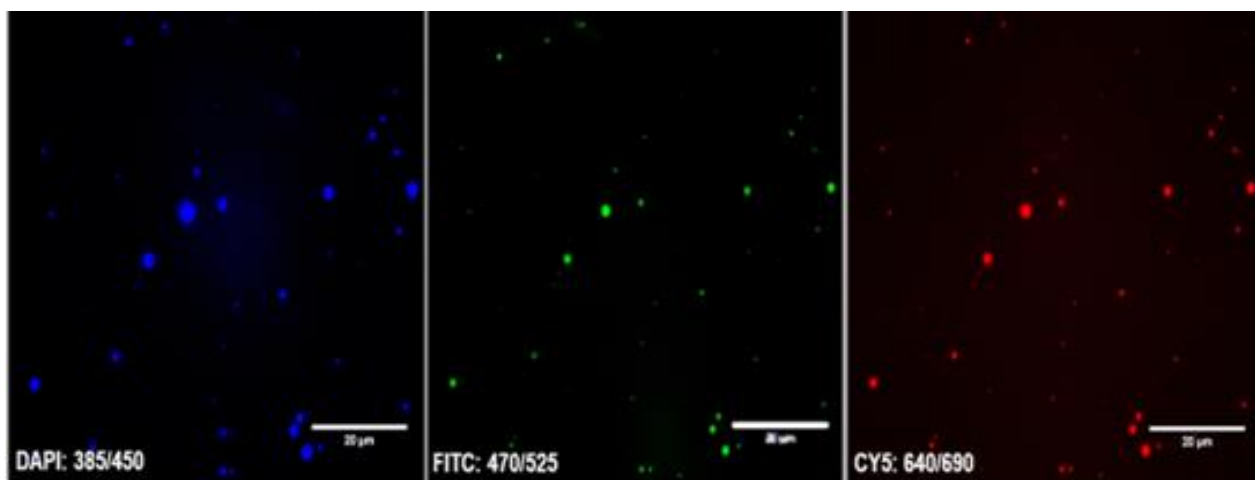


Figure 13. The intrinsic fluorescent properties of DINPs. The blank DINPs were resuspended in DI water at 10 μg/ml concentration. 100 μl DINPs suspension was dropped on the glass slides and let air-dry before adding one drop of the fluorescent mounting media. The sample was covered by a coverslip and fluorescent images taken in DAPI, FITC and CY5 channels. The results showed that fluorescent images of blank DINPs were visualized in different channels. The scale bar is 25 μm.

3.1.4. Drug release profiles

EpoR DINPs at a concentration of 1 mg/ml were used for the plasmid release study in PBS 1x pH 7.40 for various time points. Then plasmids released were precipitated for measuring the concentration. The results showed the biphasic release curve of EpoR DINPs was determined with the burst release phase (11% of EpoR released) for the first 12 hours followed by the sustained release phase (**Figure 14**).

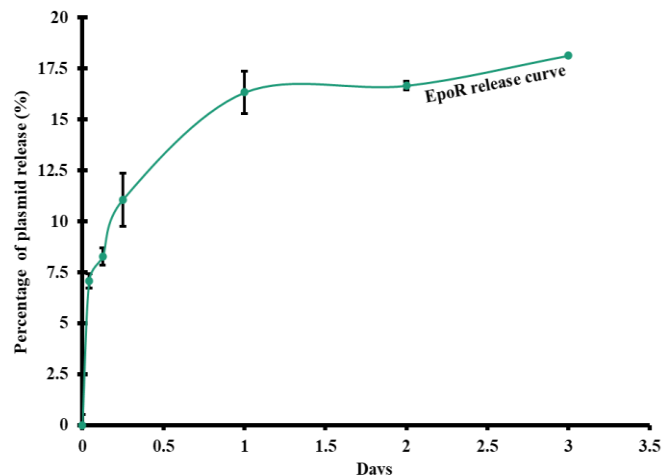


Figure 14. The release profile of EpoR DINPs. The kinetic of EpoR released from DINPs in PBS solution at 37°C. The biphasic release curve of EpoR DINPs was seen including burst released phase with 11% EpoR in the first 12 hours and the sustained released phase up to 17% at day 3. Data presented as Mean±SEM.

3.1.5. DIMP stability

The stability of DINPs in 10% FBS, saline, stimulated body fluid, and DI water over time (72 hours) was examined. The results showed that the particle sizes of DINPs changed similarly to these of PLGA NPs throughout the incubation time (**Figure 15**). There were no signs of aggregation during the study although the sizes were slightly increased or decreased between timepoints; however, they are not significant differences.

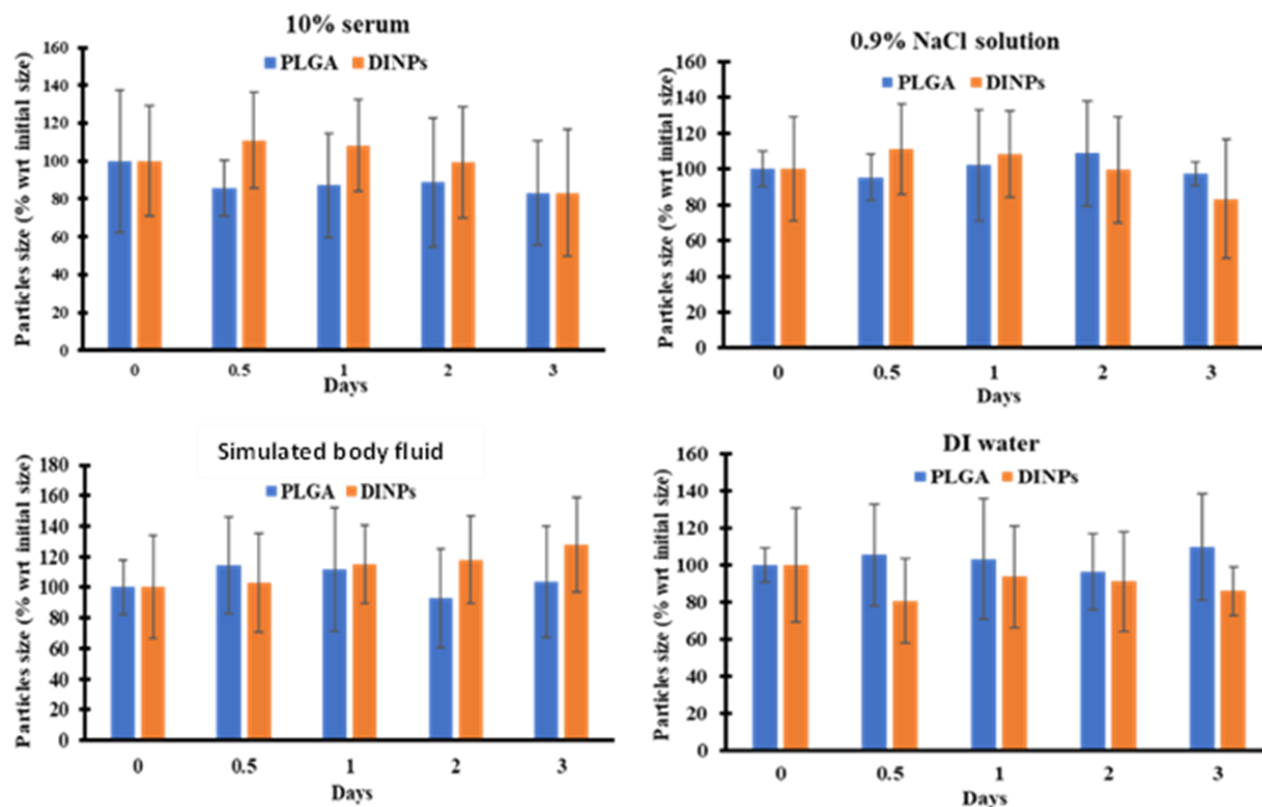


Figure 15. Size stability of DINPs. 1 mg/ml DINPs were prepared in various solvents including 10% serum, saline (0.9% NaCl), simulated body fluid, and DI water. Their sizes were measured over 72 hours for size stability study. The results showed there were no significantly different sizes (no particle aggregates) between DINPs and PLGA NPs at various timepoints (0, 0.5, 1, 2, and 3 days).

3.2. In vitro studies of EpoR DINPs

3.2.1. GFP expression

LentiX cells were used to transfect with free plasmids to confirm functions, expression of GFP. The results showed empty vectors, h.EpoR, and m.EpoR plasmids were able to transfect LentiX cells to express GFP signals under the fluorescent microscope on the 1st and 3rd days (**Figure 16**). GFP intensity as well as the numbers of transfected cells was low on day 1 and increased on day 3. The transfection efficiency was higher with the empty vector compared to

EpoR plasmids, whereas a similar transfection efficiency was seen between m.EpoR and h.EpoR.

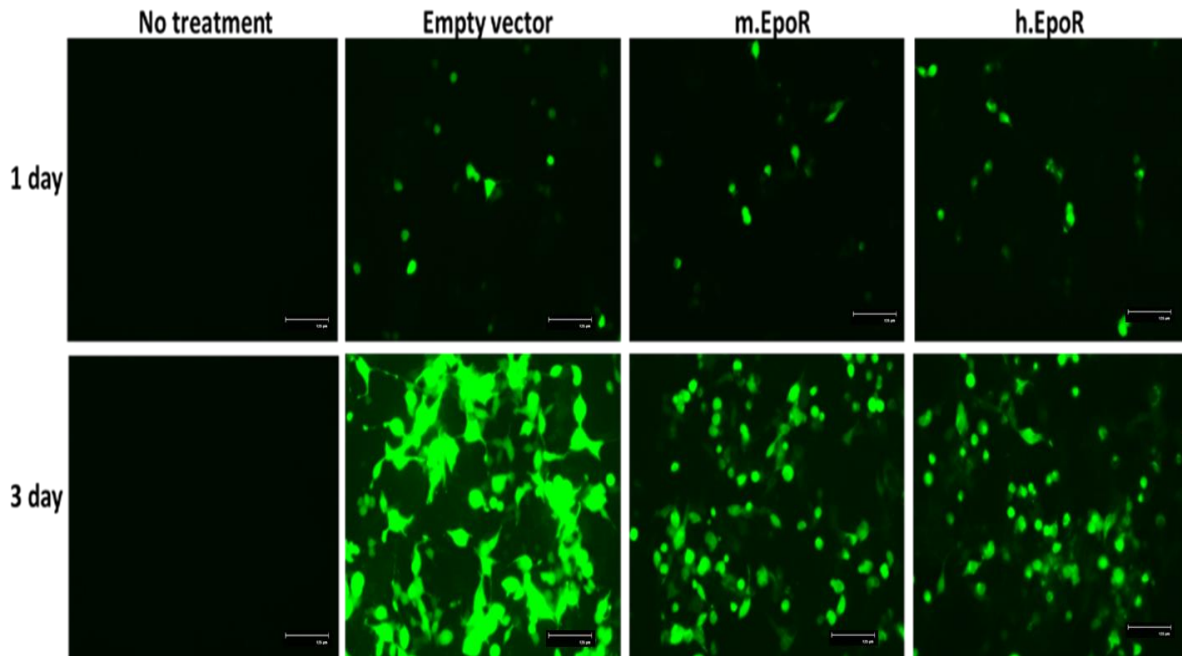


Figure 16. Transfection study of free plasmids on LentiX cells. LentiX cells (500,000 cells/well) were seeded on 6-well-plates overnight in 10% FBS DMEM. Purified plasmids (5 μ g) with lipofectamine 3000 were added and incubated for 2 hours in 1% FBS in DMEM for gene transfection studies. Then Lenti-X cells were supplemented with 10% FBS DMEM. GFP expression protein was observed under fluorescent imaging system (20X) over time (1 day and 3 days). The results showed cell transfection started at day 1 and increased at day 3. The empty vector showed high fluorescent intensity compared to the other plasmids at day 3. The scale bar is 125 μ m.

3.2.2. EpoR expression on EPCs

The mCherry plasmids were used for this experiment and DINP transfection study on EPCs to improve the fluorescent intensity for monitoring transfection efficiency easily. The confirmation of EpoR expression was performed to verify EpoR plasmid encoding EpoR transmembrane protein on the surface of transfected EPCs. PEI polymers were used to enhance transfection efficiency on EPCs while empty vectors served as the negative control of EpoR expression. Cy5 tagged EpoR antibodies were used to stain transfected cells on the first day to determine the EpoR expressed on the surface of EPCs. The results showed that the PEI:plasmid complexes were able to transfect

EPCs on the first day. The empty vectors only expressed mCherry fluorescent protein while EpoR plasmids showed the colocalization of mCherry and Cy5 fluorescent signals (**Figure 17**).

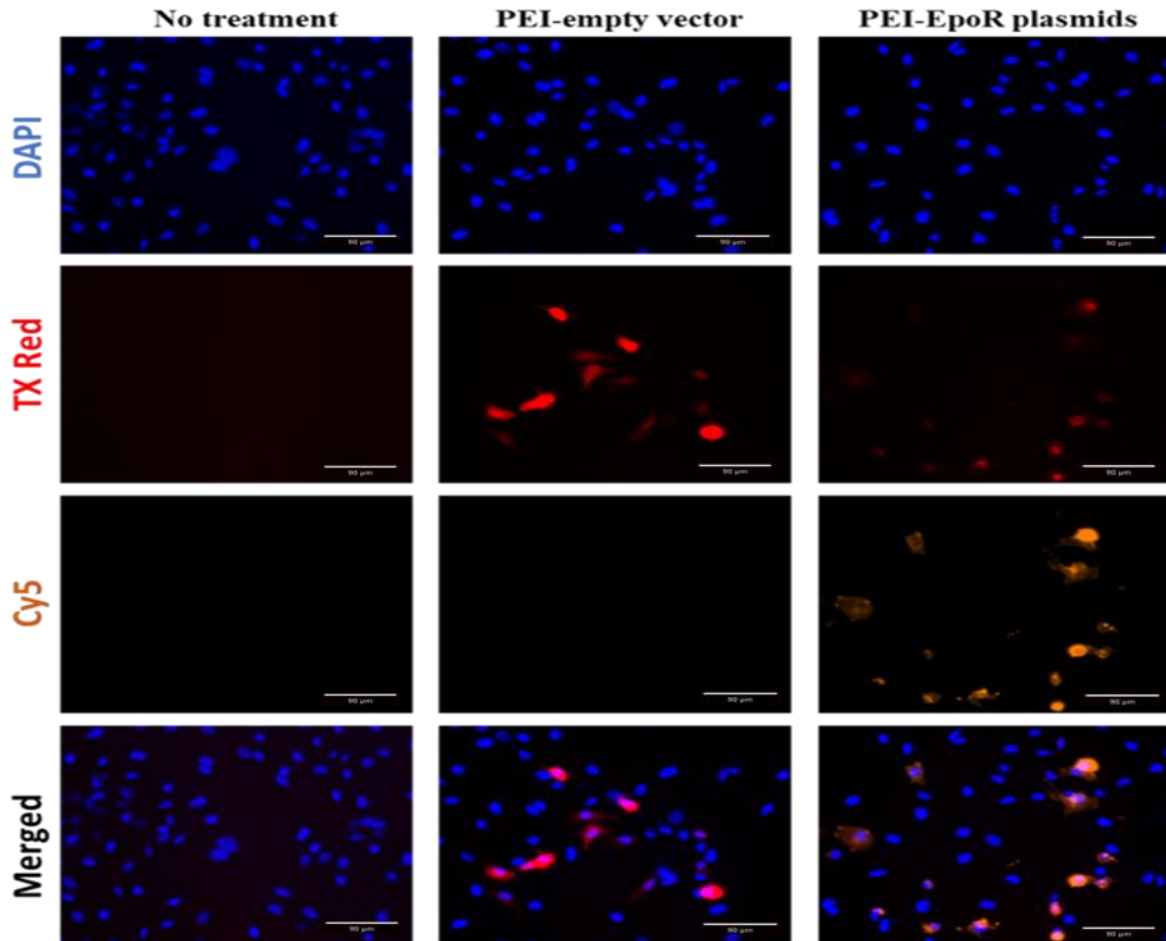


Figure 17. *Transfection study of PEI: plasmids complexes on EPCs for one day. EPCs (50,000 cells/well) are seeded on a 48-well plate overnight. 8 µg plasmids/mg with 1:3 (w/w) PEI:plasmids were added to EPCs and incubated for 2 hours. Empty vectors were used for the negative control of EpoR expression. DAPI was stained for nuclei. TX red was mCherry fluorescent protein expressed from empty vectors and EpoR plasmids while Cy5 was only labeled for EpoR transmembrane protein expression on EPCs. Fluorescence images (20X) were taken using Echo Revolve microscope. Images were then processed using ImageJ for brightness and contrast adjustment. The results showed empty vectors only expressed mCherry fluorescent protein while EpoR plasmids showed the colocalization mCherry and Cy5 fluorescent signals. The scale bar is 90 µm.*

3.2.3. EpoR DINPs transfection study on EPCs

To verify the transfection capacity of EpoR DINPs on EPCs, the dose-dependent study of EpoR DINPs was performed to find the optimal concentration for transfection. Three different

doses of EpoR DINPs including 50 $\mu\text{g/ml}$, 75 $\mu\text{g/ml}$, and 100 $\mu\text{g/ml}$ were examined on EPCs for 2 days (**Figure 18**). Blank DINPs were used at the highest concentration 100 $\mu\text{g/ml}$ to subtract the intrinsic fluorescent properties of DINPs. The results showed that EpoR DINPs at 75 $\mu\text{g/ml}$ showed highest mCherry fluorescent intensities compared to that of the other group. Its fluorescent intensity also increased on the second day of the transfection. EpoR DINPs at 50 $\mu\text{g/ml}$ showed

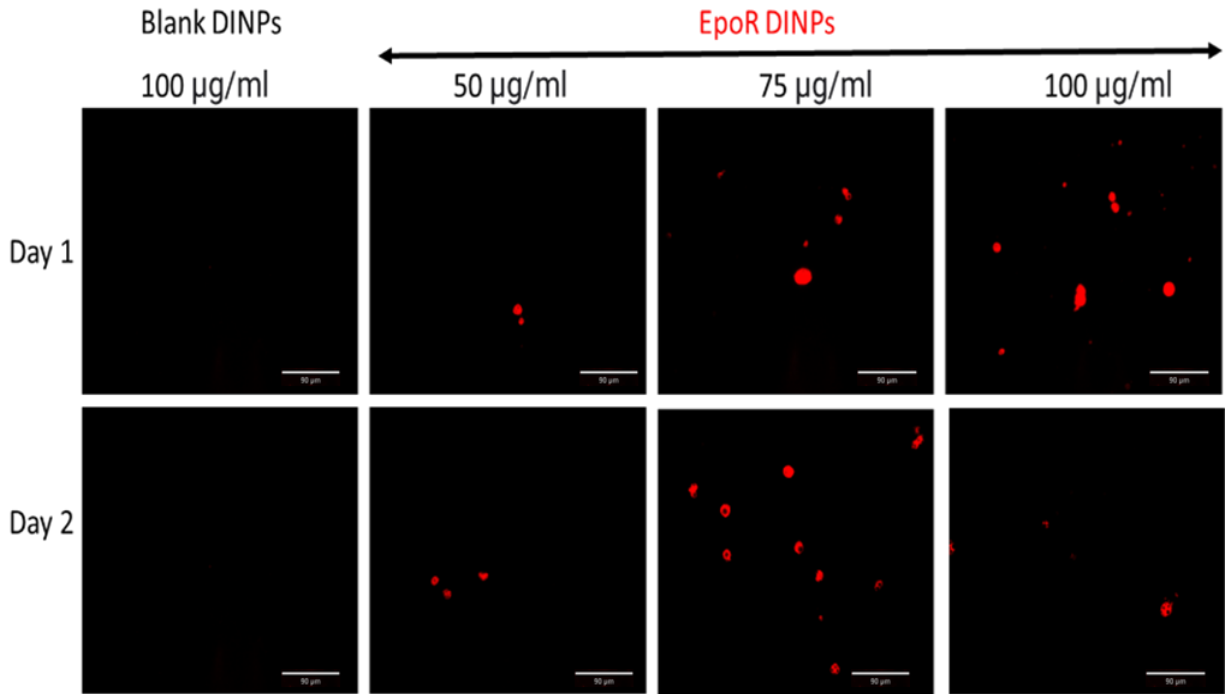


Figure 18. The dose-dependent study of EpoR DINPs on EPCs for two days. EPCs (17,000 cells/well) were seeded on a 96-well-plate overnight in 10% FBS completed media. EPCs were put into quiescent state for 2 hours in incomplete media and incubated to EpoR DINPs (in 1% FBS media) at various concentrations (50, 75, and 100 $\mu\text{g/ml}$) for 2 hours. Then EPCs were supplemented with 5% FBS media. Blank DINPs were used for the negative control group. Treated cells were washed with 1x PBS and observed for mCherry fluorescent protein expression for 1- and 2-days using Echo Revolve fluorescent microscope (20X). Images were then processed using ImageJ for brightness and contrast adjustment. The results showed that EpoR DINPs at 75 $\mu\text{g/ml}$ showed highest mCherry fluorescent intensities compared to that of the other groups. Its fluorescent intensity also increased in the second day of the transfection. EpoR DINPs at 50 $\mu\text{g/ml}$ showed less transfection on both days while 100 $\mu\text{g/ml}$ of EpoR DINPs showed less signals on the 2nd day compared to the 1st day. There were no fluorescent signals observed on the blank DNP group. The scale bar is 90 μm .

less transfection on both days, whereas 100 $\mu\text{g/ml}$ of EpoR DINPs showed less signals on the 2nd day compared to the 1st day. There were no fluorescent signals observed in the blank DNP group.

3.2.4. DINPs uptake study

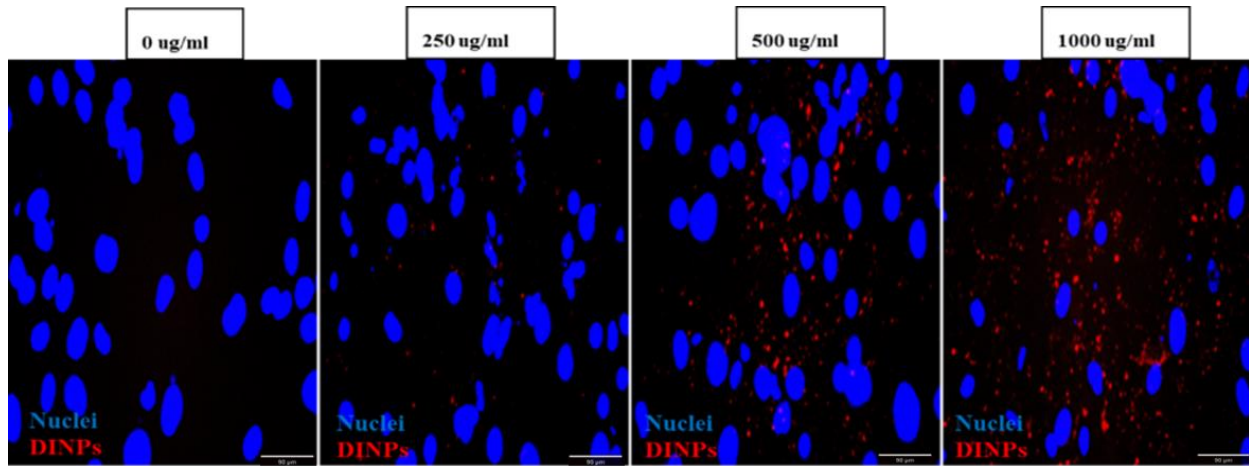


Figure 19. The uptake study of **DINPs** on EPCs. EPCs (25,000 cells/well) were seeded on collagen coated coverslips (22x22 mm) overnight. Cells were put into a quiescent state for 2 hours in incomplete media before being incubated another 2 hours in different concentrations of DINPs (0, 250, 500, and 1000 µg/ml). After 2 hours, EC nuclei were stained with DAPI, then fluorescent images were taken to trace DINPs (Cy5) inside ECs using Echo Revolve fluorescent microscope. Images were then processed using ImageJ software for brightness and contrast adjustment. The results showed EPC uptake was increased when the concentration of DINPs was higher. There was no fluorescent signal observed at 0 µg/ml DNP concentration.

Cy5 fluorescent channels were used to trace DINPs while DAPI fluorescent channels represented EC nuclei. **Figure 19** shows representative fluorescent images of **DINPs** (red) were uptaken to the EPCs at various concentrations of DINPs (0, 250, 500, and 1000 µg/ml in low serum media) after 2 hours incubation. No DINPs signals were observed in ECs at 0 µg/ml concentration which served as the negative control for the study. Cy5

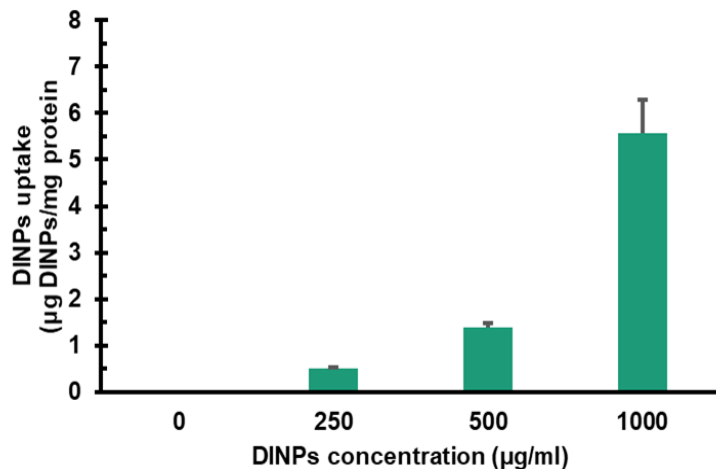


Figure 20. The quantitative analysis of **DINPs** uptake on EPCs. Cells after incubating with DINPs at different concentrations (0, 250, 500, and 1000 µg/ml) were lysed with 1% Triton 100X for 30 minutes to measure fluorescent intensity of DINPs and total protein concentration. The data were analyzed in µg DINPs/mg cell protein. The results showed that EPCs absorbed 0.5 µg, 1.4 µg, and 5.6 µg per mg protein at 250, 500, and 1000 µg/ml DINPs, respectively.

fluorescent intensities of DINPs were visualized on various treatment groups. EPCs uptake was increased when the concentration of DINPs was higher. Treated EPCs were lysed with 1% Triton X-100 for 30 minutes to quantitate the amount of DINPs in EPCs at various concentrations. The results showed that EPCs uptook 0.5 μg , 1.4 μg , and 5.6 μg DINPs per mg protein according to incubated concentrations of 250, 500, and 1000 $\mu\text{g}/\text{ml}$ DINPs, respectively (**Figure 20**). The

detailed cellular uptake was also visualized using the Cytovia microscope. For this study, 500 $\mu\text{g}/\text{ml}$ DINPs were chosen for the representative EPCs uptake DINPs by using DAPI fluorescent properties of

DINPs. **Figure 21** showed that DAPI fluorescent signals were scattered in distribution in the cytosol of EPCs while no fluorescent signals were observed on the control group (without incubation of DINPs).

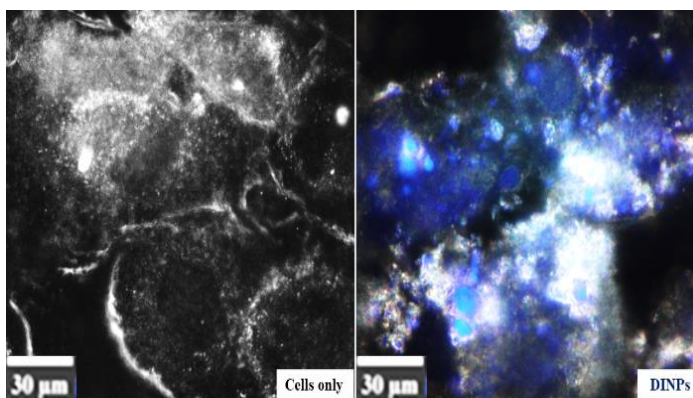


Figure 21. *The Cytovia images of DINPs absorbed HMMECs. Cells were seeded on coverslips overnight before being incubated to DINPs at 500 $\mu\text{g}/\text{ml}$ for 2 hours before being visualized under the Cytovia microscope in DAPI channels. The merge images were the overlay images between phase contrast and fluorescent images. The results showed fluorescent signals of DINPs unevenly distributed in the cell cytosol while no fluorescent signals were observed in the control group.*

3.2.5. *In vitro* therapeutic effects of EpoR DINPs on HMMECs

The therapeutic efficacy of EpoR plasmids released from DINPs was assessed in HMMECs because they were ECs derived from skeletal muscles, which have similar properties of ECs from PADs. I selected only the most effective concentration of EpoR plasmids (50 ng/ml) for our cell studies. HMMECs were treated with various treatments, including no treatment as a negative

control, VEGF, free EpoR, and EpoR DINPs (**Figure 22**). The protection study was performed in

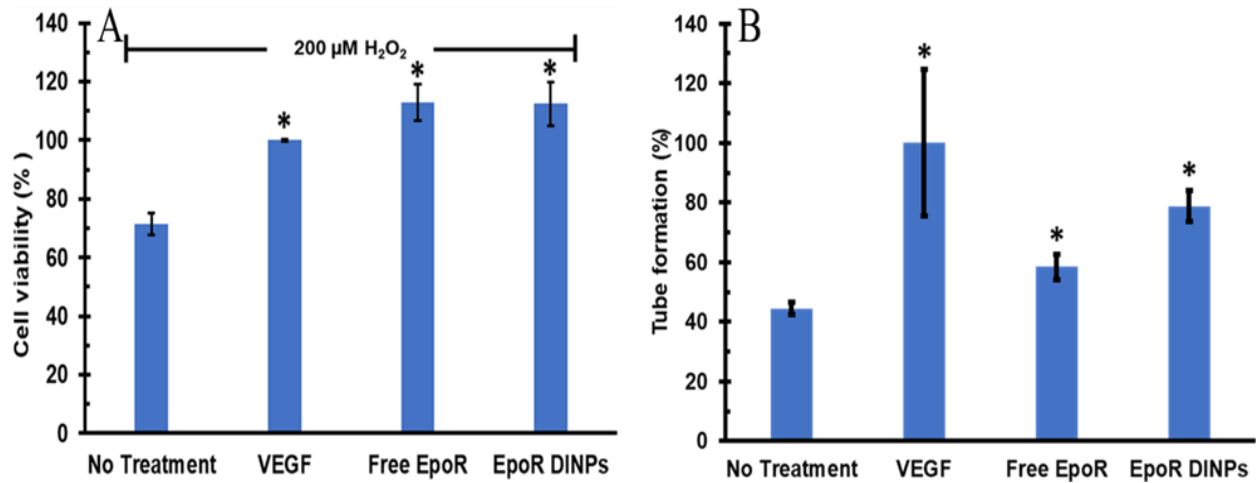


Figure 22: In vitro therapeutic effects of EpoR DINPs on Human Muscular Microvascular Endothelial Cells (HMMECs). HMMECs were pre-transfected with various treatment groups for 4 hours and used as cell sources for seeding in protection study (A) and angiogenesis (B). A) Cells were seeded onto 96 well plates at confluent density overnight. Cells were washed and replenished with 200 μM H_2O_2 in low serum media for 1 day. Then cell viability was analyzed via MTS assays ($n = 3$). No treatment (cells in low serum media with H_2O_2) served as negative control. The results demonstrated EpoR DINPs, free EpoR, and VEGF significantly protected HMMECs under stress conditions. B) Pre-transfected HMMECs in low serum media were seeded on Matrigel for 12 hours ($n=3$). Angiogenesis images were taken at 0 hours and 12 hours by using a phase contrast microscope and analyzed using ImageJ software. EpoR DINPs significantly enhanced angiogenesis compared to that of the no treatment group and showed similar angiogenesis effects as the VEGF group. Data presented as Mean \pm SD. Student's t -tests were run and * indicated significant difference ($P < 0.05$) with respect to the no treatment group in protection and angiogenesis study.

the presence of ROS species (200 μM H_2O_2) in low serum culture media to determine the *in vitro* protective capability of EpoR DINPs. 200 μM H_2O_2 caused HMMECs survival to be reduced up to 70% in one day. EpoR DINPs significantly protected stressed HMMECs compared to the control group (no treatment) as shown by the induced cell viability after 24 hours of exposure. EpoR DINPs and the free EpoR group had similar cell protection capabilities, which was better protection than the VEGF group; however, there were no significant differences between these groups. The results determined cell viability was higher with EpoR DINPs and free EpoR (both 112% survival) compared to that of VEGF (100%), and significantly better compared to that of the non-treatment group (71%, $p < 0.05$). Angiogenesis was studied in the matrigel placed hypoxia

chamber (1% O₂, 5% CO₂ at 37⁰C) to mimic ischemic tissues in PAD patients. Phase-contrast images were taken at 12 hours to observe HMMECs facilitate angiogenesis (**Figure 23**). The

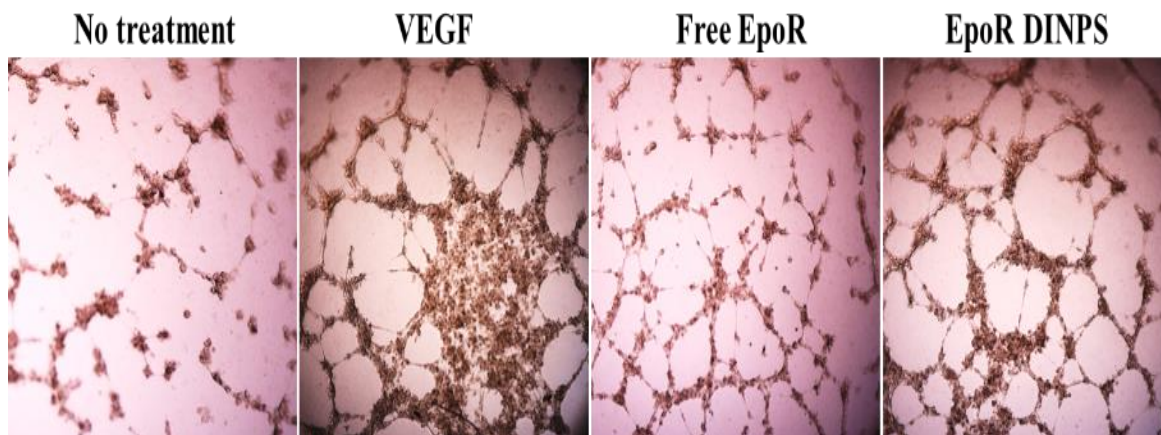


Figure 23. *The representative images of in vitro tube formation of EpoR DINPs in hypoxic conditions. Phase-contrast images were taken at 0 and 12 hours to observe HMMECs facilitate angiogenesis. The results showed a significant induction of angiogenesis in groups (VEGF, free EpoR, and EpoR DINPs) when compared to that of the no treatment group ($p < 0.05$).*

analyzed data demonstrated significant induction of angiogenesis ($p < 0.05$) in all groups (VEGF, free EpoR, and EpoR DINPs) when compared to that of the no-treatment group. According to the study, HMMECs could induce tube formation within 12 hours. EpoR DINPs (79%) significantly enhanced tube formation on the matrigel compared to the no treatment (44%) and free EpoR (58%) groups (**Figure 22B**). The percentage of tube formation induced in the EpoR DINPs group increased almost 2 times compared to that of the no-treatment group. VEGF enhanced higher tube formation compared to the EpoR DINPs group, but there were no significant differences between these groups.

3.3. *In vivo* studies of EpoR DINPs

3.3.1. PAD models

The PAD models were created by ligating the left femoral artery and its branches following the published procedure.¹ LSCI was used to quantify the percentage of blood perfusion reduced on the damaged legs compared to the normal legs (**Figure 24**). The ischemic paw showed pallor color,

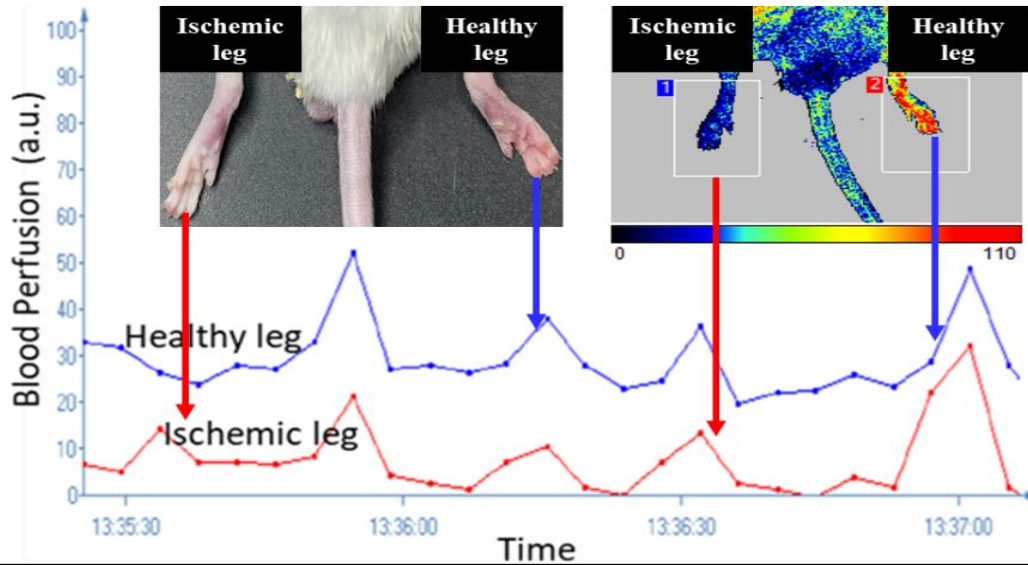


Figure 24. LSCI of the established PAD mice. The PAD models were created by ligating the left femoral artery and its branches following the published procedure.¹ LSCI were immediately used to measure the percentage of blood perfusion reduced on the damaged legs compared to the normal legs. On the upper-left corner image, the ischemic paw showed pallor or pale color while the healthy paw was reddish in the real image. Correspondingly, LSCI images of the ischemic paw was blue and black, which is low or no blood perfusion, whereas the healthy one was visualized red, which is high blood perfusion. The line graph showed the blood perfusion of the healthy leg (blue line) and the ischemic leg (red line). The ischemic leg significantly reduced the blood perfusion compared to these in the healthy leg.

while the healthy paw was reddish in clinical images. Correspondingly, LSCI images of the ischemic paw were blue and black, which is low or no blood perfusion, whereas the healthy one was visualized red, which is high blood perfusion. The line graph showed the blood perfusion of the healthy leg (blue line) was 5 times higher than that of the ischemic leg (red line) measured immediately after the ligation. The ischemic leg significantly reduced the blood perfusion compared to that of the healthy leg. The combined data of 25 retired Balb/c mice aged 6-8 months showed that the ratio of blood perfusion significantly reduced from 97% to 13% right after the surgery (**Figure 25**). However, the blood perfusion ratio varied highly from mouse to mouse, as seen in the dot graph on the left side. The analyzed data demonstrated the blood perfusion was

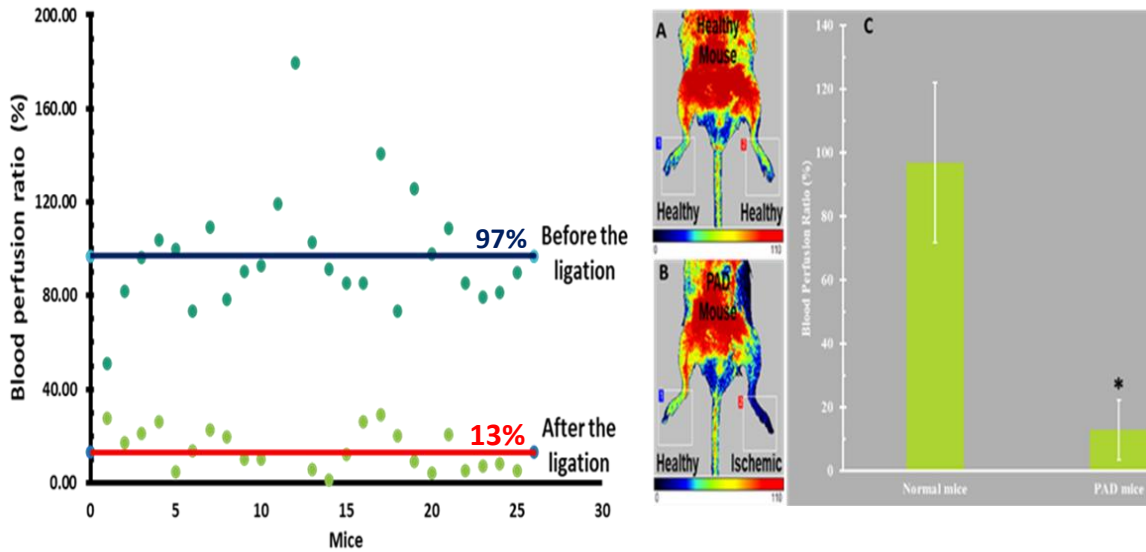


Figure 25. The quantitative analysis of blood perfusion on PAD mice (n = 25). The left graph showed the LSCI data before and after the ligation of the left femoral arteries and its branches in 25 Balb/c mice. Figure A and B showed the representative images of the same mouse before and after the ligation procedure on the left femoral arteries and its branches. The ischemic leg was observed as blue and black color, which is low and no blood perfusion while the healthy leg showed red and yellowish color, which is high blood perfusion. The right bar graph (C) demonstrated the significantly reduced blood perfusion in PAD mice compared to healthy mice. (*) indicated a significant difference ($P < 0.001$).

significantly reduced on the bar graph on the right side. Besides using LSCI for blood perfusion

measurement, MSOT was also investigated in Dr.

Mason's lab at UTSW after IM injecting 5

mg/50 μ l of the blank DINPs on the ischemic

gastrocnemius muscle (PAD model was created

by clamping the leg at UTSW) to study

hemoglobin saturation and DIMP tracking

(Figure 26). Figure 26A showed the ischemic leg

had less oxygen saturation compared to the

normal leg on the transaxial view at the thigh level

under MSOT imaging. Figure 26B also showed

DINPs (green) were observed right after IM

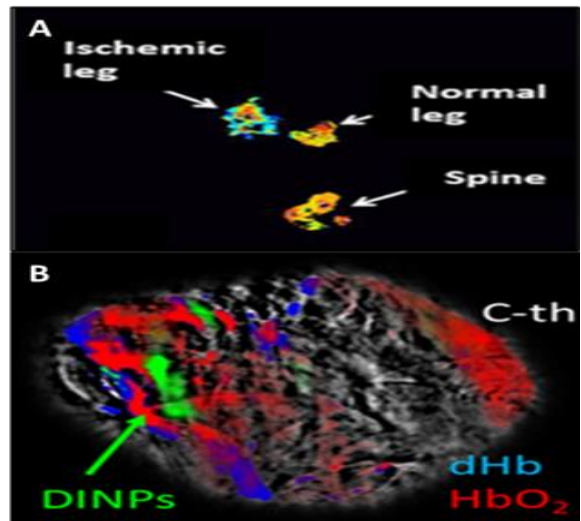


Figure 26. MSOT images of blank DINPs on a PAD mouse. PAD mouse was created and IM injected 100 μ l of blank DINPs (5 mg/ml) along the gastrocnemius muscle. The animal was prepared for taking MSOT images. The results showed that DINPs were visualized in the ischemic tissue in green color on the transaxial view at the thigh level.

injection on the ischemic thigh, which showed less oxygen-hemoglobin (red) and presence of deoxygen-hemoglobin (blue) compared with the normal thigh (C-th).

3.3.2. Bio-distribution of ICG DINPs on PAD mice

To determine the best administration routes for PAD treatment, our group previously performed a biodistribution study using ICG PLGA NPs to investigate IM injection and IV injection in PAD mice (**Figure 27**). The published data showed that IM injection not only provided

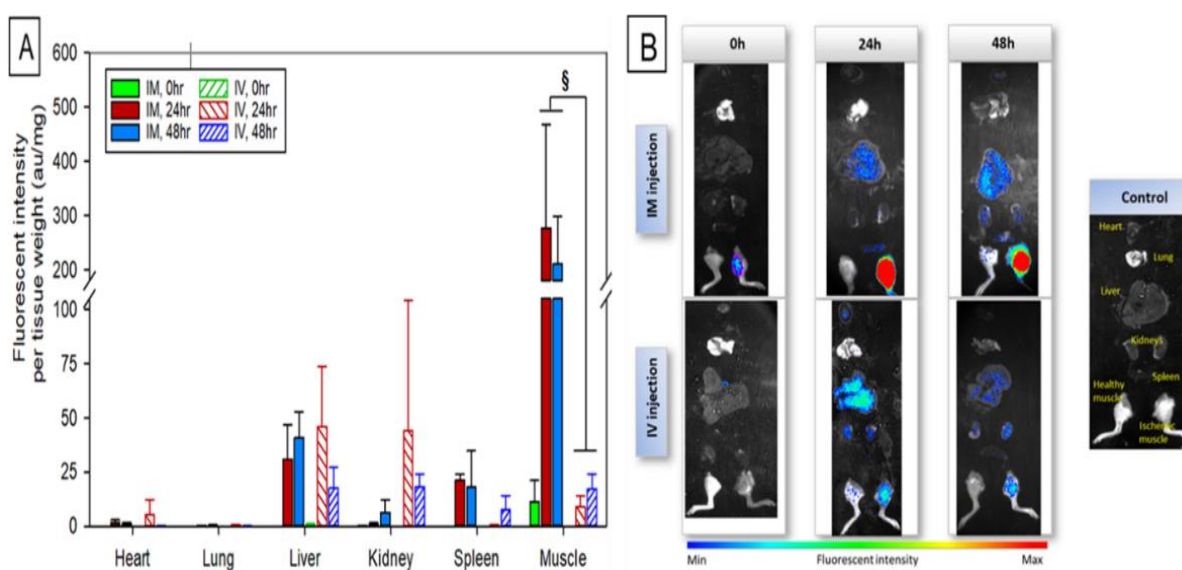


Figure 27. The biodistribution study of ICG-loaded PLGA nanoparticles through intravenous (IV) and intramuscular (IM) injections. A) Fluorescent intensity of collected tissues and organs at different time points; B) Quantified dye loaded NPs accumulated in tissues and organs at different time points. Data presented as Mean±SD. Student's and Welch's t-test were run and § indicated significant difference ($P<0.01$) with respect to IV injection.²

higher accumulation in the ischemic tissues, but also caused less toxicity in the liver and kidneys at 24 and 48 hours.² Following IM injection, the majority of ICG PLGA NPs were retained in the leg muscle for 48 hours, while low fluorescent signals of ICG revealed in livers and spleens at 24 hours and kidneys at 48 hours. Therefore, IM injection was selected as the main administrative route to test DINPs on PAD mice for various experiments later. The biodistribution of DINPs was performed on 10 PAD mice including saline (n=2) and DINPs (n=8) to study the retention of

DINPs at ischemic legs and other organs at 3 different timepoints (0 hours, 4 hours, and 24 hours). The results demonstrated the fluorescent intensities were observed over time points at the ischemic legs under the *in vivo* imaging (**Figure 28**). The fluorescent signals of DINPs at time-point 0 hours (right after injection) showed less intensity compared to 4 and 24 hours. The investigated mice were sacrificed at 4 hours and 24 hours for *ex vivo* imaging to evaluate

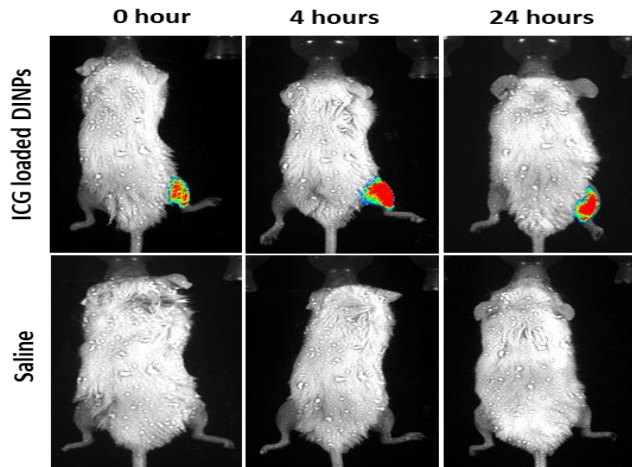


Figure 28. The representative *in vivo* images of DINPs in the gastrocnemius muscle of PAD mice at timepoint 0h, 4h, and 24h. PAD mice were IM injected with ICG DINPs and taken the fluorescent images at 0h, 4h, and 24h. The results determined that DINPs still remained in the ischemic tissues at 4 and 24 hours.

DINPs that remained at the ischemic tissues as well as accumulated in organs.

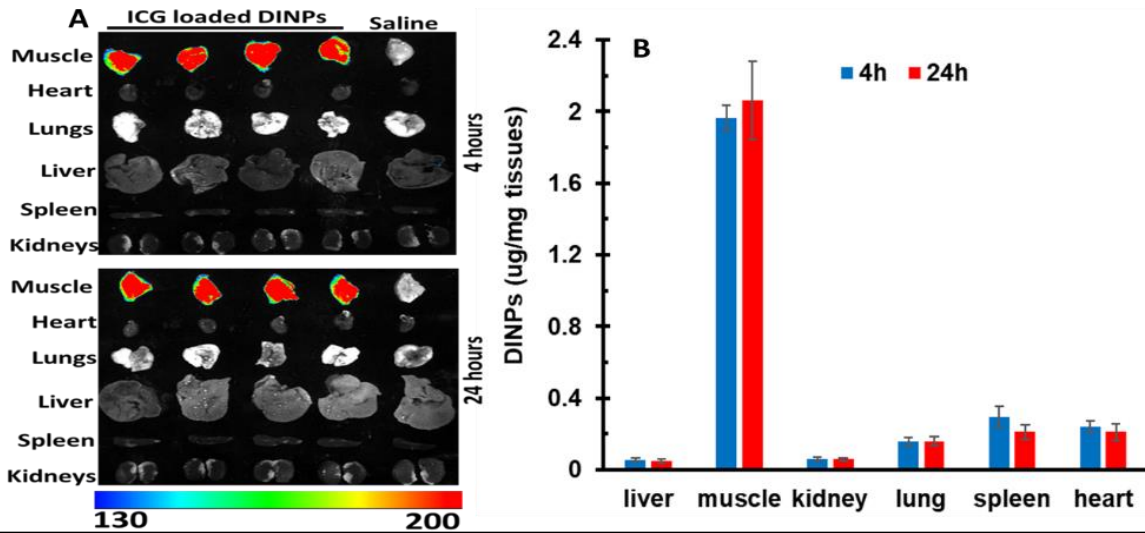


Figure 29. The *ex vivo* biodistribution study of DINPs on PAD mice at 4 and 24 hours. PAD mice were injected with ICG DINPs along the gastrocnemius muscle; then treated mice were sacrificed at 4 and 24 hours for *ex vivo* imaging. **A)** *Ex vivo* images of DINPs in organs. The results showed that DINPs remained at ischemic tissues at 4 and 24 hours. There were no fluorescent signals observed in the other tissues. **B)** The analyzed data of DINPs in homogenized tissues. The collected tissues were homogenized and centrifuged to collect supernatant for measuring fluorescent signals of DINPs. The quantitative data evaluated approximately 2 ug DINPs/mg tissues at 4 and 24 hours in gastrocnemius muscle while DINPs also appeared in other organs such as spleen, heart, lung, kidneys, and liver subsequently.

Figure 29A shows similar fluorescent intensities observed at the ischemic muscle at both timepoints, while no signals presented in the hearts, lungs, livers, spleens, and kidneys. No fluorescent signals were seen in any tissues in the saline group at all different timepoints. To quantify the amount of DINPs on each tissue, all tissues were weighed, homogenized, and measured for fluorescent intensities by using a spectrophotometer (**Figure 29B**). The amount of DINPs per tissues ($\mu\text{g}/\text{gm}$) at 4 hours and 24 hours were determined including livers (0.06 and 0.05), ischemic legs (1.96 and 2.06), kidneys (0.06 and 0.06), lungs (0.16 and 0.16), spleens (0.29 and 0.21), and hearts (0.24 and 0.21).

3.3.3. Therapeutic effect of EpoR DINPs in LSCI and treadmill

The pilot study of EpoR DINPs was performed on 8 PAD mice to determine the optimal dose for the therapeutic study. The results determined 80 μg EpoR DINPs/g (equivalent to 294 ng EpoR plasmids/g mice) and 40 μg EpoR DINPs/g groups enhanced blood perfusion at the first week and the third week compared to that of the saline group (data not shown). Blood perfusion recovery was similar in the first week between the two DNP groups; however, the 80 μg EpoR DINPs group enhanced 13% higher blood perfusion compared to the 40 μg EpoR DINPs group. Therefore, I chose 80 μg EpoR DINPs/g mice as the effective dose for the *in vivo* therapeutic study.

To determine *in vivo* therapeutic effects of EpoR DINPs, 50 μl of each treatment group was intramuscularly injected to the left gastrocnemius muscle (the injured legs) of Balb/c mice (n=3-5 per group) on the 2nd day post-surgery. The four animal groups included saline (sham, control), free EpoR (294 ng EpoR plasmid/g), VEGF (28 ng VEGF/g) and EpoR DINPs (80 μg EpoR DINPs/g). The normal legs on the right side of the same mouse served as a control for normalizing the blood perfusion ratio (ischemic leg/normal leg ratio). LSCI was used to measure blood

perfusion at day 0, week 1 and week 3 to determine blood perfusion changes. The results demonstrated that EpoR DINPs significantly improved blood perfusion of the injured hindlimb compared to the sham group (**Figure 30B**).

All animals in the control group developed necrotic toes and/or limbs within 1-2 weeks. Free EpoR plasmids showed similar blood perfusion to the sham group, likely due to a quick clearance of free plasmids by the animal immune system. Mice treated with VEGF showed better blood perfusion compared to the saline and free EpoR treatment, but less perfusion compared to EpoR

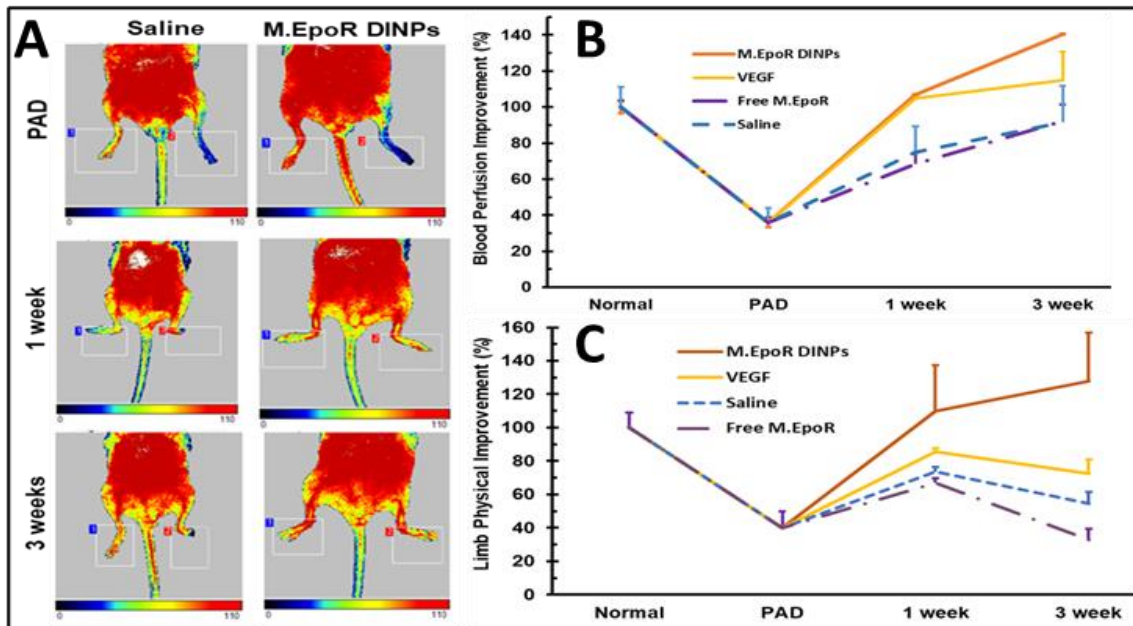


Figure 30. In vivo therapeutic effects of EpoR DINPs on PAD mice. **A)** Representative blood perfusion images of Balb/c PAD mice treated with saline and EpoR DINPs. EpoR DINPs restored blood perfusion quickly and protected PAD mice from autoamputation compared to the saline group (n=3-5). Spectrum colors show various levels of blood perfusion: Red is high blood perfusion, blue is low blood perfusion, and black is completely no blood perfusion. **B)** Blood perfusion improvement of treated PAD mice were evaluated by analyzing non-ischemic leg/ischemic leg blood perfusion ratio. EpoR DINPs enhanced the blood perfusion ratio better than those in the VEGF, saline, and free EpoR groups. **C)** Physical improvement of treated PAD mice was analyzed by treadmill endurance tests. The results demonstrated that EpoR DINPs restored physical capability better compared to the other groups.

DINPs. Treadmill endurance tests showed similar physical restoration of treated mice in concern with blood perfusion improvement. Mice treated with EpoR DINPs showed stronger physical

abilities than VEGF, free EpoR, and saline groups (**Figure 30C**). The results proved that intramuscular administration of EpoR DINPs to injured legs in PAD mice prolonged the retention time needed for improving the bioavailability of therapeutic EpoR plasmids released from DINPs and improved *in vivo* therapeutic responses. The effectiveness of EpoR DINPs enhanced blood perfusion and restored the physical ability of injured legs in PAD mice, a promising potential for similar efficacy in humans.

3.3.4. Histology staining

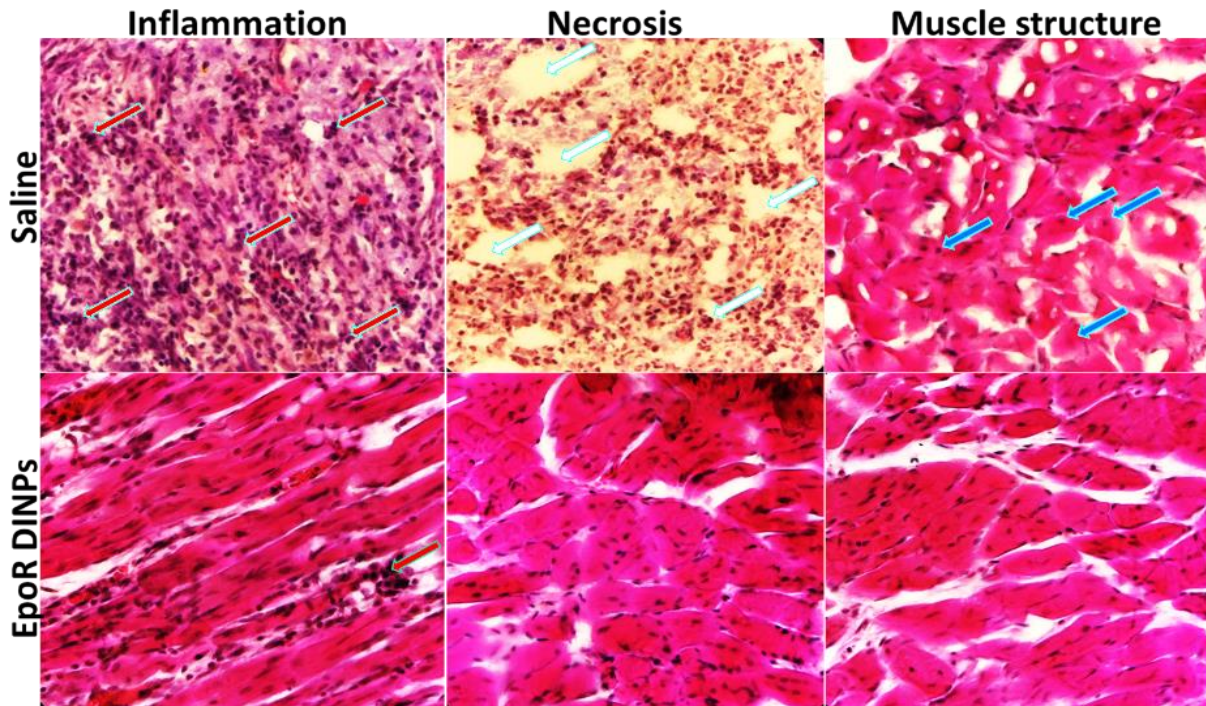


Figure 31. H&E staining of the gastrocnemius muscle on treated PAD mice. The gastrocnemius muscles from the mice treated with saline and EpoR DINPs groups (n=4) were harvested and embedded in OCT before tissue sectioning 5 μ m per section. Then tissue slides were stained with H&E staining and observed under the bright field microscope (40X). On the saline group, the ischemic muscle experienced serious inflammation (red arrow), muscle necrosis replaced by adipocytes (white arrow), and atrophy muscle (blue arrow). On the other hand, EpoR DINPs were able to protect ischemic muscle from inflammation and necrosis although some inflamed sites were observed on the staining areas.

The treated mice in the saline and EpoR DINPs group were sacrificed to collect the gastrocnemius muscle for H&E staining and immunohistology staining to determine muscle

structure and assess EpoR expression, angiogenesis, and EPC recruitment. Ischemic muscles were gently dissected from the tibia bone and fixed with 4% paraformaldehyde overnight before being embedded in the paraffin for tissue sections. H&E staining of muscle cross-sections showed that EpoR DINPs protected the ischemic muscles from serious inflammation and necrosis for maintaining their normal structures (**Figure 31**). The saline group showed muscle fibers changed the shape, becoming atrophy muscle (blue arrow). The muscle bundles became separated and thinner. The central nucleated muscle fibers were observed in several sites in the area while most of them were degenerated nuclei around the muscle fiber. There was the presence of adipocytes (white arrow) and severe inflammatory areas (red arrow). In the EpoR DINP group, the muscle fibers still maintained a healthy structure. A few inflammatory sites were observed in the staining areas as well as in the adipocytes. The significantly higher number of central nucleated muscle fibers was presented on muscle fibers compared to the saline group.

For immunohistochemical staining, the tissue sections were stained with anti-CD31 (EC biomarker), anti-CD 34 (EPC biomarker), and anti-EpoR (EpoR expression) antibodies following the double staining immunohistochemistry protocol posted on the Abcam website. The same secondary antibody conjugated to FITC was used for all immunostaining of CD31, CD34, and EpoR markers, so the positive cells with these biomarkers were visualized to the green color of the FITC channel (**Figure 32**). The results determined that mice treated with EpoR DINPs significantly increased the number of cells positive CD31 in **Figure 32A**, CD34 in **Figure 32B**, and highly expressed EpoR protein in **Figure 32C**. The quantitative analysis in **Figure 32D** showed EpoR DINPs enhanced capillary density 92 times compared to the saline group. Slightly increasing EPC recruitment was observed in the treatment group, which was 4 times higher compared to the saline group. EpoR expression was significantly increased 58 times higher than

that of the saline group.

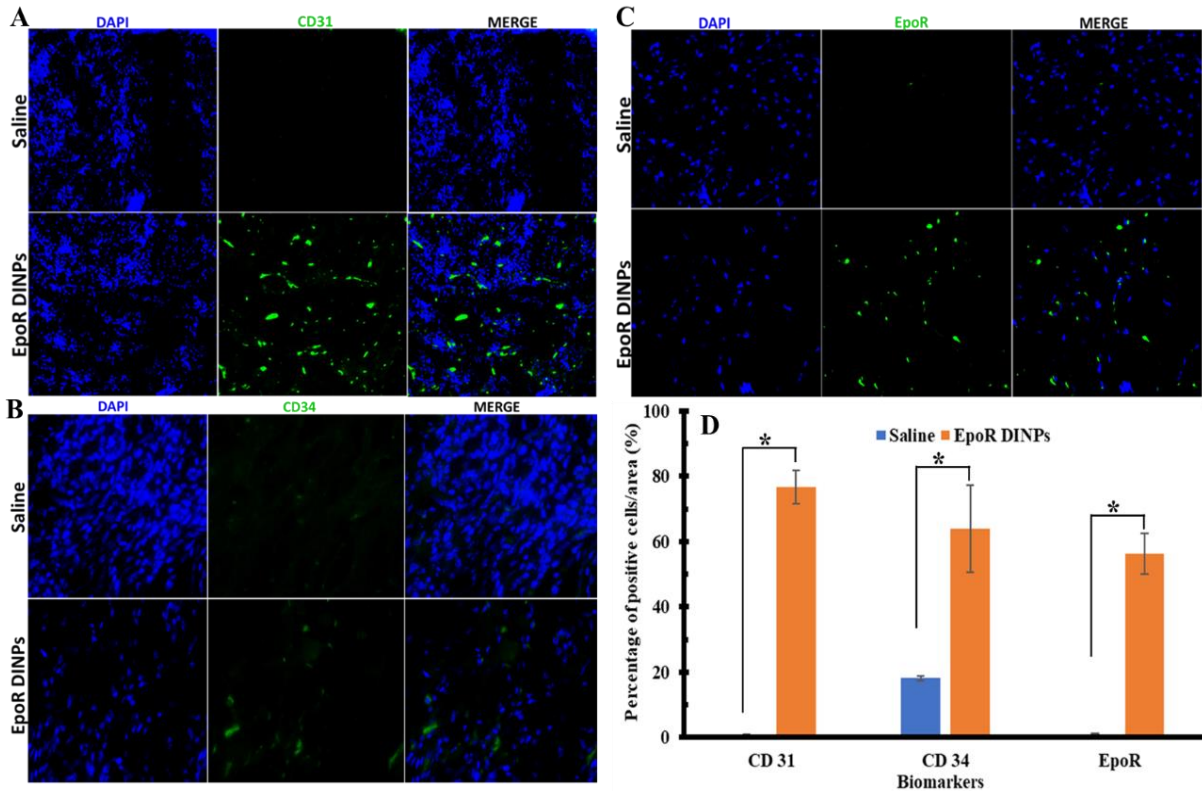


Figure 32. Immunohistochemistry tissue staining of CD31, CD34, and EpoR biomarkers on treated PAD mice. Double immunohistochemical staining technique was used to stain gastrocnemius sections (5 um per section). The primary antibodies were mouse anti-CD31, mouse anti-CD34, and mouse anti-EpoR antibodies where the secondary antibodies tagged with FITC were against the primary correspondingly. Cell nuclei were stained with DAPI as counterstaining. A) Representative images of CD31 staining. B) Representative images of CD34 staining. C) Representative images of EpoR staining. D) The analyzed data of cells expressed CD31, CD34, and EpoR per field of view microscope. EpoR DINPs significantly increased the number of cells staining positive with CD31, CD34, and EpoR. Data presented as Mean±SD for percentage of various biomarkers positive per field of view. Student's and Welch's t-test were run and * indicated significant difference ($P < 0.01$) with respect to corresponding saline groups.

Chapter 4

DISCUSSION/CONCLUSION

Although PLGA NPs have been developed for the treatment of PAD, translational aspects of PLGA NPs could be limited as they could not provide the imaging properties for the detection. PLGA, a common FDA-approved polymer, possesses superior encapsulating properties for probucol delivery to tissues and retention in rabbit femoral arteries and the hindlimb muscle.¹⁰⁸ VEGF plasmid loaded PLGA NPs induced significant angiogenesis with dense capillaries, improved collateral circulation, and enhanced gene expression compared to that of naked plasmids.¹⁰⁹ Furthermore, IM injection of sphingosine-1-phosphate (S1P) loaded PLGA NPs demonstrated their effectiveness as suitable carriers of pro-angiogenic factors^{110,111}. The major disadvantage of PLGA is non-imaging materials. To overcome this limitation, PLGA needs to load both dyes and drugs inside NPs or one in the core and the other on the shells; however, this limited drug loading complicates the fabrication process. Thus, the intrinsic imaging materials are developed to satisfy the high demand for detection and treatment on the same NP design for PADs.

In the last decade, several imaging biomaterials have been developed to apply for treatment management or image-guided surgery. The multifunctional citric acid-derived, biodegradable elastomers is one such novel bioimaging material¹²³⁻¹³² with intrinsic photoluminescent properties served as *in vitro* and *in vivo* imaging tools for detection. Besides these materials, the inorganic NPs demonstrated their benefits on imaging application; however, they cause cytotoxicity and impair NO production¹⁷⁴⁻¹⁷⁶. Recently, novel biodegradable photoluminescent polymers (BPLPs) have been investigated because of the need for bio-imaging materials without conjugating photobleaching organic dyes and/or cytotoxic quantum dots¹³⁰. BPLPs can be used to formulate

NPs that could be used for tracking during treatment due to their tunable fluorescent properties¹²⁹; however, it is limited in detecting in deep tissues, which is a challenge for *in vivo* imaging application. To overcome this limitation, aniline tetramer (AT) was introduced to BPLPs for bringing deep tissue photoacoustic imaging ability. The fluorescent intensity of BPLPATs was decreased with the increase of AT weight ratios, while the PA signals were increased. PA images of BPLPATs can be visualized at a depth of 11 mm under chicken breast tissues *ex vivo*. Therefore, the unique photoacoustic properties of BPLPAT make it promising materials for formulating nanoparticles with desired fluorescence and photoacoustic imaging for managing treatment.

In this project, I used BPLPAT 10% (instead of BPLPAT 5% and BPLPAT 15%) to formulate and optimize DINPs to maintain the intrinsic fluorescent properties of BPLP while acquiring high PA signals of DINPs on PAD treatment. We successfully fabricated DINPs in a powder form for long-term storage with high plasmid loading efficiency (average 80%). DINPs had uniform spherical shapes with a diameter range of 150 nm-250 nm and high negative zeta potential. Its PDI ranged from 0.138-0.213, which was an acceptable index (<0.3). DLS showed larger diameters of DINPs compared to TEM images because they used different principles to evaluate the diameters. According to the release curve, DINPs provided the biphasic release profile including the burst phase (11% of EpoR released) for 12 hours followed by the sustained phase. It noted that DINPs demonstrated quick release of larger plasmids compared to PLGA NPs, which released 4% during the first 24 hours.¹⁷⁷ This can be attributed by polylactones and hydrophilic glycolic acid in BPLPs, which provide fast release and degradation.¹⁷⁸ The fast release of DINPs will benefit PAD treatment since it would improve the short-term therapeutic efficiency. The stability of DINPs was observed in different solutions, including DI water, 10% FBS, saline, and simulated body fluid over 72 hours without any signs of aggregations. The high negative charge

of DINPs helped to maintain the size stability. Therefore, DINPs are not aggregates in the studied solutions and safe to use for *in vivo* study.

DINPs were visualized on three different fluorescent channels including DAPI, FITC, and Cy5; however, they were taken at a high intensity of light sources. As discussed above, the BPLPAT polymers had strong photoluminescent properties, so it demonstrated that the intrinsic fluorescent properties of BPLPATs were weakened in DINPs. I speculate the low fluorescent signals of DINPs were due to the differential density of BPLPATs and DINPs, where BPLPATs have higher density than DINPs. This can be a drawback of tracking DINPs in cell cultures for a long-term study. To investigate the benefits of DINPs as imaging probes to keep track of EPCs, various concentrations of DINPs were incubated with EPCs for 2 hours. Treated cells were taken by fluorescent images at Cy5 channel while DAPI was counter-staining. The results demonstrated the internalization of DINPs by EPCs correlated to the concentrations of DINPs (up to 1,000 μ g/ml). Nanoparticle uptake is unique depending on cell lines and materials. For instance, human aortic endothelial cells internalized PLGA NPs up to 300 μ g/ml¹⁰¹ while Type I alveolar cells uptook to 1000 μ g/ml PLGA NPs⁹⁴. Thus, the high uptake of DINPs makes it easier to detect cells internalized in NPs.

To determine DINPs releasing EpoR plasmids for inducing *in vitro* therapeutic effects, HMMECs were used for the protection and tube formation studies since they are cell lines derived from muscle microvascular endothelial cells. Therefore, they are a representative cell line for PAD therapy which relates to muscular ECs. Protection and tube formation studies were performed to evaluate the main functions of EpoR plasmids. The results demonstrated EpoR DINPs significantly protected ECs under stressed conditions and facilitated angiogenesis in a hypoxic environment

compared to those of the controls. These results suggest the potential of novel EpoR DINPs for PAD treatments.

Finally, I investigated EpoR DINPs on PAD treatment for tracking DINPs during the treatment. At first, the imaging ability of DINPs was observed using MSOT imaging while PA images of BPLPAT NPs were demonstrated in Dr. Yang's lab to detect NPs at a depth of 11 mm. For this study, I only tested the imaging benefits of blank DINPs on PAD models created at UTSW via MSOT. MSOT not only detected DINPs in deep tissues, but also provided oxyhemoglobin and deoxyhemoglobin saturation. It is important to verify the blood perfusion collected from traditional technologies such as LSCI, which were limited to the depth signal. The results showed that MSOT were able to visualize DINPs injected to gastrocnemius muscles and oxygen saturation on PAD models. The biodistribution showed DINPs remained at the ischemic tissue for 24 hours of administration and less accumulation to livers, kidneys, and spleens, as noted in previous studies via PLGA NPs². EpoR DINPs provided a controlled, sustained release of EpoR plasmids to improve blood perfusion after 3 weeks of treatments. As the result of this, physical abilities assessed via treadmill endurance test was recovery. I demonstrated EpoR DINPs transfected cells in ischemic tissues for high expression of Epo transmembrane protein on the surface of cells, so the Epo/EpoR pathway was triggered to facilitate cell protection and pro-angiogenic signaling pathways for enhancing angiogenesis. To assess angiogenesis, immunohistochemistry staining was used; CD31, which is for ECs, and CD34 for EPCs. I determined the capillary density significantly increased 92 times while a few cells positive to CD31 were observed in the control group. Similarly, EPCs were recruited to the ischemic tissues for proliferation ECs and inducing angiogenesis. The quantitative analysis demonstrated EPC recruitment was 3.5 times higher than that of the saline group.

In conclusion, the surgical intervention for PADs often leads to serious complications and is the contraindication of elderly people, which occupies more than 20% of individuals over 80-years-old. Recently, restoration of blood perfusion via enhancing angiogenesis in ischemic tissues has been explored as an alternative strategy to overcome limitations of endovascular surgery. Although growth factors or plasmids encoding growth factors loaded NPs were investigated on PAD treatments in clinical trials phase I or II, their outcomes were limited, or no significant difference was found compared to the placebo. One of the main reasons causing the failure of current treatment was lacking the imaging method to adjust initial doses or monitor the retention of NPs in ischemic tissues. In this thesis, I have successfully developed EpoR DINPs to monitor precisely a therapeutic dose of EpoR DINPs for PAD treatment. Our work demonstrated DINPs retained the intrinsic fluorescent properties of BPLPAT polymers including DAPI, FITC, and Cy5 channels, and loaded the efficient amount of EpoR plasmids for the *in vitro* and *in vivo* studies. The *in vitro* studies determined DINPs were traced in HMMECs and EPCs via uptake studies without using any dyes or imaging agents whereas EpoR released provided cell protection and tube formation in HMMECs compared to VEGF. Our *in vivo* studies proved that DINPs were visualized in the ischemic tissues and restored blood perfusion and physical capacity via enhancing capillary density and EPC recruitment by upregulating EpoR expression in treated muscles. In general, EpoR DINPs showed the therapeutic dual-imaging benefits on PAD approach.

Chapter 5

LIMITATIONS AND FUTURE WORK

Although results from my thesis did support the potential application of our DINPs for PAD treatment and management, more work needs to be done before their use in humans. First of all, EpoR DINPs improved significantly *in vitro* and *in vivo* therapeutic efficacy; however, I have never performed the toxicity study of DINPs to determine the maximal dose causing cell damage, so the toxicity of DINPs will further be evaluated to prove safety for clinical usage of DINPs. Cell toxicity and hemocompatibility of DINPs will be investigated by incubating EPCs and heparin-anticoagulated human blood with DINPs at various concentrations to find the toxic doses of DINPs. For cell toxicity, the cell viability over a time range (24 and 48 hours) will be studied; then these cells will be immunohistochemically stained against specific EC biomarkers, KDR (VEGF receptor), and vascular endothelial cadherin (VE-cadherin). For EC functionality, low-density lipoprotein (LDL) uptake, prostacyclin production, and nitric oxide (NO) release from exposed cells will be detected using colorimetric assays and ELISA kits. The hemocompatibility of DINPs will be evaluated by detecting the number of adherent platelets via lactate dehydrogenase (LDH) assays, assessing platelet activation by flow cytometry and determining whole blood clotting kinetics. Poly(octamethylene citrate) (POC) will be used as a control due to its excellent hemocompatibility.

For *in vivo* toxicity of DINPs, potential side effects will be analyzed via blood collection for hematocrit, lipase and amylase levels for up to 4 weeks. To determine potential cardiotoxicity, I will examine biomarkers such as troponins, myeloperoxidase, and cystatin C via staining of heart tissue sections. We will study lung toxicity by detection of the Clara cell protein, tumor necrosis

factor, and beta-glucuronidase; kidney toxicity via serum creatinine, blood urea nitrogen, and kidney injury molecule-1, and liver toxicity using alanine aminotransferase, aspartate aminotransferase, and LDH.

For fluorescent imaging limitations, although DINPs maintained intrinsic fluorescent properties for BPLPAT 10%, the fluorescent signal reduced significantly. To track cell uptake, high levels of a power source were used to visualize DINPs. To improve the imaging properties of DINPs, BPLPAT polymers with various AT ratios will be applied to improve fluorescent intensity. The percentage of AT in BPLPAT materials will be optimized to enhance fluorescent signals of DINPs where PA images will be retained to visualize DINPs in deep tissues for tracking the doses of DINPs.

The PAD model was created by following the published procedures reduced by 87% blood perfusion. However, the remaining blood perfusion of 13% seems to create too severe a model. The significant reduction of blood flow will quickly damage muscles, then causing necrosis if the blood perfusion will not restore immediately. I have seen much necrosis at different levels including skin, one toe or multiple toes, paw, or even the whole legs within the second day of the surgery, which is day 0 of treatment. I noted that when necrosis happens, it is impossible to observe the improvement of blood perfusion on treated mice; however, tissue staining of gastrocnemius still demonstrates the improvement of angiogenesis, EPCs, and EpoR expression. Therefore, the model should be modified to prevent necrosis quickly post-surgery for future study. I may ligate only the femoral arteries and/or one branch to get more blood supply to prevent necrosis. The expected model will show only ischemic tissues in the first week where no necrosis is observed.

The IM administration route is another limitation of the project. I used IM injection of EpoR DINPs for the investigated project since it showed a high accumulation of DINPs at the ischemic

tissue while less toxicity in organs was speculated at the first 24 hours. As noted, several PAD projects use IM injection on the gastrocnemius muscle, and the improvement of blood perfusion varied a lot in the treatment group. This can be due to model issues or different doses of EpoR available for ischemic tissues. To understand the issue, histology staining will be investigated to explore real reasons. I speculated that some sites showed significant improvement while other sites showed muscle necrosis or inflammation. Similarly, staining against CD31, CD34, and EpoR expression also showed unevenly enhancing angiogenesis. The major problem of IM injections for large therapeutic agents is that the drug will not diffuse around tissues. It has been reported in the literature, especially IM injections for gene therapy.¹⁷⁹ They concluded the transfection only happened around the needles. To overcome this limitation, the pilot study of the effective doses should be approached for IV injection and IM injection on PAD mice to compare the therapeutic effects at two timepoints (1 week and 3 weeks). Although IV injection shows limited drug delivery to ischemic tissues, it evenly distributes therapeutic agents to diseased tissues, which have leaky capillaries. To enhance drug delivery efficacy, targeting ligands may also be used. Our unpublished data showed intercellular adhesion molecule 1 (ICAM1) significantly upregulated at ischemic tissues on the first day of the model. Therefore, I may need to conjugate anti-ICAM1 on DINPs to improve the delivery of DINPs via IV injection.

References

1. Niiyama H, Huang NF, Rollins MD, Cooke JP. Murine model of hindlimb ischemia. *J Vis Exp*. 2009. doi: 10.3791/1035
 2. Hinkle L, Le D, Nguyễn T, Tran V, Amankwa C, Weston C, Shen H, Nguyen K, Rahimi M, Acharya S. Nano encapsulated novel compound SA-10 with therapeutic activity in both acute and chronic murine Hindlimb ischemia models. *Nanomedicine: Nanotechnology, Biology and Medicine*. 2021;35:102400. doi: 10.1016/j.nano.2021.102400
 3. https://www.cdc.gov/dhbsp/data_statistics/fact_sheets/fs_pad.htm. Peripheral arterial disease (PAD) fact sheet.
 4. Hirsch AT, Criqui MH, Treat-Jacobson D, Regensteiner JG, Creager MA, Olin JW, Krook SH, Hunninghake DB, Comerota AJ, Walsh ME, et al. Peripheral arterial disease detection, awareness, and treatment in primary care. *JAMA: The Journal of the American Medical Association*. 2001;286:1317-1324.
 5. Song P, Rudan D, Zhu Y, Fowkes FJI, Rahimi K, Fowkes FGR, Rudan I. Global, regional, and national prevalence and risk factors for peripheral artery disease in 2015: an updated systematic review and analysis. *The Lancet Global Health*. 2019;7:e1020-e1030. doi: [https://doi.org/10.1016/S2214-109X\(19\)30255-4](https://doi.org/10.1016/S2214-109X(19)30255-4)
 6. Go AS, Mozaffarian D, Roger VL, Benjamin EJ, Berry JD, Borden WB, Bravata DM, Dai S, Ford ES, Fox CS, et al. Executive summary: heart disease and stroke statistics--2013 update: a report from the American Heart Association. *Circulation*. 2013;127:143-152. doi: 10.1161/CIR.0b013e318282ab8f
 7. Stoyioglou A, Jaff MR. Medical treatment of peripheral arterial disease: a comprehensive review. *J Vasc Interv Radiol*. 2004;15:1197-1207.
 8. Fowkes FGR, Aboyans V, Fowkes FJ, McDermott MM, Sampson UK, Criqui MH. Peripheral artery disease: epidemiology and global perspectives. *Nature Reviews Cardiology*. 2017;14:156.
 9. Camci-Unal G, Alemdar N, Annabi N, Khademhosseini A. Oxygen releasing biomaterials for tissue engineering. *Polymer International*. 2013;62:843-848. doi: 10.1002/pi.4502
 10. Topfer LA, Spry C. New Technologies for the Treatment of Peripheral Artery Disease. In: *CADTH Issues in Emerging Health Technologies*. Ottawa (ON): Canadian Agency for Drugs and Technologies in Health
- Copyright (c) CADTH 2018. You are permitted to reproduce this document for non-commercial purposes, provided it is not modified when reproduced and appropriate credit is given to CADTH.; 2016:1-19.
11. Virani SS, Alonso A, Aparicio HJ, Benjamin EJ, Bittencourt MS, Callaway CW, Carson AP, Chamberlain AM, Cheng S, Delling FN, et al. Heart Disease and Stroke Statistics2014; 2021 Update. *Circulation*. 2021;143:e254-e743. doi: doi:10.1161/CIR.0000000000000950
 12. Doyle BJ, Rihal CS, Gastineau DA, Holmes DR, Jr. Bleeding, blood transfusion, and increased mortality after percutaneous coronary intervention: implications for contemporary practice. *J Am Coll Cardiol*. 2009;53:2019-2027. doi: 10.1016/j.jacc.2008.12.073

13. Orford JL, Selwyn AP, Ganz P, Popma JJ, Rogers C. The comparative pathobiology of atherosclerosis and restenosis. *The American Journal of Cardiology*. 2000;86:6H-11H.
14. Cully M. Diabetes: Drug-eluting balloons for the treatment of critical limb ischaemia. *Nature Reviews Cardiology*. 2013;10:430. doi: 10.1038/nrcardio.2013.102
15. Davies MG, Anaya-Ayala JE. Endovascular techniques in limb salvage: cutting, cryo, brachy, and drug-eluting balloons. *Methodist DeBakey Cardiovascular Journal*. 2013;9:69-72.
16. Arena FJ. Arterial kink and damage in normal segments of the superficial femoral and popliteal arteries abutting nitinol stents--a common cause of late occlusion and restenosis? A single-center experience. *J Invasive Cardiol*. 2005;17:482-486.
17. Nessa A, Latif SA, Siddiqui NI, Hussain MA, Bhuiyan MR, Hossain MA, Akther A, Rahman M. Angiogenesis-a novel therapeutic approach for ischemic heart disease. *Mymensingh Medical Journal : MMJ*. 2009;18:264-272.
18. Patra C, Boccaccini AR, Engel FB. Vascularisation for cardiac tissue engineering: the extracellular matrix. *Thrombosis and Haemostasis*. 2014;113. doi: 10.1160/TH14-05-0480
19. Thomas CE, Ehrhardt A, Kay MA. Progress and problems with the use of viral vectors for gene therapy. *Nature Reviews Genetics*. 2003;4:346-358. doi: 10.1038/nrg1066
20. Yockman JW, Kastenmeier A, Erickson HM, Brumbach JG, Whitten MG, Albanil A, Li DY, Kim SW, Bull DA. Novel polymer carriers and gene constructs for treatment of myocardial ischemia and infarction. *Journal of Controlled Release: Official Journal of the Controlled Release Society*. 2008;132:260-266. doi: 10.1016/j.jconrel.2008.06.024
21. Pack DW, Hoffman AS, Pun S, Stayton PS. Design and development of polymers for gene delivery. *Nature Reviews Drug Discovery*. 2005;4:581-593. doi: 10.1038/nrd1775
22. Danhier F, Ansorena E, Silva JM, Coco R, Le Breton A, Preat V. PLGA-based nanoparticles: an overview of biomedical applications. *Journal of Controlled Release: Official Journal of the Controlled Release Society*. 2012;161:505-522. doi: 10.1016/j.jconrel.2012.01.043
23. Remant Bahadur KC, Uludag H. A comparative evaluation of disulfide-linked and hydrophobically-modified PEI for plasmid delivery. *Journal of Biomaterials Science Polymer edition*. 2011;22:873-892. doi: 10.1163/092050610X496297
24. Zhang XZ, Zeng X, Sun YX, Zhuo RX. 8 - Bioactive materials in gene therapy. In: Zhao X, Courtney JM, Qian H, eds. *Bioactive Materials in Medicine*. Woodhead Publishing; 2011:179-219.
25. Jiang X, Abedi K, Shi J. Polymeric nanoparticles for RNA delivery. In: *Reference Module in Materials Science and Materials Engineering*. Elsevier; 2021.
26. Kang SW, Lim HW, Seo SW, Jeon O, Lee M, Kim BS. Nanosphere-mediated delivery of vascular endothelial growth factor gene for therapeutic angiogenesis in mouse ischemic limbs. *Biomaterials*. 2008;29:1109-1117. doi: 10.1016/j.biomaterials.2007.11.004
27. Yi F, Wu H, Jia GL. Formulation and characterization of poly (D,L-lactide-co-glycolide) nanoparticle containing vascular endothelial growth factor for gene delivery. *Journal of Clinical Pharmacy and Therapeutics*. 2006;31:43-48. doi: 10.1111/j.1365-2710.2006.00702.x
28. Park JS, Yang HN, Yi SW, Kim JH, Park KH. Neoangiogenesis of human mesenchymal stem cells transfected with peptide-loaded and gene-coated PLGA nanoparticles. *Biomaterials*. 2016;76:226-237. doi: 10.1016/j.biomaterials.2015.10.062

29. Collinson DJ, Donnelly R. Therapeutic angiogenesis in peripheral arterial disease: can biotechnology produce an effective collateral circulation? *European Journal of Vascular and Endovascular Surgery: The Official Journal of the European Society for Vascular Surgery*. 2004;28:9-23. doi: 10.1016/j.ejvs.2004.03.021
30. Grochot-Przeczek A, Dulak J, Jozkowicz A. Therapeutic angiogenesis for revascularization in peripheral artery disease. *Gene*. 2013;525:220-228. doi: 10.1016/j.gene.2013.03.097
31. Jones WS, Annex BH. Growth factors for therapeutic angiogenesis in peripheral arterial disease. *Current Opinion in Cardiology*. 2007;22:458-463. doi: 10.1097/HCO.0b013e328236741b
32. Shimamura M, Nakagami H, Koriyama H, Morishita R. Gene therapy and cell-based therapies for therapeutic angiogenesis in peripheral artery disease. *BioMed Research International*. 2013;2013:186215. doi: 10.1155/2013/186215
33. Noukeu LC, Wolf J, Yuan B, Banerjee S, Nguyen KT. Nanoparticles for detection and treatment of peripheral arterial disease. *Small*. 2018;14:e1800644. doi: 10.1002/smll.201800644
34. Kidane AG, Salacinski H, Tiwari A, Bruckdorfer KR, Seifalian AM. Anticoagulant and antiplatelet agents: their clinical and device application(s) together with usages to engineer surfaces. *Biomacromolecules*. 2004;5:798-813. doi: 10.1021/bm0344553
35. Harder S, Klinkhardt U, Alvarez JM. Avoidance of bleeding during surgery in patients receiving anticoagulant and/or antiplatelet therapy: pharmacokinetic and pharmacodynamic considerations. *Clinical Pharmacokinetics*. 2004;43:963-981. doi: 10.2165/00003088-200443140-00002
36. Randomized placebo-controlled trial of effect of eptifibatid on complications of percutaneous coronary intervention: IMPACT-II. *The Lancet*. 1997;349:1422-1428. doi: [https://doi.org/10.1016/S0140-6736\(96\)10172-0](https://doi.org/10.1016/S0140-6736(96)10172-0)
37. Hoareau GL, Tibbits EM, Beyer CA, Simon MA, DeSoucy ES, Faulconer ER, Neff LP, Grayson JK, Stewart IJ, Williams TK, et al. Resuscitative endovascular balloon occlusion of the aorta: review of the literature and applications to veterinary emergency and critical care. *Front Vet Sci*. 2019;6:197-197. doi: 10.3389/fvets.2019.00197
38. Fanelli F, Cannavale A, Corona M, Lucatelli P, Wlderck A, Salvatori FM. The "DEBELLUM"--lower limb multilevel treatment with drug eluting balloon--randomized trial: 1-year results. *The Journal of Cardiovascular Surgery*. 2014;55:207-216.
39. Fanelli F, Cannavale A, Corona M, Lucatelli P, Wlderck A, Salvatori FM. The "debellum" - lower limb multilevel treatment with drug eluting balloon - randomized trial: 1-year results. *The Journal of Cardiovascular Surgery*. 2014.
40. Kakkar AM, Abbott JD. Percutaneous versus surgical management of lower extremity peripheral artery disease. *Current Atherosclerosis Reports*. 2015;17:479. doi: 10.1007/s11883-014-0479-0
41. Kinlay S. Management of critical limb ischemia. *Circulation Cardiovascular interventions*. 2016;9:e001946. doi: 10.1161/CIRCINTERVENTIONS.115.001946
42. Bosiers M, Deloose K, Verbist J, Peeters P. Update management below knee intervention. *Minerva Cardioangiologica*. 2009;57:117-129.
43. Couto M, Figueroa A, Sotolongo A, Perez R, Ojeda JM. Endovascular intervention in the treatment of peripheral artery disease. *Boletin de la Asociacion Medica de Puerto Rico*. 2015;107:47-51.

44. Dominguez A, 3rd, Bahadorani J, Reeves R, Mahmud E, Patel M. Endovascular therapy for critical limb ischemia. *Expert Rev Cardiovasc Ther.* 2015;13:429-444. doi: 10.1586/14779072.2015.1019472
45. Thukkani AK, Kinlay S. Endovascular intervention for peripheral artery disease. *Circ Res.* 2015;116:1599-1613. doi: 10.1161/CIRCRESAHA.116.303503
46. Vartanian SM, Conte MS. Surgical intervention for peripheral arterial disease. *Circ Res.* 2015;116:1614-1628. doi: 10.1161/CIRCRESAHA.116.303504
47. Blum A, Balkan W, Hare JM. Advances in cell-based therapy for peripheral vascular disease. *Atherosclerosis.* 2012;223:269-277.
48. Fadini GP, Agostini C, Avogaro A. Autologous stem cell therapy for peripheral arterial disease meta-analysis and systematic review of the literature. *Atherosclerosis.* 2010;209:10-17.
49. Cooke JP, Losordo DW. Modulating the vascular response to limb ischemia: angiogenic and cell therapies. *Circ Res.* 2015;116:1561-1578. doi: 10.1161/CIRCRESAHA.115.303565
50. Gertz ZM, Wilensky RL. Local drug delivery for treatment of coronary and peripheral artery disease. *Cardiovascular Therapeutics.* 2011;29:e54-66.
51. Bonaca MP, Creager MA. Pharmacological treatment and current management of peripheral artery disease. *Circ Res.* 2015;116:1579-1598. doi: 10.1161/CIRCRESAHA.114.303505
52. Mughal NA, Russell DA, Ponnambalam S, Homer-Vanniasinkam S. Gene therapy in the treatment of peripheral arterial disease. *The British Journal of Surgery.* 2012;99:6-15.
53. Bonaca Marc P, Creager Mark A. Pharmacological treatment and current management of peripheral artery disease. *Circulation Research.* 2015;116:1579-1598. doi: 10.1161/CIRCRESAHA.114.303505
54. Iyer SR, Annex BH. Therapeutic angiogenesis for peripheral artery disease: lessons learned in translational science. *JACC Basic Transl Sci.* 2017;2:503-512. doi: 10.1016/j.jacbts.2017.07.012
55. Weiss DJ. Stem cells, cell therapies, and bioengineering in lung biology and diseases. Comprehensive review of the recent literature 2010-2012. *Ann Am Thorac Soc.* 2013;10:S45-S97. doi: 10.1513/AnnalsATS.201304-090AW
56. Teraa M, Sprengers Ralf W, Schutgens Roger EG, Slaper-Cortenbach Ineke CM, van der Graaf Y, Algra A, van der Tweel I, Doevendans Pieter A, Mali Willem PTM, Moll Frans L, et al. Effect of repetitive intra-arterial infusion of bone marrow mononuclear cells in patients with no-option limb ischemia. *Circulation.* 2015;131:851-860. doi: 10.1161/CIRCULATIONAHA.114.012913
57. Magee JA, Piskounova E, Morrison SJ. Cancer stem cells: impact, heterogeneity, and uncertainty. *Cancer Cell.* 2012;21:283-296. doi: 10.1016/j.ccr.2012.03.003
58. Kusumanto YH, Hospers GA, Mulder NH, Tio RA. Therapeutic angiogenesis with vascular endothelial growth factor in peripheral and coronary artery disease: a review. *International Journal of Cardiovascular Interventions.* 2003;5:27-34.
59. Aviles RJ, Annex BH, Lederman RJ. Testing clinical therapeutic angiogenesis using basic fibroblast growth factor (FGF-2). *Brit J Pharmacol.* 2003;140:637-646. doi: DOI 10.1038/sj.bjp.0705493
60. van der Linde D, Konings EE, Slager MA, Witsenburg M, Helbing WA, Takkenberg JJ, Roos-Hesselink JW. Birth prevalence of congenital heart disease worldwide: a systematic

- review and meta-analysis. *J Am Coll Cardiol.* 2011;58:2241-2247. doi: 10.1016/j.jacc.2011.08.025
61. Anderson EM, Silva EA, Hao Y, Martinick KD, Vermillion SA, Stafford AG, Doherty EG, Wang L, Doherty EJ, Grossman PM, et al. VEGF and IGF delivered from alginate hydrogels promote stable perfusion recovery in ischemic hind limbs of aged mice and young rabbits. *J Vasc Res.* 2017;54:288-298. doi: 10.1159/000479869
 62. Tang J, Wang J, Zheng F, Kong X, Guo L, Yang J, Zhang L, Huang Y. Combination of chemokine and angiogenic factor genes and mesenchymal stem cells could enhance angiogenesis and improve cardiac function after acute myocardial infarction in rats. *Molecular and Cellular Biochemistry.* 2010;339:107-118. doi: 10.1007/s11010-009-0374-0
 63. Madeddu P. Therapeutic angiogenesis and vasculogenesis for tissue regeneration. *Experimental Physiology.* 2005;90:315-326. doi: 10.1113/expphysiol.2004.028571
 64. Kusumanto YH, van Weel V, Mulder NH, Smit AJ, van den Dungen JJ, Hooymans JM, Sluiter WJ, Tio RA, Quax PH, Gans RO, et al. Treatment with intramuscular vascular endothelial growth factor gene compared with placebo for patients with diabetes mellitus and critical limb ischemia: a double-blind randomized trial. *Human Gene Therapy.* 2006;17:683-691. doi: 10.1089/hum.2006.17.683
 65. Beleslin-Cokic BB, Cokic VP, Yu X, Weksler BB, Schechter AN, Noguchi CT. Erythropoietin and hypoxia stimulate erythropoietin receptor and nitric oxide production by endothelial cells. *Blood.* 2004;104:2073-2080. doi: 10.1182/blood-2004-02-0744
 66. Trincavelli ML, Da Pozzo E, Ciampi O, Cuboni S, Daniele S, Abbracchio MP, Martini C. Regulation of erythropoietin receptor activity in endothelial cells by different erythropoietin (EPO) derivatives: an in vitro study. *International Journal of Molecular Sciences.* 2013;14:2258-2281. doi: 10.3390/ijms14022258
 67. Anagnostou A, Lee ES, Kessimian N, Levinson R, Steiner M. Erythropoietin has a mitogenic and positive chemotactic effect on endothelial cells. *Proc Natl Acad Sci U S A.* 1990;87:5978-5982.
 68. Heeschen C, Aicher A, Lehmann R, Fichtlscherer S, Vasa M, Urbich C, Mildner-Rihm C, Martin H, Zeiher AM, Dimmeler S. Erythropoietin is a potent physiologic stimulus for endothelial progenitor cell mobilization. *Blood.* 2003;102:1340-1346. doi: 10.1182/blood-2003-01-0223
 69. Nakano M, Satoh K, Fukumoto Y, Ito Y, Kagaya Y, Ishii N, Sugamura K, Shimokawa H. Important role of erythropoietin receptor to promote VEGF expression and angiogenesis in peripheral ischemia in mice. *Circ Res.* 2007;100:662-669. doi: 10.1161/01.RES.0000260179.43672.fe
 70. Cai Z, Manalo DJ, Wei G, Rodriguez ER, Fox-Talbot K, Lu H, Zweier JL, Semenza GL. Hearts from rodents exposed to intermittent hypoxia or erythropoietin are protected against ischemia-reperfusion injury. *Circulation.* 2003;108:79-85. doi: 10.1161/01.CIR.0000078635.89229.8A
 71. Joshi D, Abraham D, Shiwen X, Baker D, Tsui J. Potential role of erythropoietin receptors and ligands in attenuating apoptosis and inflammation in critical limb ischemia. *J Vasc Surg.* 2014;60:191-201, 201 e191-192. doi: 10.1016/j.jvs.2013.06.054
 72. Rezaeian F, Wettstein R, Amon M, Scheuer C, Schramm R, Menger MD, Pittet B, Harder Y. Erythropoietin protects critically perfused flap tissue. *Ann Surg.* 2008;248:919-929. doi: 10.1097/SLA.0b013e31818f678e

73. Satoh K, Fukumoto Y, Nakano M, Kagaya Y, Shimokawa H. Emergence of the erythropoietin/erythropoietin receptor system as a novel cardiovascular therapeutic target. *J Cardiovasc Pharmacol*. 2011;58:570-574. doi: 10.1097/FJC.0b013e318235e7bb
74. Joshi D, Tsui J, Ho TK, Selvakumar S, Abraham DJ, Baker DM. Review of the role of erythropoietin in critical leg ischemia. *Angiology*. 2010;61:541-550. doi: 10.1177/0003319709358697
75. Sinclair AM, Coxon A, McCaffery I, Kaufman S, Paweletz K, Liu L, Busse L, Swift S, Elliott S, Begley CG. Functional erythropoietin receptor is undetectable in endothelial, cardiac, neuronal, and renal cells. *Blood*. 2010;115:4264-4272. doi: 10.1182/blood-2009-10-248666
76. Sanchis-Gomar F, Garcia-Gimenez JL, Pareja-Galeano H, Romagnoli M, Perez-Quilis C, Lippi G. Erythropoietin and the heart: physiological effects and the therapeutic perspective. *International Journal of Cardiology*. 2014;171:116-125. doi: 10.1016/j.ijcard.2013.12.011
77. Ribatti D, Poliani PL, Longo V, Mangieri D, Nico B, Vacca A. Erythropoietin/erythropoietin receptor system is involved in angiogenesis in human neuroblastoma. *Histopathology*. 2007;50:636-641. doi: 10.1111/j.1365-2559.2007.02653.x
78. Jelkmann W, Bohlius J, Hallek M, Sytkowski AJ. The erythropoietin receptor in normal and cancer tissues. *Critical Reviews in Oncology/Hematology*. 2008;67:39-61. doi: 10.1016/j.critrevonc.2008.03.006
79. Zvezdaryk KJ, Coffelt SB, Figueroa YG, Liu J, Phinney DG, LaMarca HL, Florez L, Morris CB, Hoyle GW, Scandurro AB. Erythropoietin, a hypoxia-regulated factor, elicits a pro-angiogenic program in human mesenchymal stem cells. *Experimental Hematology*. 2007;35:640-652. doi: 10.1016/j.exphem.2007.01.044
80. Jelkmann W, Elliott S. Erythropoietin and the vascular wall: the controversy continues. *Nutrition, Metabolism, and Cardiovascular Diseases: NMCD*. 2013;23 Suppl 1:S37-43. doi: 10.1016/j.numecd.2012.04.002
81. Satoh K, Kagaya Y, Nakano M, Ito Y, Ohta J, Tada H, Karibe A, Minegishi N, Suzuki N, Yamamoto M, et al. Important role of endogenous erythropoietin system in recruitment of endothelial progenitor cells in hypoxia-induced pulmonary hypertension in mice. *Circulation*. 2006;113:1442-1450. doi: 10.1161/CIRCULATIONAHA.105.583732
82. Zhang Q, Zhang J, Moe OW, Hsia CCW. Synergistic upregulation of erythropoietin receptor (EPO-R) expression by sense and antisense EPO-R transcripts in the canine lung. *Proceedings of the National Academy of Sciences of the United States of America*. 2008;105:7612-7617. doi: 10.1073/pnas.0802467105
83. Kunath K, von Harpe A, Fischer D, Petersen H, Bickel U, Voigt K, Kissel T. Low-molecular-weight polyethylenimine as a non-viral vector for DNA delivery: comparison of physicochemical properties, transfection efficiency and in vivo distribution with high-molecular-weight polyethylenimine. *Journal of Controlled Release: Official Journal of the Controlled Release Society*. 2003;89:113-125.
84. Moghimi SM, Symonds P, Murray JC, Hunter AC, Debska G, Szewczyk A. A two-stage poly(ethylenimine)-mediated cytotoxicity: implications for gene transfer/therapy. *Molecular Therapy: The Journal of the American Society of Gene Therapy*. 2005;11:990-995. doi: 10.1016/j.ymthe.2005.02.010

85. Ramezani M, Ebrahimian M, Hashemi M. Current strategies in the modification of PLGA-based gene delivery system. *Current Medicinal Chemistry*. 2017;24:728-739. doi: 10.2174/0929867324666161205130416
86. Bauters C, Asahara T, Zheng LP, Takeshita S, Bunting S, Ferrara N, Symes JF, Isner JM. Site-specific therapeutic angiogenesis after systemic administration of vascular endothelial growth factor. *J Vasc Surg*. 1995;21:314-324; discussion 324-315.
87. Mitsos S, Katsanos K, Koletsis E, Kagadis GC, Anastasiou N, Diamantopoulos A, Karnabatidis D, Dougenis D. Therapeutic angiogenesis for myocardial ischemia revisited: basic biological concepts and focus on latest clinical trials. *Angiogenesis*. 2012;15:1-22. doi: 10.1007/s10456-011-9240-2
88. Liew A, Bhattacharya V, Shaw J, Stansby G. Gene therapy for peripheral arterial disease. *Cochrane Database of Systematic Reviews*. 2016. doi: 10.1002/14651858.CD012058
89. Shimamura M, Nakagami H, Taniyama Y, Morishita R. Gene therapy for peripheral arterial disease. *Expert Opinion on Biological Therapy*. 2014;14:1175-1184. doi: 10.1517/14712598.2014.912272
90. Ravikumar P, Menon JU, Punnakitikashem P, Gyawali D, Togao O, Takahashi M, Zhang J, Ye J, Moe OW, Nguyen KT, et al. Nanoparticle facilitated inhalational delivery of erythropoietin receptor cDNA protects against hyperoxic lung injury. *Nanomedicine: Nanotechnology, Biology, and Medicine*. 2016;12:811-821. doi: 10.1016/j.nano.2015.10.004
91. Menon JU, Tumati V, Hsieh JT, Nguyen KT, Saha D. Polymeric nanoparticles for targeted radiosensitization of prostate cancer cells. *Journal of Biomedical Materials Research Part A*. 2015;103:1632-1639. doi: 10.1002/jbm.a.35300
92. Wadajkar AS, Santimano S, Tang L, Nguyen KT. Magnetic-based multi-layer microparticles for endothelial progenitor cell isolation, enrichment, and detachment. *Biomaterials*. 2014;35:654-663. doi: 10.1016/j.biomaterials.2013.10.015
93. Sundaresan V, Menon JU, Rahimi M, Nguyen KT, Wadajkar AS. Dual-responsive polymer-coated iron oxide nanoparticles for drug delivery and imaging applications. *Int J Pharm*. 2014;466:1-7. doi: 10.1016/j.ijpharm.2014.03.016
94. Menon JU, Ravikumar P, Pise A, Gyawali D, Hsia CC, Nguyen KT. Polymeric nanoparticles for pulmonary protein and DNA delivery. *Acta Biomater*. 2014;10:2643-2652. doi: 10.1016/j.actbio.2014.01.033
95. Xu H, Kona S, Su LC, Tsai YT, Dong JF, Brilakis ES, Tang L, Banerjee S, Nguyen KT. Multi-ligand poly(L-lactic-co-glycolic acid) nanoparticles inhibit activation of endothelial cells. *J Cardiovasc Transl Res*. 2013;6:570-578. doi: 10.1007/s12265-013-9460-5
96. Wadajkar AS, Menon JU, Tsai YS, Gore C, Dobin T, Gandee L, Kangasniemi K, Takahashi M, Manandhar B, Ahn JM, et al. Prostate cancer-specific thermo-responsive polymer-coated iron oxide nanoparticles. *Biomaterials*. 2013;34:3618-3625. doi: 10.1016/j.biomaterials.2013.01.062
97. Wadajkar AS, Kadapure T, Zhang Y, Cui W, Nguyen KT, Yang J. Dual-imaging enabled cancer-targeting nanoparticles. *Adv Healthc Mater*. 2012;1:450-456. doi: 10.1002/adhm.201100055
98. Wadajkar AS, Bhavsar Z, Ko CY, Koppolu B, Cui W, Tang L, Nguyen KT. Multifunctional particles for melanoma-targeted drug delivery. *Acta Biomater*. 2012;8:2996-3004. doi: 10.1016/j.actbio.2012.04.042

99. Patel RH, Wadajkar AS, Patel NL, Kavuri VC, Nguyen KT, Liu H. Multifunctionality of indocyanine green-loaded biodegradable nanoparticles for enhanced optical imaging and hyperthermia intervention of cancer. *J Biomed Opt.* 2012;17:046003. doi: 10.1117/1.JBO.17.4.046003
100. Koppolu B, Bhavsar Z, Wadajkar AS, Nattama S, Rahimi M, Nwariaku F, Nguyen KT. Temperature-sensitive polymer-coated magnetic nanoparticles as a potential drug delivery system for targeted therapy of thyroid cancer. *J Biomed Nanotechnol.* 2012;8:983-990.
101. Kona S, Dong JF, Liu Y, Tan J, Nguyen KT. Biodegradable nanoparticles mimicking platelet binding as a targeted and controlled drug delivery system. *Int J Pharm.* 2012;423:516-524. doi: 10.1016/j.ijpharm.2011.11.043
102. Rahimi M, Wadajkar A, Subramanian K, Yousef M, Cui W, Hsieh JT, Nguyen KT. In vitro evaluation of novel polymer-coated magnetic nanoparticles for controlled drug delivery. *Nanomedicine: Nanotechnology, Biology, and Medicine.* 2010;6:672-680.
103. Rahimi M, Meletis EI, You S, Nguyen K. Formulation and characterization of novel temperature sensitive polymer-coated magnetic nanoparticles. *J Nanosci Nanotechnol.* 2010;10:6072-6081.
104. Rahimi M, Yousef M, Cheng Y, Meletis EI, Eberhart RC, Nguyen K. Formulation and characterization of a covalently coated magnetic nanogel. *J Nanosci Nanotechnol.* 2009;9:4128-4134.
105. Panyam J, Labhasetwar V. Biodegradable nanoparticles for drug and gene delivery to cells and tissue. *Adv Drug Deliv Rev.* 2003;55:329-347.
106. Wickline SA, Neubauer AM, Winter P, Caruthers S, Lanza G. Applications of nanotechnology to atherosclerosis, thrombosis, and vascular biology. *Arterioscler Thromb Vasc Biol.* 2006;26:435-441.
107. Gentile P, Chiono V, Carmagnola I, Hatton PV. An overview of poly(lactic-co-glycolic) acid (PLGA)-based biomaterials for bone tissue engineering. *International Journal of Molecular Sciences.* 2014;15:3640-3659. doi: 10.3390/ijms15033640
108. Klugherz BD, Meneveau N, Chen W, Wade-Whittaker F, Papandreou G, Levy R, Wilensky RL. Sustained intramural retention and regional redistribution following local vascular delivery of polylactic-coglycolic acid and liposomal nanoparticulate formulations containing probucol. *Journal of Cardiovascular Pharmacology and Therapeutics.* 1999;4:167-174. doi: 10.1054/jcpt.1999.0167
109. Xu YY, Li YJ, Guan H, Liu CW, Zheng YH, Liu B, Yang J, Song CX. [The effect of vascular endothelia growth factor encapsulated in nanoparticles on chronic limb ischemia]. *Zhonghua wai ke za zhi [Chinese Journal of Surgery].* 2004;42:58-61.
110. Qi X, Okamoto Y, Murakawa T, Wang F, Oyama O, Ohkawa R, Yoshioka K, Du W, Sugimoto N, Yatomi Y, et al. Sustained delivery of sphingosine-1-phosphate using poly(lactic-co-glycolic acid)-based microparticles stimulates Akt/ERK-eNOS mediated angiogenesis and vascular maturation restoring blood flow in ischemic limbs of mice. *European Journal of Pharmacology.* 2010;634:121-131. doi: 10.1016/j.ejphar.2010.02.038
111. Guzman LA, Labhasetwar V, Song CX, Jang YS, Lincoff AM, Levy R, Topol EJ. Local intraluminal infusion of biodegradable polymeric nanoparticles - A novel approach for prolonged drug delivery after balloon angioplasty. *Circulation.* 1996;94:1441-1448.

112. Nair AM, Tsai YT, Shah KM, Shen J, Weng H, Zhou J, Sun X, Saxena R, Borrelli J, Jr., Tang L. The effect of erythropoietin on autologous stem cell-mediated bone regeneration. *Biomaterials*. 2013;34:7364-7371. doi: 10.1016/j.biomaterials.2013.06.031
113. Thevenot PT, Nair AM, Shen J, Lotfi P, Ko CY, Tang L. The effect of incorporation of SDF-1alpha into PLGA scaffolds on stem cell recruitment and the inflammatory response. *Biomaterials*. 2010;31:3997-4008. doi: 10.1016/j.biomaterials.2010.01.144
114. Xu H, Deshmukh R, Timmons R, Nguyen KT. Enhanced endothelialization on surface modified poly(L-lactic acid) substrates. *Tissue Eng Part A*. 2011;17:865-876. doi: 10.1089/ten.TEA.2010.0129
115. Xu H, Nguyen KT, Brilakis ES, Yang J, Fuh E, Banerjee S. Enhanced endothelialization of a new stent polymer through surface enhancement and incorporation of growth factor-delivering microparticles. *J Cardiovasc Transl Res*. 2012;5:519-527. doi: 10.1007/s12265-012-9381-8
116. Menon JU, Jadeja P, Tambe P, Vu K, Yuan B, Nguyen KT. Nanomaterials for photo-based diagnostic and therapeutic applications. *Theranostics*. 2013;3:152-166. doi: 10.7150/thno.5327
117. Wadajkar AS, Menon JU, Kadapure T, Tran RT, Yang J, Nguyen KT. Design and Application of Magnetic-based Theranostic Nanoparticle Systems. *Recent Patents on Biomedical Engineering*. 2013;6:47-57. doi: 10.2174/1874764711306010007
118. Kang C, Cho W, Park M, Kim J, Park S, Shin D, Song C, Lee D. H₂O₂-triggered bubble generating antioxidant polymeric nanoparticles as ischemia/reperfusion targeted nanotheranostics. *Biomaterials*. 2016;85:195-203. doi: 10.1016/j.biomaterials.2016.01.070
119. Lee D, Bae S, Ke Q, Lee J, Song B, Karumanchi SA, Khang G, Choi HS, Kang PM. Hydrogen peroxide-responsive copolyoxalate nanoparticles for detection and therapy of ischemia-reperfusion injury. *Journal of Controlled Release: Official Journal of the Controlled Release Society*. 2013;172:1102-1110. doi: 10.1016/j.jconrel.2013.09.020
120. Song Y, Huang Z, Xu J, Ren D, Wang Y, Zheng X, Shen Y, Wang L, Gao H, Hou J, et al. Multimodal SPION-CREKA peptide based agents for molecular imaging of microthrombus in a rat myocardial ischemia-reperfusion model. *Biomaterials*. 2014;35:2961-2970. doi: 10.1016/j.biomaterials.2013.12.038
121. Xie F, Li ZP, Wang HW, Fei X, Jiao ZY, Tang WB, Tang J, Luo YK. Evaluation of liver ischemia-reperfusion injury in rabbits using a nanoscale ultrasound contrast agent targeting ICAM-1. *PLoS One*. 2016;11:e0153805. doi: 10.1371/journal.pone.0153805
122. Ximendes EC, Rocha U, Del Rosal B, Vaquero A, Sanz-Rodriguez F, Monge L, Ren F, Vetrone F, Ma D, Garcia-Sole J, et al. In vivo ischemia detection by luminescent nanothermometers. *Adv Healthc Mater*. 2017;6. doi: 10.1002/adhm.201601195
123. Dey J, Xu H, Nguyen KT, Yang J. Crosslinked urethane doped polyester biphasic scaffolds: Potential for in vivo vascular tissue engineering. *Journal of Biomedical Materials Research Part A*. 2010;95:361-370. doi: 10.1002/jbm.a.32846
124. Dey J, Xu H, Shen J, Thevenot P, Gondi SR, Nguyen KT, Sumerlin BS, Tang L, Yang J. Development of biodegradable crosslinked urethane-doped polyester elastomers. *Biomaterials*. 2008;29:4637-4649. doi: 10.1016/j.biomaterials.2008.08.020
125. Guo J, Xie Z, Tran RT, Xie D, Jin D, Bai X, Yang J. Click chemistry plays a dual role in biodegradable polymer design. *Advanced Materials*. 2014;26:1906-1911. doi: 10.1002/adma.201305162

126. Gyawali D, Zhou S, Tran RT, Zhang Y, Liu C, Bai X, Yang J. Fluorescence imaging enabled biodegradable photostable polymeric micelles. *Adv Healthc Mater.* 2014;3:182-186. doi: 10.1002/adhm.201300145
 127. Mehdizadeh M, Weng H, Gyawali D, Tang L, Yang J. Injectable citrate-based mussel-inspired tissue bioadhesives with high wet strength for sutureless wound closure. *Biomaterials.* 2012;33:7972-7983. doi: 10.1016/j.biomaterials.2012.07.055
 128. Su LC, Xu H, Tran RT, Tsai YT, Tang L, Banerjee S, Yang J, Nguyen KT. In situ re-endothelialization via multifunctional nanoscaffolds. *ACS Nano.* 2014;8:10826-10836. doi: 10.1021/nn504636n
 129. Xie Z, Zhang Y, Liu L, Weng H, Mason RP, Tang L, Nguyen KT, Hsieh JT, Yang J. Development of intrinsically photoluminescent and photostable polylactones. *Adv Mater.* 2014;26:4491-4496. doi: 10.1002/adma.201306070
 130. Yang J, Zhang Y, Gautam S, Liu L, Dey J, Chen W, Mason RP, Serrano CA, Schug KA, Tang L. Development of aliphatic biodegradable photoluminescent polymers. *Proc Natl Acad Sci U S A.* 2009;106:10086-10091.
 131. Yang J, Webb AR, Ameer GA. Novel citric acid-based biodegradable elastomers for tissue engineering. *Advanced Materials.* 2004;16:511-516.
 132. Yang J, Webb AR, Pickerill SJ, Hageman G, Ameer GA. Synthesis and evaluation of poly(diols citrate) biodegradable elastomers. *Biomaterials.* 2006;27:1889-1898.
 133. Mason EA, Lopez R, Mason RP. Wavelength shifting of chemiluminescence using quantum dots to enhance tissue light penetration. *Optical Mater Exp.* 2016;6:1392-1401.
 134. Atturu G, Homer-Vanniasinkam S, Russell DA. Pharmacology in peripheral arterial disease: what the interventional radiologist needs to know. *Semin Intervent Radiol.* 2014;31:330-337. doi: 10.1055/s-0034-1393969
 135. Suarez S, Almutairi A, Christman KL. Micro- and nanoparticles for treating cardiovascular disease. *Biomaterials Science.* 2015;3:564-580. doi: 10.1039/C4BM00441H
 136. Ding C, Zhu A, Tian Y. Functional surface engineering of C-dots for fluorescent biosensing and in vivo bioimaging. *Acc Chem Res.* 2014;47:20-30. doi: 10.1021/ar400023s
 137. Priem B, Tian C, Tang J, Zhao Y, Mulder WJ. Fluorescent nanoparticles for the accurate detection of drug delivery. *Expert Opinion on Drug Delivery.* 2015;12:1881-1894. doi: 10.1517/17425247.2015.1074567
 138. Qin S, Fite BZ, Gagnon MK, Seo JW, Curry FR, Thorsen F, Ferrara KW. A physiological perspective on the use of imaging to assess the in vivo delivery of therapeutics. *Annals of Biomedical Engineering.* 2014;42:280-298. doi: 10.1007/s10439-013-0895-2
 139. Kimakova P, Solar P, Solarova Z, Komel R, Debeljak N. Erythropoietin and its angiogenic activity. *International Journal of Molecular Sciences.* 2017;18:E1519. doi: 10.3390/ijms18071519
 140. Krishna SM, Omer SM, Golledge J. Evaluation of the clinical relevance and limitations of current pre-clinical models of peripheral artery disease. *Clin Sci (Lond).* 2016;130:127-150. doi: 10.1042/CS20150435
 141. Liang GF, Zhu YL, Sun B, Hu FH, Tian T, Li SC, Xiao ZD. PLGA-based gene delivering nanoparticle enhance suppression effect of miRNA in HePG2 cells. *Nanoscale Res Lett.* 2011;6. doi: Artn 447
- 10.1186/1556-276x-6-447

142. Sah E, Sah H. Recent Trends in Preparation of Poly(lactide-co-glycolide) Nanoparticles by mixing polymeric organic solution with antisolvent. *Journal of Nanomaterials*. 2015;2015:794601. doi: 10.1155/2015/794601
143. Saha D, Kumar S, Ray D, Kohlbrecher J, Aswal VK. Role of physicochemical parameters associated with the hydrophobic vs. amphiphilic biodegradable polymer nanoparticles formation. *Journal of Molecular Liquids*. 2020;318:113977. doi: <https://doi.org/10.1016/j.molliq.2020.113977>
144. Sahana DK, Mittal G, Bhardwaj V, Kumar MN. PLGA nanoparticles for oral delivery of hydrophobic drugs: influence of organic solvent on nanoparticle formation and release behavior in vitro and in vivo using estradiol as a model drug. *Journal of Pharmaceutical Sciences*. 2008;97:1530-1542. doi: 10.1002/jps.21158
145. Shan D, Kothapalli S-R, Ravnicek DJ, Gerhard E, Kim JP, Guo J, Ma C, Guo J, Gui L, Sun L, et al. Development of citrate-based dual-imaging enabled biodegradable electroactive polymers. *Adv Funct Mater*. 2018;28:1801787. doi: 10.1002/adfm.201801787
146. Bozkir A, Saka OM. Chitosan nanoparticles for plasmid DNA delivery: effect of chitosan molecular structure on formulation and release characteristics. *Drug Delivery*. 2004;11:107-112. doi: 10.1080/10717540490280705
147. Fay F, Quinn DJ, Gilmore BF, McCarron PA, Scott CJ. Gene delivery using dimethyldidodecylammonium bromide-coated PLGA nanoparticles. *Biomaterials*. 2010;31:4214-4222. doi: 10.1016/j.biomaterials.2010.01.143
148. Le DQ, Kuriakose AE, Nguyen DX, Nguyen KT, Acharya S. Hybrid nitric oxide donor and its carrier for the treatment of peripheral arterial diseases. *Scientific Reports*. 2017;7:8692. doi: 10.1038/s41598-017-08441-9
149. Dey J, Tran RT, Shen J, Tang L, Yang J. Development and long-term in vivo evaluation of a biodegradable urethane-doped polyester elastomer. *Macromol Mater Eng*. 2011;296:1149-1157. doi: 10.1002/mame.201100074
150. Motlagh D, Allen J, Hoshi R, Yang J, Lui K, Ameer G. Hemocompatibility evaluation of poly(diols citrate) in vitro for vascular tissue engineering. *Journal of Biomedical Materials Research Part A*. 2007;82:907-916.
151. Yang J, Motlagh D, Webb AR, Ameer GA. Novel biphasic elastomeric scaffold for small-diameter blood vessel tissue engineering. *Tissue Eng*. 2005;11:1876-1886.
152. Parikh PP, Castilla D, Lassance-Soares RM, Shao H, Regueiro M, Li Y, Vazquez-Padron R, Webster KA, Liu ZJ, Velazquez OC. A reliable mouse model of hind limb gangrene. *Ann Vasc Surg*. 2018;48:222-232. doi: 10.1016/j.avsg.2017.10.008
153. Rivard A, Fabre JE, Silver M, Chen D, Murohara T, Kearney M, Magner M, Asahara T, Isner JM. Age-dependent impairment of angiogenesis. *Circulation*. 1999;99:111-120. doi: 10.1161/01.cir.99.1.111
154. Couffinhal T, Silver M, Zheng LP, Kearney M, Witzienbichler B, Isner JM. Mouse model of angiogenesis. *The American Journal of Pathology*. 1998;152:1667-1679.
155. Dutta S, Sengupta P. Men and mice: Relating their ages. *Life Sciences*. 2016;152:244-248. doi: 10.1016/j.lfs.2015.10.025
156. Krishna SM, Omer SM, Li J, Morton SK, Jose RJ, Golledge J. Development of a two-stage limb ischemia model to better simulate human peripheral artery disease. *Scientific Reports*. 2020;10:3449. doi: 10.1038/s41598-020-60352-4
157. Padgett ME, McCord TJ, McClung JM, Kontos CD. Methods for acute and subacute murine hindlimb ischemia. *J Vis Exp*. 2016. doi: 10.3791/54166

158. Alhasan MK, Liu L, Lewis MA, Magnusson J, Mason RP. Comparison of optical and power doppler ultrasound imaging for non-invasive evaluation of arsenic trioxide as a vascular disrupting agent in tumors. *PLoS One*. 2012;7:e46106. doi: 10.1371/journal.pone.0046106
159. Dey S, Kumari S, Kalainayakan SP, Campbell J, 3rd, Ghosh P, Zhou H, FitzGerald KE, Li M, Mason RP, Zhang L, et al. The vascular disrupting agent combretastatin A-4 phosphate causes prolonged elevation of proteins involved in heme flux and function in resistant tumor cells. *Oncotarget*. 2018;9:4090-4101. doi: 10.18632/oncotarget.23734
160. Ding Y, Mason RP, McColl RW, Yuan Q, Hallac RR, Sims RD, Weatherall PT. Simultaneous measurement of tissue oxygen level-dependent (TOLD) and blood oxygenation level-dependent (BOLD) effects in abdominal tissue oxygenation level studies. *J Magn Reson Imaging*. 2013;38:1230-1236. doi: 10.1002/jmri.24006
161. Hallac RR, Ding Y, Yuan Q, McColl RW, Lea J, Sims RD, Weatherall PT, Mason RP. Oxygenation in cervical cancer and normal uterine cervix assessed using blood oxygenation level-dependent (BOLD) MRI at 3T. *NMR Biomed*. 2012;25:1321-1330. doi: 10.1002/nbm.2804
162. Jiang L, Weatherall PT, McColl RW, Tripathy D, Mason RP. Blood oxygenation level-dependent (BOLD) contrast magnetic resonance imaging (MRI) for prediction of breast cancer chemotherapy response: a pilot study. *J Magn Reson Imaging*. 2013;37:1083-1092. doi: 10.1002/jmri.23891
163. Kucejova B, Sunny NE, Nguyen AD, Hallac R, Fu X, Pena-Llopis S, Mason RP, Deberardinis RJ, Xie XJ, Debose-Boyd R, et al. Uncoupling hypoxia signaling from oxygen sensing in the liver results in hypoketotic hypoglycemic death. *Oncogene*. 2011;30:2147-2160. doi: 10.1038/onc.2010.587
164. Mason RP, Jeffrey FM, Malloy CR, Babcock EE, Antich PP. A noninvasive assessment of myocardial oxygen tension: ¹⁹F NMR spectroscopy of sequestered perfluorocarbon emulsion. *Magnetic Resonance in Medicine*. 1992;27:310-317.
165. Remmele S, Mason RP, O'Connor JPB. MRI hypoxia measurements. In: Luna A, ed. *Functional Imaging in Oncology*. Berlin: Springer-Verlag; 2014:269-289.
166. White DA, Zhang Z, Li L, Gerberich J, Stojadinovic S, Peschke P, Mason RP. Developing oxygen-enhanced magnetic resonance imaging as a prognostic biomarker of radiation response. *Cancer Lett*. 2016;380:69-77. doi: 10.1016/j.canlet.2016.06.003
167. Xia M, Kodibagkar V, Liu H, Mason RP. Tumour oxygen dynamics measured simultaneously by near-infrared spectroscopy and ¹⁹F magnetic resonance imaging in rats. *Phys Med Biol*. 2006;51:45-60. doi: 10.1088/0031-9155/51/1/004
168. Hallac RR, Zhou H, Pidikiti R, Song K, Stojadinovic S, Zhao D, Solberg T, Peschke P, Mason RP. Correlations of noninvasive BOLD and TOLD MRI with pO₂ and relevance to tumor radiation response. *Magnetic Resonance in Medicine*. 2014;71:1863-1873. doi: 10.1002/mrm.24846
169. Krohn KA, Link JM, Mason RP. Molecular imaging of hypoxia. *J Nucl Med*. 2008;49 Suppl 2:129S-148S. doi: 10.2967/jnumed.107.045914
170. Liu H, Song Y, Worden KL, Jiang X, Constantinescu A, Mason RP. Noninvasive investigation of blood oxygenation dynamics of tumors by near-infrared spectroscopy. *Appl Opt*. 2000;39:5231-5243. doi: 10.1364/ao.39.005231

171. O'Kelly D, Guo Y, Mason RP. Evaluating online filtering algorithms to enhance dynamic multispectral optoacoustic tomography. *Photoacoustics*. 2020;19:100184. doi: 10.1016/j.pacs.2020.100184
172. O'Kelly D, Zhou H, Mason RP. Tomographic breathing detection: a method to noninvasively assess in situ respiratory dynamics. *J Biomed Opt*. 2018;23:1-6. doi: 10.1117/1.JBO.23.5.056011
173. Kumar VA, Liu Q, Wickremasinghe NC, Shi S, Cornwright TT, Deng Y, Azares A, Moore AN, Acevedo-Jake AM, Agudo NR, et al. Treatment of hind limb ischemia using angiogenic peptide nanofibers. *Biomaterials*. 2016;98:113-119. doi: <https://doi.org/10.1016/j.biomaterials.2016.04.032>
174. Astanina K, Simon Y, Cavelius C, Petry S, Kraegeloh A, Kiemer AK. Superparamagnetic iron oxide nanoparticles impair endothelial integrity and inhibit nitric oxide production. *Acta Biomater*. 2014;10:4896-4911. doi: 10.1016/j.actbio.2014.07.027
175. Cao Y. The toxicity of nanoparticles to human endothelial cells. *Adv Exp Med Biol*. 2018;1048:59-69. doi: 10.1007/978-3-319-72041-8_4
176. Montiel-Dávalos A, Ventura-Gallegos JL, Alfaro-Moreno E, Soria-Castro E, García-Latorre E, Cabañas-Moreno JG, Ramos-Godinez MdP, López-Marure R. TiO₂ nanoparticles induce dysfunction and activation of human endothelial cells. *Chemical Research in Toxicology*. 2012;25:920-930. doi: 10.1021/tx200551u
177. López-Royo T, Sebastián V, Moreno-Martínez L, Uson L, Yus C, Alejo T, Zaragoza P, Osta R, Arruebo M, Manzano R. Encapsulation of Large-Size Plasmids in PLGA Nanoparticles for Gene Editing: Comparison of Three Different Synthesis Methods. *Nanomaterials (Basel)*. 2021;11. doi: 10.3390/nano11102723
178. Hu J, Guo J, Xie Z, Shan D, Gerhard E, Qian G, Yang J. Fluorescence imaging enabled poly(lactide-co-glycolide). *Acta Biomater*. 2016;29:307-319. doi: 10.1016/j.actbio.2015.10.010
179. Kobulnik J, Kuliszewski MA, Stewart DJ, Lindner JR, Leong-Poi H. Comparison of gene delivery techniques for therapeutic angiogenesis ultrasound-mediated destruction of carrier microbubbles versus direct intramuscular injection. *J Am Coll Cardiol*. 2009;54:1735-1742. doi: 10.1016/j.jacc.2009.07.023

Biographical Information

I was an orthopedic surgeon in Vietnam where I was a clinical fellow and an attending physician at one of the most prestigious medical hospitals– the University Medical Center in Ho Chi Minh City. In 2011, I came to the U.S. to pursue research interests in the Bioengineering field. As an undergraduate, I interned in a biochemistry lab during my undergrad to learn about protein analysis. I focused on exploring bio-conjugation applications and studying quantitative proteomics using mass spectrometry-based novel proteomic tools. I presented my research at ACES 2015 and COS 2016 and won the third prize award at ACES 2015. I then graduated Summa Cum Laude majoring in both Chemistry and Biology. In 2017, I continued my research interest by enrolling in the PhD program in the Department of Bioengineering (BE) at the University of Texas at Arlington (UTA). Here I took advantage of medical knowledge and skills to contribute to BE research fields in nanomedicine and tissue engineering. I combined my medical background and advanced nanotechnologies to develop new therapies to treat cancer, orthopedic and cardiovascular diseases. With the interdisciplinary background, I have successfully performed many *in vivo*, *ex vivo*, and *in vitro* studies for various projects including melanoma, lung cancers, eye disorders, orthopedic and cardiovascular diseases. Besides research, I have been a peer mentor at the UTA animal care facility for 4 years to help other Ph.D. students improve animal experiments. I have also served as a reviewer for many journals such as Scientific Reports, Theranostics, Drug Delivery Science and Technology, Advanced Materials, ChemistrySelect, and so on. For the past 5 years, I have contributed 8 published papers, several prepared manuscripts, and numerous posters with various topics at different national conferences.

Published Papers



ELSEVIER



BASIC SCIENCE

Nanomedicine: Nanotechnology, Biology, and Medicine
35 (2021) 102400

Original Article

nanomedjournal.com

Nano encapsulated novel compound SA-10 with therapeutic activity in both acute and chronic murine hindlimb ischemia models

Louis Hinkle, BA^{a,1}, Duong Le, PhD^{b,1}, Tam Nguyen, MD^{b,1}, Vy T^b,
Charles E. Amankwa, M^d, Courtney Weston, B^d, Haifa Shen^a, Kytai T Nguyen^b,
Maham Rahimi, MD, PhD, RPVI^{c,*}, Suchismita Acharya, PhD^{c,d,f,**}

^aHouston Methodist Research Institute, Department of Nanomedicine, Houston, TX

^bDepartment of Bioengineering, University of Texas at Arlington, Arlington, TX

^cDepartment of Pharmacology and Neuroscience, University of North Texas Health Science Center, Fort Worth, TX

^dNorth Texas Eye Research Institute, University of North Texas Health Science Center, Fort Worth, TX

^eDivision of Cardiovascular Surgery, Houston Methodist Hospital, Houston, TX

^fDepartment of Pharmaceutical Sciences, College of Pharmacy, University of North Texas Health Science Center, Fort Worth, TX

Revised 23 March 2021

Abstract

The production dysregulation of reactive oxygen species (ROS) and nitric oxide (NO) in ischemic tissues results in endothelial dysfunction, hyperinflammation and poor blood circulation. Here, we report a hybrid molecule, SA-10 with both NO donating and ROS scavenging abilities that demonstrated potent cytoprotection and tube formation activity in endothelial cells under H₂O₂-induced oxidative stress. SA-10 loaded poly(lactic-co-glycolic acid) (PLGA) nanoparticles (SA-10 NPs) were delivered intramuscularly (IM) to two murine hindlimb ischemia models. In the acute mode ischemia/reperfusion (I/R), the muscle damage, hyperinflammation, and lung edema were significantly reduced 3 days post-dose while in the chronic ischemia model, significant improvement of blood perfusion and physical endurance was observed over 30 days ($P < 0.05$). Elderly patients with acute and chronic limb ischemia have limited options for surgical or endovascular interventions, so we anticipate that a product like SA-10 NPs has potential as one of the therapeutic alternatives to surgery.

© 2021 Elsevier Inc. All rights reserved.

Peripheral arterial disease (PAD) is a disease of the lower extremities where one or several peripheral arteries are narrowed or blocked. The annual cost for PAD-related health care in the US is \$10-\$20 billion dollars.¹ According to American Heart Association (AHA) statistics, at least 200 million people worldwide^{2,3} suffer from PAD. In the US, 8.5 million PAD patients (12% of American adults)¹ are ages 40 or older, and about 20% of PAD patients are over 70 years of age.^{4,5} Progression of PAD leads critical limb ischemia (CLI), which requires either endovascular revascularization or surgery to restore blood perfusion. Endovascular revascularization includes balloon dilation (angioplasty), cutting balloons, drug-coated balloons, covered stents, drug-eluting stents, and atherectomy.

The surgical bypass is usually performed on femoral and proximal popliteal arteries where the issues of stenosis and occlusion commonly happen,⁵ and autologous vein bypass transplantation is considered first line therapy.^{1,6} Nevertheless, the intervention often causes thrombosis and restenosis, and approximately 20-30% of PAD patients with CLI are not suitable candidates to undergo either surgery or endovascular revascularization. Recently, enhancing angiogenesis to treat PAD⁷ attracted more attention from scientists due to avoiding invasive surgical intervention.

Acute limb ischemia has an incidence of 1.5 cases per 10,000 persons per year and is associated with high rates of death and complication.⁸ Acute limb ischemia results from a sudden

* Corresponding author.

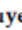

** Correspondence to: S. Acharya, Department of Pharmacology and Neuroscience, University of North Texas Health Science Center, Fort Worth, TX.

E-mail addresses: mrahimi@houstonmethodist.org, (M. Rahimi), suchismita.acharya@unthsc.edu, (S. Acharya).

¹ These authors contributed equally to this work.

Article

Novel Thiol Containing Hybrid Antioxidant-Nitric Oxide Donor Small Molecules for Treatment of Glaucoma

Charles E. Amankwa^{1,2}, Sudershan R. Gondi^{1,2}, Adnan Dibas^{1,2}, Courtney Weston^{1,2}, Arlene Funk^{1,2}, Tam Nguyen³ , Kytai T. Nguyen³, Dorette Z. Ellis^{2,4} and Suchismita Acharya^{1,2,4,*} 

- ¹ Department of Pharmacology and Neuroscience, University of North Texas Health Science Center, Fort Worth, TX 76107, USA; CharlesAmankwa@my.unthsc.edu (C.E.A.); sudershan.gondi@unthsc.edu (S.R.G.); dibasa@yahoo.com (A.D.); courtney.weston@outlook.com (C.W.); Arlene.Funk@my.unthsc.edu (A.F.)
- ² North Texas Eye Research Institute, University of North Texas Health Science Center, Fort Worth, TX 76107, USA; dorette.ellis@unthsc.edu
- ³ Department of Bioengineering, University of Texas at Arlington, Arlington, TX 76010, USA; tam.nguyen12@mavs.uta.edu (T.N.); knguyen@uta.edu (K.T.N.)
- ⁴ Department of Pharmaceutical Sciences, College of Pharmacy, University of North Texas Health Science Center, Fort Worth, TX 76107, USA
- * Correspondence: suchismita.acharya@unthsc.edu



Citation: Amankwa, C.E.; Gondi, S.R.; Dibas, A.; Weston, C.; Funk, A.; Nguyen, T.; Nguyen, K.T.; Ellis, D.Z.; Acharya, S. Novel Thiol Containing Hybrid Antioxidant-Nitric Oxide Donor Small Molecules for Treatment of Glaucoma. *Antioxidants* **2021**, *10*, 575. <https://doi.org/10.3390/antiox10040575>

Academic Editor: Urara Hasegawa

Received: 28 February 2021
Accepted: 5 April 2021
Published: 8 April 2021

Publisher's Note: MDPI stays neutral with regard to jurisdictional claims in published maps and institutional affiliations.



Copyright: © 2021 by the authors. Licensee MDPI, Basel, Switzerland. This article is an open access article distributed under the terms and conditions of the Creative Commons Attribution (CC BY) license (<https://creativecommons.org/licenses/by/4.0/>).

Abstract: Oxidative stress induced death and dysregulation of trabecular meshwork (TM) cells contribute to the increased intraocular pressure (IOP) in primary open angle (POAG) glaucoma patients. POAG is one of the major causes of irreversible vision loss worldwide. Nitric oxide (NO), a small gas molecule, has demonstrated IOP lowering activity in glaucoma by increasing aqueous humor outflow and relaxing TM. Glaucomatous pathology is associated with decreased antioxidant enzyme levels in ocular tissues causing increased reactive oxygen species (ROS) production that reduce the bioavailability of NO. Here, we designed, synthesized, and conducted in vitro studies of novel second-generation sulfur containing hybrid NO donor-antioxidants SA-9 and its active metabolite SA-10 to scavenge broad-spectrum ROS as well as provide efficient protection from *t*-butyl hydrogen peroxide (TBHP) induced oxidative stress while maintaining NO bioavailability in TM cells. To allow a better drug delivery, a slow release nanosuspension SA-9 nanoparticles (SA-9 NPs) was prepared, characterized, and tested in dexamethasone induced ocular hypertensive (OHT) mice model for IOP lowering activity. A single topical eye drop of SA-9 NPs significantly lowered IOP (61%) at 3 h post-dose, with the effect lasting up to 72 h. This class of molecule has high potential to be useful for treatment of glaucoma.

Keywords: nitric oxide; superoxide radical; hybrid small molecule; glaucoma; intra-ocular pressure; nanosuspension

1. Introduction

Primary open angle glaucoma (POAG) is among the leading causes of irreversible blindness globally. POAG is associated with compromised trabecular meshwork (TM), decreased aqueous humor outflow, increased intraocular pressure (IOP) [1], and degeneration of optic nerve head, altogether resulting in progressive vision loss. Despite damage to the TM, POAG is considered a multifactorial disease in which aging, inflammation, neurotrophic factors, genetics, and oxidative stress may play key roles in the pathophysiology [2]. However, the underlying mechanism still remains unclear. Elevated IOP is an important risk factor for the development and progression of POAG. In general, the IOP elevation in glaucoma is caused by the increased resistance to aqueous humor outflow, leading to ischemia and decreased oxygen supply to the retina, which progressively results in retinopathy. Treatment options have essentially focused on reducing IOP and increasing aqueous humor outflow or decreasing aqueous humor formation. A large variety of drug

Nanoencapsulated hybrid compound SA-2 with long-lasting intraocular pressure–lowering activity in rodent eyes

Dorota L. Stankowska,^{1,2} J. Cameron Millar,^{1,2} Bindu Kodati,^{1,2} Sumita Behera,² Renuka M. Chaphalkar,^{1,2} Tam Nguyen,³ Kytai T. Nguyen,³ Raghu R. Krishnamoorthy,^{1,2} Dorette Z. Ellis,⁴ Suchismita Acharya^{1,2,4}

¹Department of Pharmacology and Neuroscience, University of North Texas Health Science Center, Fort Worth, TX.; ²North Texas Eye Research Institute, University of North Texas Health Science Center, Fort Worth, TX.; ³Department of Bioengineering, The University of Texas at Arlington, Arlington, TX; ⁴Department of Pharmaceutical Sciences, College of Pharmacy, University of North Texas Health Science Center, Fort Worth, TX.

Purpose: Glaucoma is a neurodegenerative disease of the eye with an estimated prevalence of more than 111.8 million patients worldwide by 2040, with at least 6 to 8 million projected to become bilaterally blind. Clinically, the current method of slowing glaucomatous vision loss is to reduce intraocular pressure (IOP). In this manuscript, we describe the in vitro cytoprotective and in vivo long lasting IOP-lowering activity of the poly D, L-lactic-co-glycolic acid (PLGA) nanoparticle-encapsulated hybrid compound SA-2, possessing nitric oxide (NO) donating and superoxide radical scavenging functionalities.

Methods: Previously characterized primary human trabecular meshwork (hTM) cells were used for the study. hTM cells were treated with SA-2 (100 μ M, 200 μ M, and 1,000 μ M), SA-2 PLGA-loaded nanosuspension (SA-2 NPs, 0.1%), or vehicle for 30 min. Cyclic guanosine monophosphate (cGMP) and super oxide dismutase (SOD) levels were analyzed using commercial kits. In another experiment, hTM cells were pretreated with *tert*-butyl hydrogen peroxide (TBHP, 300 μ M) for 30 min followed by treatment with escalating doses of SA-2 for 24 h, and CellTiter 96 cell proliferation assay was performed. For the biodistribution study, the cornea, aqueous humor, vitreous humor, retina, choroid, and sclera were collected after 1 h of administration of a single eye drop (30 μ l) of SA-2 NPs (1% w/v) formulated in PBS to rat (n = 6) eyes. Compound SA-2 was quantified using high performance liquid chromatography /mass spectrometry (HPLC/MS). For the IOP-lowering activity study, a single SA-2 NPs (1%) eye drop was instilled in normotensive rats eyes and in the IOP-elevated rat eyes (n = 3/group, in the Morrison model of glaucoma), or Ad5TGF β 2-induced ocular hypertensive (OHT) mouse eyes (n = 5/group). IOP was measured at various time points up to 72 h, and the experiment was repeated in triplicate. Mouse aqueous humor outflow facility was determined with multiple flow-rate infusion and episcleral venous pressure estimated with manometry.

Results: SA-2 upregulated cGMP levels (six- to ten-fold) with an half maximal effective concentration (EC₅₀) of 20.3 μ M in the hTM cells and simultaneously upregulated (40-fold) the SOD enzyme when compared with the vehicle-treated hTM cells. SA-2 also protected hTM cells from TBHP-induced decrease in cell survival with an EC₅₀ of 0.38 μ M. A single dose of slow-release SA-2 NPs (1% w/v) delivered as an eye drop significantly lowered IOP (by 30%) in normotensive and OHT rodent eyes after 3 h post-dose, with the effect lasting up to 72 h. A statistically significant increase in aqueous outflow facility and a decrease in episcleral venous pressure was observed in rodents at this dose at 54 h.

Conclusions: Hybrid compound SA-2 upregulated cGMP in hTM cells, increased outflow facility and decreased IOP in rodent models of OHT. Compound SA-2 possessing an antioxidant moiety provided additive cytoprotective activity to oxidatively stressed hTM cells by scavenging reactive oxygen species (ROS) and increasing SOD enzyme activity. Additionally, the PLGA nanosuspension formulation (SA-2 NPs) provided longer duration of IOP-lowering activity (up to 3 days) in comparison with the free non-encapsulated SA-2 drug. The data have implications for developing novel, non-prostaglandin therapeutics for IOP-lowering and cytoprotective effects with the possibility of an eye drop dosing regimen of once every 3 days for patients with glaucoma.


It is estimated that by 2040, more than 111.8 million people worldwide will be affected with glaucoma, with the possibility of at least 6 to 8 million of them becoming bilaterally blind [1,2]. Primary open angle glaucoma (POAG), the most common form of glaucoma, is characterized by

progressive loss of retinal ganglion cell (RGC) somas and their axons, as well as axonal degeneration of the optic nerve. In many patients with POAG, there is also a rise in intraocular pressure (IOP), which is thought to be a major contributing factor to the development of the disease. Thus far, the only clinically efficacious method for treating POAG is to reduce IOP, either medically or surgically. However, lowering IOP is only partially effective; in most cases, it slows but does not arrest the progression of neurodegeneration. Furthermore,

Correspondence to: Suchismita Acharya, Department of Pharmacology and Neuroscience, University, North Texas Health Science Center, Fort Worth, TX; Phone: (817) 735-5193; email: Suchismita.acharya@unthsc.edu


Enhanced Endothelial Cell Delivery for Repairing Injured Endothelium via Pretargeting Approach and Bioorthogonal Chemistry


Min Kyung Khang,[§] Aneetta Elizabeth Kuriakose,[§] Tam Nguyen, Cynthia My-Dung Co, Jun Zhou, Thuy Thi Dang Truong, Kytai Truong Nguyen,^{*} and Liping Tang^{*}


 Cite This: *ACS Biomater. Sci. Eng.* 2020, 6, 6831–6841

 Read Online

ACCESS |

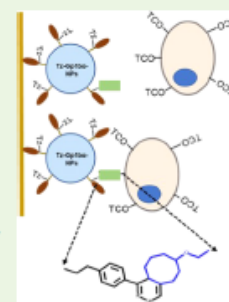
 Metrics & More

 Article Recommendations

 Supporting Information

ABSTRACT: Arterial wall injury often leads to endothelium cell activation, endothelial detachment, and atherosclerosis plaque formation. While abundant research efforts have been placed on treating the end stages of the disease, no cure has been developed to repair injured and denude endothelium often occurred at an early stage of atherosclerosis. Here, a pretargeting cell delivery strategy using combined injured endothelial targeting nanoparticles and bioorthogonal click chemistry approach was developed to deliver endothelial cells to replenish the injured endothelium via a two-step process. First, nanoparticles bearing glycoprotein 1b α (Gp1b α) proteins and tetrazine (Tz) were fabricated to provide a homogeneous nanoparticle coating on an injured arterial wall via the interactions between Gp1b α and von Willebrand factor (vWF), a ligand that is present on denuded endothelium. Second, transplanted endothelium cells bearing transcyclooctene (TCO) would be quickly immobilized on the surfaces of nanoparticles via TCO:Tz reactions. *In vitro* binding studies under both static and flow conditions confirmed that our novel Tz-labeled Gp1b α -conjugated poly(lactic- ω -glycolic acid) (PLGA) nanoparticles can successfully pretargeted toward the injured site and support rapid adhesion of endothelial cells from the circulation. *Ex vivo* results also confirm that such an approach is highly efficient in mediating the local delivery of endothelial cells at the sites of arterial injury. The results support that this pretargeting cell delivery approach may be used for repairing injured endothelium *in situ* at its early stage.

KEYWORDS: bioorthogonal click chemistry, pretargeting approach, nanoparticles, glycoprotein 1b α (Gp1b α), atherosclerosis, endothelial cells, endothelialization



1. INTRODUCTION

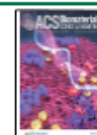
Percutaneous coronary interventions (PCI), including angioplasty, are commonly used to treat atherosclerosis, which is one of the leading causes of death worldwide. The procedures often cause arterial wall injury, resulting in inflamed or activated endothelial cells (ECs). They also promote platelet adhesion/deposition and allow migration and proliferation of smooth muscle cells (SMCs) at the site of vascular injury, leading to subsequent complications such as late thrombosis and restenosis.^{1,2} Nanoparticles (NPs) have been developed to treat various cardiovascular diseases.^{3,4} NPs, due to their low risk of causing inflammation and arterial occlusion can be intravenously injected into the circulation system to deliver therapeutic agents to the body. Active delivery of NPs to the injured arterial site via targeting ligands has also been used to improve therapeutic efficacy. For instance, intercellular adhesion molecule-1 (ICAM-1)-, sLex, and PSGL-1-conjugated micro-/nanoparticles were shown to target cytokine-activated endothelium via cell adhesion molecules both *in vitro* and *in vivo* and have shown some success in the treatment of cardiovascular diseases.^{5–8}

In addition to targeted drug delivery systems, significant progress has been made in the local delivery of therapeutic NPs in the treatment of atherosclerosis. For instance, perfusion catheters have been used to deliver drugs locally with limited availability of therapeutic agents at the injured sites.^{9,10} While drug-eluting stents (DES) were made to release therapeutic agents to injured vascular tissues,^{11–13} the released drugs were found to impede endothelial regeneration and lead to an increased risk of late stent thrombosis and restenosis.¹⁴ Drug-eluting balloons (DEBs) have also been developed to deliver paclitaxel for treating arterial obstructions with encouraging outcomes.^{15–17} However, little has been done to investigate the use of DEB sheath to deliver drug-loaded NPs and regenerative cells. Besides DES and DEBs, endothelial progenitor cells (EPCs) have been investigated as ideal

Received: June 27, 2020

Accepted: November 2, 2020

Published: November 10, 2020





Melanoma Peptide MHC Specific TCR Expressing T-Cell Membrane Camouflaged PLGA Nanoparticles for Treatment of Melanoma Skin Cancer

OPEN ACCESS

Edited by:

Stefano Leporatti,
Institute of Nanotechnology (CNR),
Italy

Reviewed by:

Paolo Bigini,
Mario Negri Institute
for Pharmacological Research
(IRCCS), Italy
Pradipta Ranjan Raut,
The University of Texas MD Anderson
Cancer Center, United States

*Correspondence:

Jon A. Weidanz
weidanz@uta.edu
Kytai T. Nguyen
knguyen@uta.edu

[†]These authors have contributed
equally to this work

Specialty section:

This article was submitted to
Nanobiotechnology,
a section of the journal
Frontiers in Bioengineering and
Biotechnology

Received: 07 May 2020

Accepted: 21 July 2020

Published: 11 August 2020

Citation:

Yaman S,
Ramachandramoorthy H, Oter G,
Zhukova D, Nguyen T, Sabnani MK,
Weidanz JA and Nguyen KT (2020)
Melanoma Peptide MHC Specific
TCR Expressing T-Cell Membrane
Camouflaged PLGA Nanoparticles
for Treatment of Melanoma Skin
Cancer.
Front. Bioeng. Biotechnol. 8:943.
doi: 10.3389/fbioe.2020.00943

Serkan Yaman^{1†}, Harish Ramachandramoorthy^{1,2†}, Gizem Oter¹, Daria Zhukova¹,
Tam Nguyen¹, Manoj K. Sabnani³, Jon A. Weidanz^{3*} and Kytai T. Nguyen^{1,2*}

¹ Department of Bioengineering, The University of Texas at Arlington, Arlington, TX, United States, ² Joint Bioengineering Program, The University of Texas Southwestern Medical Center, Dallas, TX, United States, ³ Department of Biology, University of Texas at Arlington, Arlington, TX, United States

Melanoma is one of the most aggressive skin cancers, and the American Cancer Society reports that every hour, one person dies from melanoma. While there are a number of treatments currently available for melanoma (e.g., surgery, chemotherapy, immunotherapy, and radiation therapy), they face several problems including inadequate response rates, high toxicity, severe side effects due to non-specific targeting of anti-cancer drugs, and the development of multidrug resistance during prolonged treatment. To improve chemo-drug therapeutic efficiency and overcome these mentioned limitations, a multifunctional nanoparticle has been developed to effectively target and treat melanoma. Specifically, poly (lactic-co-glycolic acid) (PLGA) nanoparticles (NPs) were coated with a cellular membrane derived from the T cell hybridoma, 19LF6 endowed with a melanoma-specific anti-gp100/HLA-A2 T-cell receptor (TCR) and loaded with an FDA-approved melanoma chemotherapeutic drug Trametinib. T-cell membrane camouflaged Trametinib loaded PLGA NPs displayed high stability, hemo- and cyto-compatibility. They also demonstrated membrane coating dependent drug release profiles with the most sustained release from the NPs proportional with the highest amount of membrane used. 19LF6 membrane-coated NPs produced a threefold increase in cellular uptake toward the melanoma cell line *in vitro* compared to that of the bare nanoparticle. Moreover, the binding kinetics and cellular uptake of these particles were shown to be membrane/TCR concentration-dependent. The *in vitro* cancer killing efficiencies of these NPs were significantly higher compared to other NP groups and aligned with binding and uptake characteristics. Particles with the higher membrane content (greater anti-gp100 TCR content) were shown to be more effective when compared to the free drug and negative controls. *In vivo* biodistribution studies displayed the theragnostic capabilities of these NPs with more than a twofold increase



Contents lists available at ScienceDirect

Journal of Controlled Release

journal homepage: www.elsevier.com/locate/jconrel

Glutathione-responsive biodegradable polyurethane nanoparticles for lung cancer treatment



Roshni Iyer^a, Tam Nguyen^a, Dona Padanilam^a, Cancan Xu^a, Debabrata Saha^c, Kytai T. Nguyen^{a,b,*}, Yi Hong^{a,b,*}

^a Department of Bioengineering, University of Texas at Arlington, Arlington, TX 76019, USA

^b Joint Biomedical Engineering Program, University of Texas Southwestern Medical Center, Dallas, TX 75390, USA

^c Department of Radiation Oncology, University of Texas Southwestern Medical Center, Dallas, TX 75390, USA

ARTICLE INFO

Keywords:

Glutathione
Nanoparticles
Lung cancer
Cisplatin
Stimuli responsive

ABSTRACT

Lung cancer is one of the major causes of cancer-related deaths worldwide. Stimuli-responsive polymers and nanoparticles, which respond to exogenous or endogenous stimuli in the tumor microenvironment, have been widely investigated for spatiotemporal chemotherapeutic drug release applications for cancer chemotherapy. We developed glutathione (GSH)-responsive polyurethane nanoparticles (GPUs) using a GSH-cleavable disulfide bond containing polyurethane that responds to elevated levels of GSH within lung cancer cells. The polyurethane nanoparticles were fabricated using a single emulsion and mixed organic solvent method. Cisplatin-loaded GSH-sensitive nanoparticles (CGPU) displayed a GSH-dose dependent release of cisplatin. In addition, a significant reduction in *in vitro* survival fraction of A549 lung cancer cells was observed compared to free cisplatin of equivalent concentration (survival fraction of ~0.5 and ~0.7, respectively). The *in vivo* biodistribution studies showed localization of fluorescently labeled GPUs (~7% of total injected dose per gram tissue) in the lung tumor regions after mouse-tail IV injections in xenograft A549 lung tumor models. The animals exposed to CGPUs also exhibited the inhibition of lung tumor growth compared to animals administered with saline (tumor growth rate of 1.5 vs. 13 in saline) and free cisplatin (tumor growth rate of 5.9) in mouse xenograft A549 lung tumor models within 14 days. These nanoparticles have potential to be used for on-demand drug release for an enhanced chemotherapy to effectively treat lung cancer.

1. Introduction

Lung cancer is one of the most common causes of cancer-related mortality in the United States, with over 230,000 new cancer cases and over 150,000 deaths in the year 2018 [1]. The major variant of lung cancer is non-small cell lung cancer (NSCLC) that accounts for over 85% of these cases, thus there is an urgent need to effectively treat this deadly disease [2]. The anti-neoplastic drug cisplatin (*cis*-diamminedichloroplatinum (II)) has been widely investigated in the clinic to treat various solid tumors, such as head and neck squamous carcinoma and ovarian cancer, and it is the first-line FDA approved treatment for NSCLC [3]. Cisplatin has decreased the overall lung cancer associated mortality by 6.9% compared to that of untreated controls [4]. Although cisplatin has been used in chemotherapy to effectively kill lung cancer cells and reduce lung tumor growth, it has several drawbacks, including severe toxicity in visceral organs and fast clearance resulted in inadequate intra-tumor drug concentrations [5]. Additionally, cisplatin is

poorly soluble in aqueous solvents affecting its bioavailability and therapeutic index [6]. The efficacy of cisplatin therapeutics is also limited by innate and acquired drug resistance [3].

The limitations of chemotherapy drugs such as their systemic toxicity, poor plasma-solubility and low bioavailability, can be potentially overcome by encapsulating them into nanoparticles (NPs). NPs as drug carriers for chemotherapy have achieved tremendous popularity because of their small size, and customizability to improve their accumulation in the tumor tissues, thereby improving drug bioavailability and distribution in the tumors [7]. Stimuli-responsive nanoparticles are a class of nanoparticles that observe low drug release in normal physiological conditions and enhance drug delivery at the targeted site upon exposure to a stimulus rendering the ability of spatial, temporal and dose-controlled drug release [8]. Thus, stimuli-responsive nanoparticles are gaining significant insight for treating various cancers that dispense various endogenous stimuli to trigger the drug release from these nanoparticles, such as changes in pH and enzyme levels in the

* Corresponding authors at: Department of Bioengineering, University of Texas at Arlington, Arlington, TX 76019, USA.
E-mail addresses: knnguyen@uta.edu (K.T. Nguyen), yihong@uta.edu (Y. Hong).

<https://doi.org/10.1016/j.jconrel.2020.02.021>

Received 9 November 2019; Received in revised form 24 January 2020; Accepted 11 February 2020

Available online 12 February 2020

0168-3659/ © 2020 Elsevier B.V. All rights reserved.

Stem Cells as Drug Delivery Vehicles

Aneetta E Kuriakose, Tam P Nguyen, Linda C Noukeu, Manoj K Sabhani, Jon A Weidanz, and Duong Q Le, University of Texas at Arlington, Arlington, TX, United States

Kytai T Nguyen, University of Texas at Arlington, Arlington, TX, United States; and University of Texas Southwestern Medical Center, Dallas, TX, United States

© 2019 Elsevier Inc. All rights reserved.

Introduction

Patient's health has been significantly improved with the discovery of novel therapeutic drugs which help us to treat and even cure some of the most challenging ailments. These drugs include small molecules, imaging agents, hormones, proteins, peptides, and nucleic acids; however, when administered into circulation, they pose many challenges due to their poor solubility, low stability, and drug side effects. Drug delivery systems (DDS) are therefore developed to carry these pharmaceuticals and deliver them specifically to the pathological sites. In the past few decades, polymeric or lipid particles have been extensively researched as prospective drug carriers. They are capable of (a) improving delivery of poorly water-soluble drugs; (b) targeting drugs to interested sites to reduce adverse effects; (c) delivering macromolecules to intracellular sites of action; (d) transporting drugs across endothelial or epithelial barriers; (e) visualizing cells/tissues by combining therapeutic agents with image probes and (f) controlling the rate of delivery by modifying their composition, size and architecture (Farokhzad and Langer, 2009). Despite its translational potential, nanotechnology mediated drug delivery has shown poor clinical outcomes due to rapid clearance from circulation, inefficient targeting, and retarded tissue penetration.

To circumvent the issues associated with nanotechnology-based drug delivery, one of the emerging approaches is to use the body's own circulating cells to deliver therapeutic reagents specifically to target regions in a controlled manner. This novel strategy takes advantage of the attractive and distinctive natural properties of cells. For instance, red blood cells (RBC), one of the most abundant circulating cells, have prolonged circulation time and stealth features that are ideal for a drug delivery system (Wang et al., 2015a; Agrahari et al., 2017; Pang et al., 2017). Platelets, on other hand, have specific targeting and release capabilities, which allow us to utilize them to deliver therapeutics specifically at a pathologic microenvironment associated with cancer or inflammation (Wu et al., 2016). Leukocytes, another major class of circulating cells are known for their role in protecting the body from infections or foreign invaders, have the intrinsic ability to migrate toward disease sites, cross tissue barriers and modulate host tissue responses (Mitchell and King, 2015). Finally, stem cells possess attributes such as pathological site-specific tropism, factor secretion and cell interactions to mediate tissue repair and remodeling (Tran and Damaser, 2015). To develop cell-based systems, these living cells are either genetically modified to secrete therapeutics or functionalized to carry drugs intercellularly or on the surface with or without the use of nanoparticles.

Significant advancements have been made in engineering biological cells to enhance their innate abilities as well as to endow with them new functionalities. In this book article, we aim to highlight engineered stem cells that are considered as a "Trojan horse" to deliver reagents including genes, nanoparticles, and small molecule therapeutics (Fig. 1). Initially, we address some key properties of stem cells and various sources of stem cells, as well as discuss current methodologies employed in preclinical studies to engineer stem cells to become "therapeutic factories" and their uses in various biomedical applications. Additionally, we elaborate on different strategies or routes employed to effectively deliver these drug releasing stem cells into the body for maximum therapeutic activity. To conclude, we address current clinical trials that used stem cells for drug delivery and the lessons that we learned from these studies to improve such systems in future.

Stem Cells and Their Sources

Stem cells are undifferentiated biological cells that can divide and self-renew for a long period of time. They are easy to harvest and have the capability to differentiate into any specialized cells in the body (Yin et al., 2016). Due to their unique potential, stem cells have emerged as the frontline regenerative medicine source to heal or restore tissues damaged due to age, trauma, inflammation, cancer, infections, congenital disorders, and other diseases (Mao and Mooney, 2015; Murphy et al., 2013). As a result, they have become a promising alternative to current treatment strategies involving tissue or organ transplantation that cannot meet the rising demands of the aged and diseased populations (Eberli and Atala, 2006; Bajaj et al., 2014). Additionally, it is now known that stem cells have the ability to secrete bio-active molecules including growth factors, morphogens, chemokines, cytokines, and extracellular vesicles can mediate greater therapeutic effects after transplantation in autocrine and paracrine manner (Mastri et al., 2014). They can suppress the local immune system, inhibit fibrosis (scar formation) and apoptosis, enhance angiogenesis, and stimulate mitosis and differentiation of tissue-intrinsic reparative or stem cells (Caplan and Dennis, 2006). The bioactive molecules synthesized by stem cells vary with respect to physiological and pathological conditions (Madrigal et al., 2014). Thus, for therapeutic applications, stem cells are exposed to relevant stimuli like hypoxia or cytokines to modulate their secretions and microenvironment. For instance, bone marrow derived MSCs (BM-MSCs) secrete high levels of growth factors such as VEGF, bFGF, IGF-1, and SDF-1, as

Hybrid Compound SA-2 is Neuroprotective in Animal Models of Retinal Ganglion Cell Death

Dorota L. Stankowska,^{1,2} Adnan Dibas,^{1,2} Linya Li,³ Wei Zhang,^{1,2} Vignesh R. Krishnamoorthy,^{1,2} Sai H. Chavala,^{1,2} Tam Phung Nguyen,⁴ Thomas Yorio,^{1,2} Dorette Z. Ellis,^{2,3} and Suchismita Acharya^{1,2}

¹Department of Pharmacology and Neuroscience, University of North Texas Health Science Center, Fort Worth, Texas, United States

²North Texas Eye Research Institute, University of North Texas Health Science Center, Fort Worth, Texas, United States

³Department of Pharmaceutical Sciences, University of North Texas Health Science Center, Fort Worth, Texas, United States

⁴Department of Bioengineering, The University of Texas at Arlington, Arlington, Texas, United States

Correspondence: Suchismita Acharya, Department of Pharmacology and Neuroscience, North Texas Eye Research Institute, University of North Texas Health Science Center, 3500 Camp Bowie Boulevard, Fort Worth, TX 76107, USA; suchismita.acharya@unthsc.edu.

Submitted: October 16, 2018

Accepted: June 8, 2019

Citation: Stankowska DL, Dibas A, Li L, et al. Hybrid compound SA-2 is neuroprotective in animal models of retinal ganglion cell death. *Invest Ophthalmol Vis Sci.* 2019;60:3064-3073. <https://doi.org/10.1167/iovs.18-25999>

PURPOSE. Determine the toxicity, bioavailability in the retina, and neuroprotective effects of a hybrid antioxidant-nitric oxide donor compound SA-2 against oxidative stress-induced retinal ganglion cell (RGC) death in neurodegenerative animal models.

METHODS. Optic nerve crush (ONC) and ischemia reperfusion (I/R) injury models were used in 12-week-old C57BL/6J mice to mimic conditions of glaucomatous neurodegeneration. Mice were treated intravitreally with either vehicle or SA-2. Retinal thickness was measured by spectral-domain optical coherence tomography (SD-OCT). The electroretinogram and pattern ERG (PERG) were used to assess retinal function. RGC survival was determined by counting RBPMS-positive RGCs and immunohistochemical analysis of superoxide dismutase 1 (SOD1) levels was carried out in the retina sections. Concentrations of SA-2 in the retina and choroid were determined using HPLC and MS. In addition, the direct effect of SA-2 treatment on RGC survival was assessed in ex vivo rat retinal explants under hypoxic (0.5% O₂) conditions.

RESULTS. Compound SA-2 did not induce any appreciable change in retinal thickness, or in a- or b-wave amplitude in naive animals. SA-2 was found to be bioavailable in both the retina and choroid after a single intravitreal injection (2% wt/vol). An increase in SOD1 levels in the retina of mice subjected to ONC and SA-2 treatment, suggests an enhancement in antioxidant activity. SA-2 provided significant ($P < 0.05$) RGC protection in all three of the tested RGC injury models in rodents. PERG amplitudes were significantly higher in both I/R and ONC mouse eyes following SA-2 treatment ($P \leq 0.001$) in comparison with the vehicle and control groups.

CONCLUSIONS. Compound SA-2 was effective in preventing RGC death and loss of function in three different rodent models of acute RGC injury: ONC, I/R, and hypoxia.

Keywords: neuroprotection, SOD, nitric oxide, hybrid small molecule, RGC, glaucoma

Retinal ganglion cells (RGCs) are output neurons that ultimately transmit visual information from the retina to the brain. Irreversible blindness worldwide¹ due to RGC degeneration includes ischemic optic neuropathies, hereditary optic neuropathies, and glaucoma. RGCs are highly susceptible to oxidative stress and ischemic insult.^{2,3} Primary open angle glaucoma and angle-closure glaucoma are characterized by elevated IOP, axonal degeneration of the optic nerve, and progressive loss of RGCs. The current approaches to slow down glaucomatous vision loss are mainly aimed at lowering IOP, which do not fully address the susceptibility to RGC degeneration.⁴

Artery, vein occlusion, or elevated IOP produce oxidative stress in both RGCs and retinal endothelial cells through decreased activity of several antioxidant enzymes, including superoxide dismutase (SOD), glutathione peroxidase, catalase, and thioredoxins (Trx1 and Trx2), and these imbalances have been implicated in promoting RGC death.⁵⁻⁷ Ischemic stress in the eye followed by reperfusion generates an outburst of detrimental superoxide free radicals. The superoxide radicals then induce oxidative stress, leading to apoptosis of RGCs⁸ as

well as dysfunction of retinal endothelial cells. Another factor contributing to ischemic neuronal damage is N-methyl-D-aspartate (NMDA)-induced entry of calcium followed by production of free radicals.⁹ In the rat hippocampus,¹⁰ the activation of NMDA receptors generates reactive oxygen species (ROS) and decreases antioxidant potential of the tissue. Furthermore, the toxic peroxynitrite¹¹ formed from the reaction of NO and superoxide anions (O₂⁻) is responsible in part for NMDA receptor-mediated neurotoxicity. Cellular SOD enzymes convert the O₂⁻ radical to O₂ and H₂O₂. In many chronic and acute neurodegenerative diseases, including glaucomatous optic neuropathy,^{12,13} decrease in SOD has been associated with oxidative stress-induced neurotoxicity. SOD is an enzyme that includes three forms: SOD1 (Cu, Zn-SOD), SOD2 (Mn-SOD), and SOD3 (containing Zn and Cu) encoded by separate genes.¹⁴ Deficiency in SOD1 but not SOD2 is known to cause RGC sensitivity to various insults, which may be the underlying condition of normal tension glaucoma.¹⁵ Significantly higher levels of superoxide anions were found in the RGC layer of 24-week-old SOD1-deficient mice compared with